

Review, Extension, and Application of Unsteady Thin Airfoil Theory

by

Christopher O. Johnston

Center for Intelligent Material Systems and Structures (CIMSS)

Virginia Polytechnic Institute and State University

Blacksburg, VA, 24060

August 8, 2004

CIMSS Report No. 04-101

Work funded by the Center for Intelligent
Material Systems and Structures (CIMSS)

Review, Extension, and Application of Unsteady Thin Airfoil Theory

(Abstract)

This report presents a general method of unsteady thin airfoil theory for analytically determining the aerodynamic characteristics of deforming camberlines. This method provides a systematic approach to the calculation of both the unsteady aerodynamic forces and the load distribution. The contributions of the various unsteady aerodynamic effects are made clear and the relationship of these effects to steady airfoil theory concepts is emphasized. A general deforming camberline, which consists of two quadratic segments with arbitrary coefficients, is analyzed using this method. It is found that the unsteady aerodynamic effect is largely dependent on the shape of the deforming camberline. The drag and power requirements for deforming or unsteady thin airfoils are investigated analytically using the unsteady thin airfoil method. Both the oscillating and transient cases are investigated. The relationship between the aerodynamic energy balance and the required actuator energy for transient and oscillating camberline cases is discussed. It is shown that the unsteady aerodynamic effects are required to accurately determine the power required to deform an airfoil. The actuator energy cost of negative and positive power is shown to be an important characteristic of an airfoil actuator. Flapping wing flight is also investigated using these actuator energy concepts and shown to benefit greatly from springs or elastic mechanisms. An approximate extension of this method to three-dimensional wings is discussed and applied to flapping wing flight.

Table of Contents

Chapter 1	Introduction and Overview of Unsteady Thin Airfoil Theory	1
1.1	Report Overview.	1
1.2	A Review of Unsteady Thin Airfoil Theory Literature.	2
1.3	Fundamental Concepts in Unsteady Thin Airfoil Theory.	4
1.4	The Unsteady Pressure Distribution.	8
Chapter 2	An Unsteady Thin Airfoil Method for Deforming Airfoils	10
2.1	Introduction.	10
2.2	Determining L_0 , L_1 , M_1 , and M_0	10
2.3	Determining Δp_0 and Δp_1	13
2.4	Determining L_2 and Δp_2	16
2.5	The Separation of Quasi-Steady Terms into “Aerodynamic Damping” and “Steady” Terms	22
2.6	The Unsteady Aerodynamics for a Sinusoidal β	27
2.7	The Equivalence of $T_{l,s}$ and $T_{0,d}$	29
Chapter 3	Application of the Theory to a General Deforming Camberline	32
3.1	Introduction.	32
3.2	Camberline Representation	33
3.3	The Quasi-Steady Load Distribution and Force Coefficients.	35
3.4	The Apparent Mass Load Distribution and Force Coefficients	45
3.5	A Variable-Camber Problem.	50
3.6	The Load Distribution and Force Coefficients for a Sinusoidal β	52

Chapter 4	Drag in Unsteady Thin Airfoil Theory	65
4.1	Introduction.	65
4.2	The Lack of Drag in Steady Airfoil Thin Theory	65
4.3	The Presence of Drag in Steady Airfoil Thin Theory	69
4.4	The Drag for a Suddenly Accelerated Flat Plate.	71
4.5	A Comparison Drag for a ΔC_l	73
4.6	The Drag on an Airfoil with a Sinusoidal β	74
Chapter 5	Aerodynamic Work and Actuator Energy Concepts	77
5.1	Introduction.	77
5.2	The Aerodynamic Energy Balance and Actuator Energy Cost	78
5.3	The Aerodynamic Work for a Ramp Input of Control Deflection	83
5.4	Application to a Pitching Flat-Plate Airfoil.	86
5.5	Application to Various Control Surface Configurations.	94
Chapter 6	Flapping Wing Propulsion	102
6.1	Introduction.	102
6.2	The Energy Required for Flapping	102
6.3	Flapping By Heave Motions	109
6.4	Flapping Wing Performance Analysis.	112
6.5	Multi-Degree-of-Freedom Flapping.	118
References		121
Appendix A	Useful Integral Formulas for Determining the Unsteady Load Distribution	137
Appendix B	The Drag for a Three-Degree-of-Freedom Oscillating Airfoil	138

Chapter 1

Introduction and Overview of Unsteady Thin Airfoil Theory

1.1 Report Overview

This report presents a convenient method for determining the unsteady aerodynamic characteristics of deforming thin airfoils in incompressible flow. In particular, equations for the lift, pitching moment, drag, work, and pressure distribution for arbitrary time-dependent camberline shapes will be presented and applied to a general deforming camberline.

This chapter presents a brief overview of the unsteady thin airfoil theory literature and then provides an instructive derivation of incompressible thin airfoil theory. This derivation, based on McCune's [1990 and 1993] derivation of nonlinear unsteady airfoil theory, is an alternative approach to obtaining von Karman and Sears's [1938] formulation of unsteady airfoil theory. Chapter 2 presents a new method of determining the unsteady lift, pitching moment and pressure distribution for arbitrary time-dependent airfoil motion. This method is based on a combination of von Karman and Sears's approach to unsteady thin airfoil theory and Glauert's [1947] approach to steady thin airfoil theory. The advantage of this method is that it makes clear the relationship between the steady and unsteady pressure distribution and force coefficients. Chapter 3 applies the method of Chapter 2 to a general deforming camberline. This general camberline consists of two quadratic curves connected at an arbitrary location along the chord. The coefficients of the quadratic curves may be chosen so that the camberline represents a wide variety of camberline shapes. Results for conventional and conformal leading and trailing edge flaps along with NACA 4-digit camberlines will be presented and discussed. Chapter 4 presents a

discussion and derivation of the drag acting on an unsteady thin airfoil. The derivation is based on the unsteady thin airfoil method presented in Chapter 2, which allows for significant simplifications of the drag equation. Both transient and oscillatory cases are discussed. The asymptotic behavior of the unsteady drag for small and large oscillation frequencies is presented. Chapter 5 investigates the aerodynamic energy balance and relates it to the aerodynamic work and the actuator energy cost required for a deforming airfoil. A general actuator model is proposed that allows the relative energy cost required by the actuator to produce positive and negative work to be specified. This is applied to the various camberline shapes discussed in Chapter 3. Chapter 6 examines flapping wing propulsion using the actuator energy concepts presented in Chapter 5. The importance of springs in a flapping wing actuation system is discussed. The application to a three-dimensional wing is discussed and examples presented.

1.2 An Overview of Unsteady Thin Airfoil Theory Literature

The two popular (in the English-speaking literature) formulations of unsteady thin airfoil theory for an incompressible flow were presented by Theodorsen [1935] and von Karman and Sears [1938]. Although they produce identical results, their representative equations appear significantly different. Theodorsen's approach requires "circulatory" and "noncirculatory" velocity potentials to be determined and then used in the unsteady Bernoulli equation to determine the resulting pressure distribution. Although the unsteady pressure distribution is implied with this method, Theodorsen did not present any results for it. von Karman and Sears formulated the problem in the framework of steady thin airfoil theory, as will be discussed in Section 1.3. This makes their approach more appealing to those familiar with steady thin airfoil theory. They also did not discuss the unsteady pressure distribution, although in Sears's dissertation (Sears [1938], pp. 68-74), the problem is solved for an oscillating airfoil.

Independently of Theodorsen and von Karman and Sears, Russian and German researchers developed analogous approaches to unsteady airfoil theory. An excellent discussion of the global development of unsteady theory is given in the translated article by Neskarov [1947]. Discussions (in English) of these alternate methods are given by Sedov [1965] and Garrick [1952 and 1957].

It is emphasized that these methods are for incompressible flow; compressibility effects significantly complicate the theory (Miles [1950]). Introductions to the theory of unsteady thin

airfoils in compressible flow can be found in, for example, Bisplinghoff *et al.* [1955], Dowell [1995], Lomax [1960], Fung [1969] and Garrick [1957]. Some other relevant methods and discussions are given by Kemp [1973 and 1978], Graham [1970], Kemp and Homicz [1978], Osbourne [1973], Williams [1977 and 1980], and Amiet [1974].

Unsteady thin airfoil theory is an inviscid theory which ignores thickness and applies the linearized boundary condition on a mean surface. Therefore, the validity of the theory for various airfoil motions and Reynolds numbers is of interest. For airfoils oscillating in pitch and plunge, Silverstein and Joyner [1939], Reid and Vincenti [1940], Halfman [1952], and Rainey [1957] present experimental results that show acceptable agreement with theory for the lift and pitching moment (see Lishman [2000] pp. 316-319 for a comparison). Satyanarayana and Davis [1978] show agreement, except at the trailing edge, between the theoretical and experimental pressure distribution for an airfoil oscillating in pitch. The apparent failure of thin airfoil theory at the trailing edge has led to some debate over the validity of enforcing the Kutta condition for unsteady flows (Giesing [1969], Yates [1978a and 1978b], Katz and Weihs [1981], McCrosky [1982], Poling and Telionis [1986], and Ardonneau [1989]). Albano and Rodden [1969] show that theory slightly over predicts the magnitude, but correctly predicts the shape, of the pressure distribution for an airfoil with an oscillating control surface. For a ramp input of control surface deflection, Rennie and Jumper [1996] show reasonable agreement between theory and experiment for both the lift and pressure distribution. Fung [1969] (pp. 454-457) also presents a comparison that shows agreement between theory and experiment. Rennie and Jumper [1997] argue that at low Reynolds number (2×10^5) and high deflection rates, the viscous and unsteady effects cancel out and steady thin airfoil theory is then valid.

A topic of considerable interest in applied unsteady aerodynamics is dynamic stall and unsteady boundary-layer separation. Semi-empirical methods of modeling dynamic stall in the framework of unsteady thin airfoil theory have been proposed by Ericsson and Redding [1971] and Lishman and Beddoes [1989]. These methods must be tuned by experimental data. Sears [1956 and 1976] proposed a method of predicting boundary-layer separation for an unsteady airfoil. This method uses the unsteady thin airfoil theory vorticity distribution along with a thickness induced velocity distribution to represent the outer flow. Unsteady boundary layer separation concepts may then be applied to determine flow separation (Sears and Telionis [1975]). The treatment of separated flow regions was discussed by Sears [1976]. Sears's approach would allow dynamic stall to be determined analytically without any empiricism. Application of this method has not been

presented in the literature. McCroskey [1973] presents a modification to unsteady thin airfoil theory to account for the effect of thickness, which would be useful for the application of Sears's proposed method.

1.3 Fundamental Concepts in Unsteady Thin Airfoil Theory

The following discussion is based on McCune's [1990 and 1993] derivation of nonlinear unsteady airfoil theory. The derivation for the linear case is presented here because it is felt that it provides insight into the meaning of the three separate lift terms found by von Karman and Sears. Also, this derivation does not seem to be present in the literature.

The fundamental differences between steady (time-independent) and unsteady (time-dependent) incompressible airfoil theory stem from two concepts; the unsteady Bernoulli equation and Kelvin's theorem. Under the assumptions of thin airfoil theory, the unsteady Bernoulli equation can be written as (Katz and Plotkin [2001], Eq. 13.35)

$$\Delta p = \rho \left[U(t)\gamma(x, t) + \frac{\partial}{\partial t} \int_0^x \gamma(x_0, t) dx_0 \right] \quad (1.1)$$

where γ is the vorticity (which is a function of time) on an airfoil that extends from $x = 0$ to c . Eq. (1.1) identifies the first fundamental difference between steady and unsteady airfoil theory, which is that Δp is no longer proportional to γ (meaning the Kutta-Joukowski theorem no longer applies). It is instructive to examine the consequences of Eq. (1.1) on the airfoil lift. From Eq. (1.1), the lift can be written as

$$L = \rho U(t) \int_0^c \gamma(x, t) dx + \rho \int_0^c \frac{\partial}{\partial t} \int_0^x \gamma(x_0, t) dx_0 dx \quad (1.2)$$

Integrating the second term by parts results in

$$L = \rho U(t) \int_0^c \gamma(x, t) dx + \frac{\partial}{\partial t} \rho \left[x \int_0^x \gamma(x_0, t) dx_0 \right]_0^c - \int_0^c \gamma(x, t) x dx \quad (1.3)$$

If it is recognized that

$$x \int_0^x \gamma(x_0, t) dx_0 \Big|_0^c = c \int_0^c \gamma(x, t) dx \quad (1.4)$$

then Eq. (1.3) can be written as

$$L = \rho U(t) \int_0^c \gamma(x,t) dx + \frac{\partial}{\partial t} \rho \left[\int_0^c (c-x) \gamma(x,t) dx \right] \quad (1.5)$$

The first term in Eq. (1.5) will be defined as the Joukowski lift (L_j), because it corresponds to the lift due to the Kutta-Joukowski theorem, and the second term will be defined as apparent mass lift (L_a). Before the significance of Eq. (1.5) is recognized, the nature of γ must be discussed. This discussion is based on Kelvin's condition, which is the second fundamental difference between steady and unsteady airfoil theory. Kelvin's condition states that the circulation (Γ) in a flow must remain constant. The circulation around an airfoil is related to γ as follows

$$\Gamma_a = \int_0^c \gamma(x,t) dx \quad (1.6)$$

From the definition of unsteady motion

$$\frac{d}{dt} \int_0^c \gamma(x,t) dx \neq 0 \quad (1.3)$$

which implies that vorticity is shed into a wake as follows

$$\frac{d}{dt} \int_0^c \gamma(x,t) dx = \frac{d}{dt} \int_c^\infty \gamma_w(\xi,t) d\xi \quad (1.7)$$

From Helmholtz's vortex laws, the strength of the wake vortices remain constant as they convect downstream. An assumption of linear unsteady airfoil theory is that the wake vortices convect downstream with the freestream velocity and not with the local velocity. This implies that the wake is planar and therefore wake rollup effects are ignored. The presence of wake vortices means that γ may be written as

$$\gamma = \gamma_0 + \gamma_1 \quad (1.8)$$

where γ_0 is the "quasi-steady" component and γ_1 is the "wake induced" component of vorticity on the airfoil. The quasi-steady component is the vorticity due to the instantaneous state of the airfoil as predicted from steady thin airfoil theory. The wake induced component is the component of vorticity induced from the wake vortices. Considering Figure 1.1, the induced vorticity from a single vortex can be written as

$$\gamma_1' = \frac{1}{2\pi} \frac{\gamma_w'}{(\xi-x)} \sqrt{\frac{c-x}{x}} \sqrt{\frac{\xi}{\xi-c}} \quad (1.9)$$

From this equation, the induced vorticity for the entire wake can be written as

$$\gamma_1 = \frac{1}{2\pi} \int_c^\infty \frac{\gamma_w(\xi)}{(\xi-x)} \sqrt{\frac{c-x}{x}} \sqrt{\frac{\xi}{\xi-c}} d\xi \quad (1.10)$$

where the wake starts at c and extends to infinity.

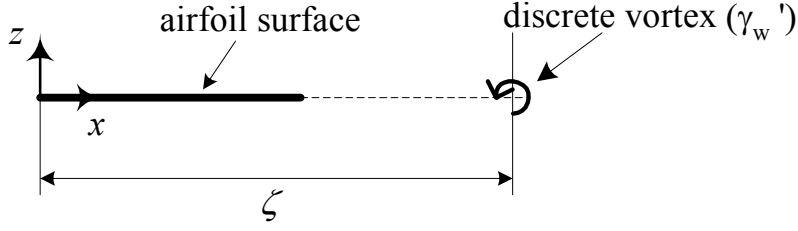


Figure 1.1: Airfoil and a single wake vortex

With it now known that $\gamma = \gamma_0 + \gamma_1$, with the expression for γ_1 given in Eq. (1.10), it useful to return to Eq. (1.5) for the lift. Substituting Eqs. (1.8) and (1.10) into Eq. (1.5) results in

$$L = \rho U(t) \int_0^c (\gamma_0 + \gamma_1) dx + \frac{\partial}{\partial t} \rho \left[\int_0^c (c-x)(\gamma_0 + \gamma_1) dx \right] \quad (1.11)$$

Eq. (1.11) can be separated into the two following terms

$$\Delta L (\text{due to } \gamma_0) = \rho U(t) \Gamma_0 - \frac{\partial}{\partial t} \rho \left[\int_0^c (x-c/2) \gamma_0 dx \right] + \rho \frac{c}{2} \frac{\partial \Gamma_0}{\partial t} \quad (1.12)$$

$$\Delta L (\text{due to } \gamma_1) = \rho U(t) \Gamma_1 - \frac{\partial}{\partial t} \rho \left[\int_0^c (x-c/2) \gamma_1 dx \right] + \rho \frac{c}{2} \frac{\partial \Gamma_1}{\partial t} \quad (1.13)$$

These two equations can be further reduced by manipulating the second and third term in Eq. (1.13). From Eq. (1.10), the wake induced circulation can be evaluated as

$$\begin{aligned} \Gamma_1 &= \int_0^c \gamma_1 dx \\ &= \int_c^\infty \gamma_w(\xi) \left(\sqrt{\frac{\xi}{\xi-c}} - 1 \right) d\xi \end{aligned} \quad (1.14)$$

Furthermore, the integral in the second term of Eq. (1.13) can be evaluated as follows

$$\int_0^c \gamma_1 (x-c/2) dx = \int_c^\infty \gamma_w(\xi) \left(\sqrt{\xi^2 - \xi c} - \xi + c/2 \right) d\xi \quad (1.15)$$

The key to the cancellations occurring in Eq. (1.12) and (1.13) is taking the time derivative of Eq. (1.14). This derivative is similar to von Karman and Sears's Eq. (15), except in the current case, $f(c) \neq 0$, which leaves an extra term. Following von Karman and Sears's discussion, the derivative is evaluated as follows

$$\begin{aligned}
& \frac{d}{dt} \int_c^\infty \gamma_w(\xi) \left(\sqrt{\xi^2 - \xi c} - \xi + c/2 \right) d\xi \\
&= -\rho_\infty \frac{c}{2} \frac{d\Gamma_w}{dt} + \rho_\infty U_\infty \int_c^\infty \gamma_w(\xi) \left(\sqrt{\frac{\xi}{\xi - c}} - 1 - \frac{c/2}{\sqrt{\xi^2 - \xi c}} \right) d\xi \\
&= -\rho_\infty \frac{c}{2} \frac{d\Gamma_w}{dt} + \rho_\infty U_\infty \Gamma_1 - \rho_\infty U_\infty \int_c^\infty \gamma_w(\xi) \frac{c/2}{\sqrt{\xi^2 - \xi c}} d\xi
\end{aligned} \tag{1.16}$$

Substituting Eq. (1.16) into (1.13) identifies the cancellation of the $\rho_\infty U_\infty \Gamma_1$ terms. This is a cancellation between, as previously defined, a Joukowski lift term and an apparent mass lift term. In fact, this cancellation eliminates all of the Joukowski lift terms due to γ_l . Considering now both Eqs. (1.9) and (1.10), the next cancellation occurs because of the Kelvin condition of Eq. (1.4), which implies

$$\frac{\partial \Gamma_0}{\partial t} + \frac{\partial \Gamma_1}{\partial t} + \frac{\partial \Gamma_w}{\partial t} = 0 \tag{1.17}$$

This cancellation is between apparent mass lift terms only, but is a combination of terms due to γ_0 and γ_l . Recognizing these two cancellations, the total lift from Eqs. (1.12), (1.13) and (1.16) can be written as

$$L = \rho U(t) \Gamma_0 - \frac{\partial}{\partial t} \rho \int_0^c (x - c/2) \gamma_0 dx + \rho_\infty U_\infty \int_c^\infty \gamma_w(\xi) \frac{c/2}{\sqrt{\xi^2 - \xi c}} d\xi \tag{1.18}$$

This is von Karman and Sears's result. They label the first term the quasi-steady lift (L_0), the second terms the apparent mass (L_l), and the third term the wake induced component (L_2). Thus, in von Karman and Sears's notation, the separate lift terms are written as follows

$$\begin{aligned}
L_0 &= \rho U(t) \Gamma_0 \\
L_l &= -\frac{\partial}{\partial t} \rho \int_0^c (x - c/2) \gamma_0 dx \\
L_2 &= \rho_\infty U_\infty \int_c^\infty \gamma_w(\xi) \frac{c/2}{\sqrt{\xi^2 - \xi c}} d\xi
\end{aligned} \tag{1.19}$$

The significance of the derivation presented here is that it shows the mechanism of lift that produces each term of Eq. (1.19). L_0 is the complete Joukowski lift term due to γ_0 , which can be determined from steady airfoil theory. L_l is only a fragment of the apparent mass term due to γ_0 because the cancelled $\rho \frac{c}{2} \frac{\partial \Gamma_0}{\partial t}$ term is not present. But, if $\frac{\partial \Gamma_0}{\partial t} = 0$, then L_l is the entire apparent mass term due to γ_0 . von Karman and Sears make this observation by noting that L_l is

the total apparent mass lift component of an airfoil without circulation. From the current discussion, a more precise statement would be that L_l is the total apparent mass component of lift for an airfoil with a constant circulation (which still allows for a non-constant vorticity distribution). The equivalence of this statement with von Karman and Sears's statement may be obvious since a constant circulatory vorticity distribution can always be superimposed on an unsteady airfoil without changing the lift due to the unsteady motion. A surprising result of Eq. (1.19) is that L_2 , which is the wake-induced component of lift, is due entirely to the apparent mass of the wake induced vorticity, and not the Joukowski lift of the wake induced vorticity.

Equations analogous to the lift terms in Eq. (1.19) can be derived for the quarter-chord pitching moment. The resulting expressions are

$$\begin{aligned}
 M_0 &= \frac{\rho U_\infty}{4} \int_0^c \gamma_0(x)(c - 4x)dx \\
 M_1 &= \frac{\rho(d/dt)}{16} \int_0^c \gamma_0(x)[8x^2 - 4xc - c^2]dx \\
 M_2 &= 0
 \end{aligned} \tag{1.20}$$

This shows that the wake induces no quarter-chord pitching moment on the airfoil.

1.4 The Unsteady Pressure Distribution

Eqs. (1.19) and (1.20) present the total airfoil lift values. von Karman and Sears do not discuss the problem of determining the unsteady lift distribution. Neumark [1952] presents equations for the unsteady load distribution that corresponds to the three lift and moment terms of Eq. (1.19) and (1.20). The resulting equations are

$$\begin{aligned}
 \Delta p_0 &= \rho U \gamma_0 \\
 \Delta p_1 &= \rho(d/dt) \int_0^x \gamma_{0n}(x)dx \\
 \Delta p_2 &= \frac{\rho U}{\pi} \sqrt{\frac{c-x}{x}} \int_c^\infty \frac{\gamma(\xi)}{\sqrt{\xi^2 - c}} d\xi
 \end{aligned} \tag{1.21}$$

Neumark shows that the connection between Δp_0 and Δp_2 and their total force equivalents given in Eq. (1.19) and (1.20), is proved by simply integrating Δp_0 and Δp_2 over x . The important contribution of Neumark is the Δp_1 term in Eq. (1.21). This term requires γ_{0n} , which is defined as the non-circulatory vorticity. Neumark uses a result obtained by Betz [1920] which states that the

vorticity on an airfoil may be separated into a circulatory (γ_c) and non-circulatory (γ_n) component. The term non-circulatory means that integrating the vorticity over the chord results in a value of zero.

Chapter 2

An Unsteady Thin Airfoil Method for Deforming Airfoils

2.1 Introduction

This chapter will present a formulation of unsteady thin airfoil theory that is convenient for the analysis of deforming airfoils. This method provides a systematic approach to the calculation of both the unsteady aerodynamic forces and the load distribution. For the quasi-steady force coefficient and load distribution calculation, this method combines Glauret's [1947] and Allen's [1943] approaches. von Karman and Sears's [1938] approach to the unsteady force coefficient calculation is adopted along with Neumark's [1952] method for the unsteady load distribution. The wake-effect terms are calculated using either the Wagner or Theodorsen function. The breakup of "steady" and "damping" terms are discussed and shown to allow for a physical interpretation of the apparent mass terms.

2.2 Determining L_0 , L_1 , M_1 , and M_0

Applying the following transformation

$$x = \frac{c}{2}(1 - \cos \theta) \quad (2.1)$$

to Eqs. (1.19) and (1.20) results in the following

$$L_0 = \rho U \Gamma_0$$

$$L_1 = \frac{\rho c^2}{4} \frac{\partial}{\partial t} \left(\int_0^\pi \gamma_0(\theta) \cos \theta \sin \theta d\theta \right) \quad (2.2)$$

$$L_2 = \frac{\rho U c}{2} \int_c^\infty \frac{\gamma(\xi)}{\sqrt{\xi^2 - c^2}} d\xi$$

$$M_0 = \frac{\rho U c^2}{4} \int_0^\pi \gamma_0(\theta) (\cos \theta - 1/2) \sin \theta d\theta$$

$$M_1 = \frac{\rho c^3}{16} \frac{\partial}{\partial t} \left(\int_0^\pi \gamma_0(\theta) [\cos^2 \theta - 1/2 - \cos \theta] \sin \theta d\theta \right) \quad (2.3)$$

$$M_2 = 0$$

It is convenient to represent γ_0 using Glauert's Fourier series, which is written as

$$\gamma_0(\theta, t) = 2U \left(A_0(t) \left[\frac{1 + \cos \theta}{\sin \theta} \right] + \sum_{n=1}^{\infty} A_n(t) \sin n\theta \right) \quad (2.4)$$

where the Fourier coefficients are defined as

$$A_0 = -\frac{1}{\pi} \int_0^\pi w(\theta, t) d\theta \quad (2.5)$$

$$A_n = \frac{2}{\pi} \int_0^\pi w(\theta, t) \cos(n\theta) d\theta$$

In these equations, w is the instantaneous boundary condition for no flow through the camberline, which is written as

$$w = \frac{1}{U} \frac{\partial z_c}{\partial t} + \frac{\partial z_c}{\partial x} \quad (2.5b)$$

where z defines the camberline and the x -axis is specified to be parallel to the free-stream velocity.

A benefit of representing γ_0 by the Fourier series is that it allows for the simple evaluation of L_l and M_l as well as the conventional representations of L_0 and M_0 . For L_l , substituting Eq. (2.4) into Eq. (2.2) leads to the following

$$L_1 = \frac{\rho c^2 U}{2} \frac{\partial}{\partial t} \int_0^\pi \left(A_0 \left[\frac{1 + \cos \theta}{\sin \theta} \right] + \sum_{n=1}^{\infty} A_n \sin n\theta \right) \cos \theta \sin \theta d\theta \quad (2.6)$$

Recall that

$$\int_0^{\pi} \left[\frac{1 + \cos \theta}{\sin \theta} \right] \cos \theta \sin \theta d\theta = \frac{\pi}{2} \quad (2.7)$$

and

$$\begin{aligned} & \int_0^{\pi} \sin n\theta \cos \theta \sin \theta d\theta \\ &= \int_0^{\pi} \sin n\theta \frac{1}{2} \sin 2\theta d\theta \\ &= \begin{cases} 0, & n \neq 2 \\ (1/4)\pi, & n = 2 \end{cases} \end{aligned} \quad (2.8)$$

Substituting Eq. (2.7) and (2.8) into (2.6) results in

$$L_1 = \frac{\rho c^2 U}{8} \pi (2\dot{A}_0 + \dot{A}_2) \quad (2.9)$$

where the dot represents differentiation with respect to t . For M_l , substituting Eq. (2.4) into Eq. (2.3) leads to the following

$$M_1 = \frac{\rho c^3 U}{8} \frac{\partial}{\partial t} \int_0^{\pi} \left(A_0 \left[\frac{1 + \cos \theta}{\sin \theta} \right] + \sum_{n=1}^{\infty} A_n \sin n\theta \right) (\cos^2 \theta - 1/2 - \cos \theta) \sin \theta d\theta \quad (2.10)$$

where the integrals are evaluated as follows

$$\int_0^{\pi} \left[\frac{1 + \cos \theta}{\sin \theta} \right] (\cos^2 \theta - 1/2 - \cos \theta) \sin \theta d\theta = -\frac{\pi}{2} \quad (2.11)$$

$$\begin{aligned} & \int_0^{\pi} \sin n\theta (\cos^2 \theta - 1/2 - \cos \theta) \sin \theta d\theta \\ &= \begin{cases} -\pi/8, & n = 1 \\ -\pi/4, & n = 2 \\ \pi/8, & n = 3 \\ 0, & n \geq 4 \end{cases} \end{aligned} \quad (2.12)$$

Thus, M_l can be written as

$$M_1 = -\frac{\rho c^3 U \pi}{64} (4\dot{A}_0 + \dot{A}_1 + 2\dot{A}_2 - \dot{A}_3) \quad (2.13)$$

Also, recall from steady theory that L_0 and M_0 may be represented as

$$L_0 = \rho U^2 c \pi (A_0 + A_1/2) \quad (2.14)$$

$$M_0 = \frac{\rho U^2 c^2 \pi}{8} (A_2 - A_1) \quad (2.15)$$

Eqs. (2.9), (2.13), (2.14) and (2.15) provide the relationships between the Fourier coefficients defined in Eq. (2.5) and the apparent mass and quasi-steady lift force and pitching moment. Note that M_l requires A_3 to be calculated, which is the only new term required in addition to those needed for the steady thin airfoil theory.

2.3 Determining Δp_0 and Δp_l

In Section 1.3, the equations for the three unsteady pressure distribution terms were presented. This section will discuss the practical calculation of two of these terms, Δp_0 and Δp_l . The majority of this section will be on the calculation of Δp_l . From Eq. (2.4), Δp_0 is written as

$$\Delta p_0 = \rho U \gamma_0(\theta) = 2\rho U^2 \left(A_0 \left[\frac{1 + \cos \theta}{\sin \theta} \right] + \sum_{n=1}^{\infty} A_n \sin n\theta \right) \quad (2.16)$$

Applying the transformation of Eq. (2.1) to Eq. (1.21) results in the following equation for Δp_l

$$\Delta p_l = \rho \frac{c}{2} (d/dt) \int_0^{\theta} \gamma_{0n}(\theta) \sin \theta d\theta \quad (2.17)$$

Eq. (2.16) requires that the circulatory (γ_{0c}) and noncirculatory (γ_{0nc}) quasi-steady vorticity distributions be defined. Recall that the term non-circulatory means that integrating the vorticity over the chord results in a value of zero. From Neumark [1952], γ_{0c} and γ_{0nc} can be written as

$$\begin{aligned} \gamma_{0c}(\theta) &= \frac{2\Gamma_0}{\pi c \sin \theta} \\ \gamma_{0n}(\theta) &= \frac{2U}{\pi \sin \theta} \int_0^{\pi} \frac{w(\theta_0, t) \sin^2 \theta_0}{\cos \theta_0 - \cos \theta} d\theta_0 \end{aligned} \quad (2.17b)$$

where w represents the unsteady boundary condition on the airfoil, and Γ_0 is defined as

$$\Gamma_0 = 2Ub \int_0^{\pi} w(\theta, t) \sqrt{\frac{1 - \cos \theta}{1 + \cos \theta}} \sin \theta d\theta \quad (2.18)$$

Instead of using Eqs. (2.17b) and (2.18) for the calculation of γ_0 , it is convenient to continue our use of Glauert's Fourier series defined in Eq. (2.4). To do this, we must separate Eq. (2.4) into circulatory and noncirculatory components using Eq. (2.17b) as a guide. The quasi-steady circulation strength (Γ_0) in Eq. (2.18) is obtained by integrating Eq. (2.4) across the chord, resulting in

$$\Gamma_0 = \pi c U \left(A_0 + \frac{A_1}{2} \right) \quad (2.19)$$

Substituting this representation of Γ_0 into the γ_{0c} expression in Eq. (2.17) results in the following

$$\boxed{\gamma_{0c}(\theta) = \frac{U(2A_0 + A_1)}{\sin \theta}} \quad (2.20)$$

This equation is interesting because it shows that the entire $2U_\infty A_1 \sin \theta$ component of γ_0 is not present in γ_{0c} , as one may expect from the symmetry of $\sin \theta$ from zero to π . Instead, the $2U_\infty A_1 \sin \theta$ component of γ_0 is separated into a circulatory and noncirculatory component by recognizing the following identity

$$\sin \theta = \frac{1}{2} \left[\frac{1}{\sin \theta} - \frac{\cos 2\theta}{\sin \theta} \right] \quad (2.21)$$

where the first term is the circulatory contribution present in Eq. (2.20) and the second term is the noncirculatory contribution of A_1 . The portion of Eq. (2.4) not present in Eq. (2.20) is the noncirculatory component of the vorticity distribution (γ_{0n}). With the help of Eq. (2.21), this is written as

$$\gamma_{0n}(\theta) = 2UA_0 \frac{\cos \theta}{\sin \theta} - UA_1 \frac{\cos 2\theta}{\sin \theta} + 2U \sum_{n=2}^{\infty} A_n \sin n\theta \quad (2.22)$$

To avoid the infinite series in Eq. (2.22), the following relationship is applied (Allen [1943])

$$\sum_{n=1}^{\infty} A_n \sin n\theta = \frac{1}{\pi} \int_0^\pi \frac{w(\theta_0, t) \sin \theta}{\cos \theta_0 - \cos \theta} d\theta_0 \quad (2.23)$$

which can also be written as

$$\sum_{n=2}^{\infty} A_n \sin n\theta = \frac{1}{\pi} \int_0^\pi \frac{w(\theta_0, t) \sin \theta}{\cos \theta_0 - \cos \theta} d\theta_0 - A_1 \sin \theta \quad (2.24)$$

Substituting this into Eq. (2.22) results in the following

$$\gamma_{0n}(\theta) = 2UA_0 \frac{\cos \theta}{\sin \theta} - UA_1 \left[\frac{\cos 2\theta}{\sin \theta} + 2 \sin \theta \right] + \frac{2U}{\pi} \int_0^\pi \frac{w(\theta_0, t) \sin \theta}{\cos \theta_0 - \cos \theta} d\theta_0 \quad (2.25)$$

which simplifies to

$$\boxed{\gamma_{0n}(\theta) = 2UA_0 \frac{\cos \theta}{\sin \theta} - UA_1 \frac{1}{\sin \theta} + \frac{2U}{\pi} \int_0^\pi \frac{w(\theta_0, t) \sin \theta}{\cos \theta_0 - \cos \theta} d\theta_0} \quad (2.26)$$

Eqs. (2.20) and (2.26) are exactly equivalent to Eq. (2.17), but are in terms of the Fourier coefficients and a somewhat simpler integral to evaluate. Substituting Eq. (2.26) into Δp_l in Eq. (2.16) and performing the integration results in

$$\boxed{\Delta p_l = \rho_\infty \frac{c}{2} (d/dt) \left[2UA_0 \sin \theta - UA_1 \theta + \int_0^\theta \gamma_b(\theta) \sin \theta d\theta \right]} \quad (2.27)$$

where the basic load distribution (γ_b) is written as

$$\gamma_b(\theta) = \frac{2U}{\pi} \int_0^\pi \frac{w(\theta_0, t) \sin \theta}{\cos \theta_0 - \cos \theta} d\theta_0 \quad (2.28)$$

Eqs. (2.27) and (2.28) provide a convenient method for calculating the apparent mass load distribution. This representation allows the relationship to be seen between the time-rate-of-change of quasi-steady load distribution parameters and the apparent mass load distribution. Note that Garrick [1957]^{*} presented an equation for the load distribution on an oscillating airfoil following Theodorsen's [1935] approach. This prompted Scanlan [1952] to criticize that Neumark's equations for the load distribution, based on the von Karman and Sears approach, were unnecessary. On the contrary, the present author believes that Neumark's equations, or more specifically the formulation presented in this report based on Neumark's equations, are superior in many ways to Garrick's equations[†]. The reason for this is that the current approach writes the apparent mass load distribution explicitly in terms of the components of the quasi-steady load distribution (Eq. (2.27)). There are two benefits of this. The first is that the physical nature of the apparent mass terms is made clear. This is because, as shown in Chapter 1 for the lift force, the apparent mass terms are dependent only on the time-rate-of-change of the quasi-steady terms. The second benefit is that the current approach requires simpler and fewer integral evaluations because the Fourier coefficients (as well as γ_b) required for the quasi-steady terms are reused for the apparent mass terms. The only difficult integral to evaluate is the integral in Eq. (2.27), but this has been found easier to evaluate than Garrick's equivalent equation. Furthermore, Section 2.7 will discuss cases for which this integral does not have to be evaluated at all.

With the circulatory and noncirculatory vorticity distributions known in terms of the Fourier coefficients (Eqs. (2.20 and 2.26)), equations for the circulatory and noncirculatory quasi-steady pitching moment may be written as

$$M_{0,c} = \frac{\rho U^2 c^2 \pi}{8} (2A_0 + A_2) \quad (2.29)$$

$$M_{0,n} = -\frac{\rho U^2 c^2 \pi}{8} (2A_0 + A_1) \quad (2.30)$$

^{*} Fung [1969], pp. 408, presents the same equation, but credits it to Kussner and Schwarz [1940]

[†] Garrick's equation is recovered if the order of integration is reversed in Eq. (2.27) and the integration over θ is evaluated (see Eqs. (2.94) and (2.95)).

These equations will be useful for comparing results with those obtained by Theodorsen, whose method requires the separation of the lift and pitching moment into circulatory and noncirculatory components (note that, by definition, $L_{0,n}$ is zero). In terms of Theodorsen's notation, though, the apparent mass components are included in the noncirculatory terms.

2.4 Determining L_2 and Δp_2

There are two different approaches available for determining the wake effect terms L_2 and Δp_2 (recall that from Eq. (2.3), $M_2 = 0$ around the quarter chord). The first of these, based on the concept of superimposing step functions, uses Wagner's solution (Wagner's function) for an impulsively started airfoil (Wagner [1925]), or more specifically a step change in the quasi-steady circulation (Γ_0), to construct solutions for arbitrary time dependent changes in Γ_0 . The second approach, intended for oscillatory motion, is based on Theodorsen's solution for a harmonically oscillating airfoil. In both of these cases, the wake effect terms (L_2 and Δp_2) are functions of only the time-rate-of-change of Γ_0 . From Eq. (1.19) it is seen that L_0 is proportional to Γ_0 . Thus, the wake effect terms can be thought of as functions of L_0 . Note that, as mentioned in Chapter 1, the wake is assumed to be planar. The effect of a nonplanar wake is discussed, for example, by Chopra [1976] and Homentcovschi [1985].

a) Applying the Wagner Function to Transient Variations in L_0

For transient variations in L_0 , the wake-effect terms (L_2 and Δp_2) are determined using the Wagner function[‡] ($\phi(t)$). The Wagner function, which represents the wake integral in Eqs. (1.19 and 1.21), allows L_2 to be written for a step input in L_0 as: $\phi(t)\Delta L_0$. Although there is no exact analytic representation of the Wagner function, accurate approximations have been suggested (Garrick [1938], von Karman and Sears [1938], and Jones [1940]). It will be most convenient to use the approximation suggested by Jones, which is written as

$$\phi(\tau) = -0.165e^{-0.091\tau} - 0.335e^{-0.6\tau} \quad (2.31)$$

where $\tau = \frac{U_\infty t}{c}$, which is the number of chord lengths traveled between $t = 0$ and $t = t$. Note that this approximation does not approach the asymptotic value of ϕ (equal to zero) at the correct rate. For limiting purposes, the Wagner function is written as

[‡] Fung [1969], pp. 208, presents the exact form of ϕ , which requires the integration of Bessel functions.

$$\phi(\tau) = -\frac{1}{2\tau} + \dots \quad (2.31b)$$

for τ approaching infinity (Lomax [1960]).

For arbitrary time-dependent L_0 variations, the concept of linear superposition is exploited using the Duhamel integral (Appendix C of Bisplinghoff, *et al.*, [1955]). This can be thought of as creating an arbitrary time variation in airfoil circulation by combining the effect of many infinitesimal step changes in circulation. Using the Duhamel integral and the Wagner function, L_2 can be written as

$$L_2(\tau) = \Delta L_0(\tau_0)\phi(\tau) + \int_{\tau_0}^{\tau} \frac{dL_0}{d\sigma}(\sigma)\phi(\tau - \sigma)d\sigma \quad (2.32)$$

From Eqs. (1.20), (2.1) and (2.32), the wake-effect load distribution (Δp_2) can be written as

$$\Delta p_2(\tau) = \frac{2}{\pi} \left[\frac{1 + \cos \theta}{\sin \theta} \right] L_2(\tau) \quad (2.33)$$

Note that Δp_2 has exactly the same θ -dependence as a quasi-steady load distribution caused by angle of attack. This is similar to lifting line theory, where the effect of the wake at each spanwise location is considered an induced angle of attack. In the present case though, the induced angle of attack is time-varying.

As an example of applying the equations presented in this chapter, consider a step change in L_0 (due to a step change in angle of attack, flap deflection, etc.). The resulting *total* lift can be written as

$$L(\tau) = L_0 + \phi(\tau)L_0 + L_1(\tau) \quad (2.34)$$

where the combination of ϕ and L_0 represents L_2 . Because for a step input at $t = 0$ the time derivatives in Eq. (2.9) for L_1 are infinite at $t = 0$ and zero elsewhere, the Dirac delta function is used to represent the time-derivatives in Eq. (2.9) as follows

$$L_1 = \frac{\rho c^2 U \delta(\tau)}{8} \pi (2A_0 + A_2) \quad (2.35)$$

Recall that the Dirac delta function has the following properties

$$\begin{aligned} \delta(\tau = 0) &= \infty \\ \delta(\tau \neq 0) &= 0 \\ \int_{-\infty}^{\infty} \delta(\tau) d\tau &= 1 \end{aligned} \quad (2.36)$$

The last property in Eq. (2.36) will be important when the energy of the system is discussed in Chapter 5. Similarly to L_I , Δp_I and M_I in Eqs. (2.13 and 2.27) are obtained by exchanging the Dirac delta function for the time derivative.

As an example of applying Eq. (2.31) and (2.32), a ramp input of L_0 will be considered. For this case, L_0 is defined to change linearly from $t = 0$ to $t = t^*$. This will be written as

$$L_0 = \Delta L_0 \frac{t}{t^*} \quad (2.37)$$

where ΔL_0 is the change in L_0 achieved between t equal to zero and t^* and $L_0(t = 0) = 0$. Using this expression, Eq. (2.32) can be written as

$$L_2(\tau) = \frac{\Delta L_0}{\tau^*} \int_0^\tau \phi(\tau - \sigma) d\sigma \quad (2.38)$$

where $\tau^* = \frac{U_\infty t^*}{c}$. From Eq. (2.31), Eq. (2.38) evaluates to the following

$$L_2(\tau) = \frac{\Delta L_0}{\tau^*} \left[-2.37152 + 0.55833e^{-0.6\tau} + 1.81319e^{-0.091\tau} \right] \quad (2.39)$$

for

$$0 \leq \tau < \tau^*$$

and

$$L_2(\tau) = \frac{\Delta L_0}{\tau^*} \left[0.55833 \left(e^{-0.6\tau} - e^{0.6(\tau^* - \tau)} \right) + 1.81319 \left(e^{-0.091\tau} - e^{0.091(\tau^* - \tau)} \right) \right] \quad (2.40)$$

for

$$\tau^* < \tau \leq 10$$

Figure 2.1 illustrates Eqs. (2.39) and (2.40) and compares them with the Wagner function of Eq. (2.31).

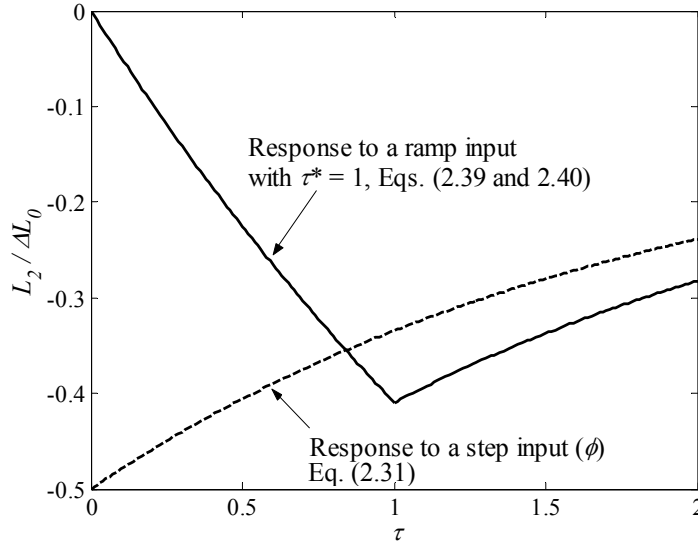


Figure 2.1: Illustrates the difference between a step input and a ramp input on L_2

Note that L_2 is *not* proportional to the wake induced circulation (Γ_1) as shown in Chapter 1. Sears [1940] showed that Γ_1 , resulting from a step input of L_0 , is given by the Kussner function (ψ). The Kussner function is the equivalent to the Wagner function for an airfoil entering a sharp-edged gust. For values of τ less than 4, Sears provides the following approximation for ψ

$$\psi = \frac{2\sqrt{\tau}}{\pi} \left(1 - \frac{\tau}{6} + \frac{\tau^2}{24} - \frac{23\tau^3}{1680} \right) \quad (2.41)$$

Analogously, Kemp [1952] shows that Γ_1 for a harmonically oscillating Γ_0 , which will be the topic of the next subsection, is given by the Sears function. The Sears function is the lift response to a infinitely long sinusoidal gust (Sears [1941]). Knowledge of Γ_1 allows the wake vorticity to be determined from Eq. (1.17).

b) Applying the Theodorsen Function to Sinusoidal Variations in L_0

For a sinusoidal variation of L_0 that has occurred for a long period of time (so that the wake extends to infinity), it is necessary to use Theodorsen's function to determine L_2 (Theodorsen [1935]). Consider the following time varying L_0

$$\begin{aligned} L_0 &= (A + iB)e^{i\omega t} \\ &= A \cos \omega t - B \sin \omega t + i(A \sin \omega t + B \cos \omega t) \end{aligned} \quad (2.42)$$

where A and B are constants and ω is the oscillation frequency. Because Eq. (2.42) represents a sinusoidal variation of L_0 , and if it is assumed that this oscillation has been occurring for a long period of time, then L_2 can be written as

$$L_2 = [C(k) - 1]L_0 \quad (2.43)$$

where $C(k)$ is Theodorsen's function and $k = \frac{\omega c}{2U}$ is the reduced frequency. Theodorsen's function is a complex number, which is defined written as

$$C(k) = F(k) + iG(k) = \frac{H_1^{(2)}(k)}{H_1^{(2)}(k) + iH_0^{(2)}(k)} \quad (2.44)$$

where H terms are Hankel functions. Figure 2.2 shows the variation of these components with k . Note that when $k = 0$, indicating steady motion, $F = 1$ and $G = 0$. For $k \ll 1$, F and G can be expanded as (Wu [1961])

$$\begin{aligned} F &= 1 - \frac{\pi}{2}k + O(k^2 \ln k) \\ G &= k \left(\gamma + \ln \frac{k}{2} \right) + O(k^2 \ln k) \end{aligned} \quad (2.45)$$

where γ is Euler's constant ($= 0.5771\dots$). For $k \gg 1$, the expansions can be written as

$$\begin{aligned} F &= \frac{1}{2} \left(1 + \frac{1}{8k^2} + O(k^{-4}) \right) \\ G &= -\frac{1}{8k} \left(1 - \frac{11}{128k^2} + O(k^{-4}) \right) \end{aligned} \quad (2.46)$$

These representations of F and G will be used in Section 2.6 to show the importance of the unsteady aerodynamic terms in aircraft stability calculations. Substituting Eqs. (2.42) and (2.44) into (2.43) allows the following general equation to be written for L_2

$$L_2 = F(k)(A \cos \omega t - B \sin \omega t) - G(k)(A \sin \omega t + B \cos \omega t) + IM - L_0 \quad (2.47)$$

where IM represent the imaginary terms, which are not of interest. Note that only in Eq. (2.47), the last step, can the imaginary terms be ignored. This is because imaginary terms in L_0 and $C(k)$ combine to form real terms. Recall also, that the final equation for L consists of the real part of L_0 and L_1 as well as the real part of L_2 . Determining Δp_2 using the Theodorsen function is exactly analogous to that for using the Wagner function in Eq. (2.34). Thus, it can be written as

$$\Delta p_2(\omega t) = \frac{2}{\pi c} \left[\frac{1 + \cos \theta}{\sin \theta} \right] L_2(\omega t) \quad (2.48)$$

where Δp_2 is, like for the transient case, seen to have the same form as a quasi-steady angle of attack increment.

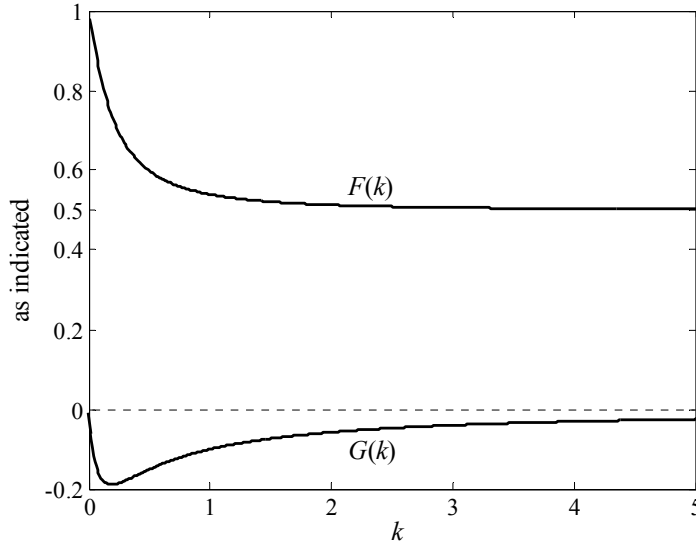


Figure 2.2: The variation with k of the components of the Theodorsen function (Eq. (2.44))

In the previous definition of k , it was assumed that k was a real number, indicating that L_0 in Eq. (2.42) was oscillating with a constant magnitude. For a damped oscillation of L_0 , the exponent in Eq. (2.42) can be written as

$$p = \mu + i\omega \quad (2.49)$$

where μ and ω are real numbers. This allows Eq. (2.42) to be rewritten as

$$\begin{aligned} L_0 &= (A + iB)e^{pt} \\ &= [A \cos \omega t - B \sin \omega t + i(A \sin \omega t + B \cos \omega t)]e^{\mu t} \end{aligned} \quad (2.50)$$

If k is redefined as $k = \frac{pc}{2U}$, can Eqs. (2.43) and (2.44) still be used to determine L_2 ? This was the topic of much discussion in the Reader's Forum of the March 1952 issue of the *Journal of the Aeronautical Sciences* (Van de Vooren [1952], Laitone [1952], Jones [1952], Dengler, *et al.* [1952]). For cases where $\mu > 0$, indicating an unstable oscillation, it was found that the conventional Theodorsen function can be used with the newly defined k . On the other hand, for a stable oscillation ($\mu < 0$), it was shown that the conventional Theodorsen function cannot be used. Instead, the Wagner function and Duhamel integral (Eq. (2.32)) must be applied, which is referred to as the "Generalized Theodorsen Function." This was not considered by Luke, *et al.* [1951], whose values of $C(k)$ for $\mu < 0$ are therefore of no value.

2.5 The Separation of Quasi-Steady Terms into “Aerodynamic Damping” and “Steady” Terms

The first step in applying the unsteady thin airfoil method described in Sections 2.1 – 2.4 is to obtain the quasi-steady terms, L_0 and Δp_0 . From Eqs. (2.5b), it is seen that these depend on both the instantaneous slope of the camberline as well as the instantaneous time-rate-of-change of the camberline. For steady motion, of course, w in Eq. (2.5b) consists of only the terms due to the slope of the camberline relative to the free-stream velocity, as shown in Figure 2.3. For unsteady motion, though, there is the additional term due to the rate of change of the camberline shape, as shown in Figure 2.4. An example of this additional term can be imagined as the aerodynamic force acting on a plate at zero free-stream velocity while in a heaving motion. This force will always damp the unsteady motion, and will therefore be labeled the aerodynamic damping.

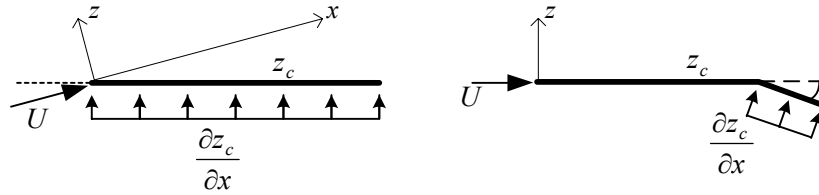


Figure 2.3: The steady terms of w (w_s) for a pitching airfoil and a deflecting flap



Figure 2.4: The damping terms of w (w_d) for a pitching airfoil and a deflecting flap

To distinguish between the aerodynamic forces resulting from these two components, w will be written as

$$w = w_s + w_d \quad (2.51)$$

where w_s is the “steady” component (Figure 2.3) and w_d is the “damping” component (Figure 2.4). Defining a nondimensional time τ as

$$\tau = \frac{Ut}{c} \quad (2.52)$$

the two terms in Eq. (2.51) can be written as

$$w_s = \frac{\partial z}{\partial x} \quad (2.53)$$

$$w_d = \frac{1}{c} \frac{\partial z}{\partial \tau} \quad (2.54)$$

For many practical applications (as shown in Chapter 3) the function z has the following form

$$z(x, \tau) = \psi(x)\beta(\tau) \quad (2.55)$$

where ψ defines the shape of camberline (for example a flapped or a parabolic camberline) and β defines the time varying magnitude of the camberline (for example the flap deflection angle or magnitude of maximum camber). Note that Eq. (2.55) cannot represent shapes such as a time varying flap-to-chord-ratio because these would require that ψ be a function of time. Using Eq. (2.55), Eqs. (2.53) and (2.54) can be rewritten as

$$w_s = \frac{\partial \psi}{\partial x} \beta \quad (2.56)$$

$$w_d = \frac{\psi}{c} \frac{\partial \beta}{\partial \tau} \quad (2.57)$$

which shows that w_s is proportional to β and w_d is proportional to $d\beta/d\tau$. Recognizing this allows the L_0 to be written as

$$\frac{L_0}{qc} \equiv C_{L,0} = K_{0,s}\beta + K_{0,d}\beta' \quad (2.58)$$

where $\beta' = \frac{\partial \beta}{\partial \tau}$. The lift due to w_s is represented by $K_{0,s}$ and that due to w_d is represented by $K_{0,d}$.

From Eq. (2.14), these K terms can be written as

$$\begin{aligned} K_{0,s} &\equiv \frac{1}{qc} \frac{dL_0}{d\beta} = \pi(2\bar{A}_{0,s} + \bar{A}_{1,s}) \\ K_{0,d} &\equiv \frac{1}{qc} \frac{dL_0}{d\beta'} = \pi(2\bar{A}_{0,d} + \bar{A}_{1,d}) \end{aligned} \quad (2.59)$$

where the steady and damping Fourier coefficients (the bar indicates that they are per-unit β or β') are defined from Eqs. (2.5), (2.56) and (2.57) as

$$\bar{A}_{0,s} = -\frac{1}{\pi} \int_0^\pi \frac{\partial \psi}{\partial x} d\theta \quad (2.59b)$$

$$\bar{A}_{n,s} = \frac{2}{\pi} \int_0^\pi \frac{\partial \psi}{\partial x} \cos(n\theta) d\theta$$

$$\bar{A}_{0,d} = -\frac{1}{\pi} \int_0^\pi \frac{\psi}{c} d\theta \quad (2.59c)$$

$$\bar{A}_{n,d} = \frac{2}{\pi} \int_0^\pi \frac{\psi}{c} \cos(n\theta) d\theta$$

Similarly, M_0 can be written as

$$\frac{M_0}{qc^2} \equiv C_{M,0} = J_{0,s}\beta + J_{0,d}\beta' \quad (2.60)$$

where from Eq. (2.15)

$$\begin{aligned} J_{0,s} &\equiv \frac{1}{qc^2} \frac{dM_0}{d\beta} = \frac{\pi}{4} (\bar{A}_{2,s} - \bar{A}_{1,s}) \\ J_{0,d} &\equiv \frac{1}{qc^2} \frac{dM_0}{d\beta'} = \frac{\pi}{4} (\bar{A}_{2,d} - \bar{A}_{1,d}) \end{aligned} \quad (2.61)$$

From Eqs. (2.16) and (2.23), the quasi-steady load distribution can also be separated into steady and damping components as follows

$$\begin{aligned} \frac{\Delta p_0(\theta)}{q} &\equiv \Delta C_{p,0} = \frac{1}{q} \frac{d\Delta p_0}{d\beta} \beta + \frac{1}{q} \frac{d\Delta p_0}{d\beta'} \beta' \\ &= [\bar{A}_{0,s} \chi(\theta) + T_{0,s}(\theta)] \beta + [\bar{A}_{0,d} \chi(\theta) + T_{0,d}(\theta)] \beta' \end{aligned} \quad (2.62)$$

$$T_{0,s}(\theta) = \frac{4}{\pi} \int_0^\pi \frac{\frac{\partial \psi}{\partial x}(\theta_0, t) \sin \theta}{\cos \theta_0 - \cos \theta} d\theta_0 \quad (2.62b)$$

$$T_{0,d}(\theta) = \frac{4}{\pi c} \int_0^\pi \frac{\psi(\theta_0, t) \sin \theta}{\cos \theta_0 - \cos \theta} d\theta_0$$

$$\chi(\theta) = 4 \left[\frac{1 + \cos \theta}{\sin \theta} \right]$$

where $T_{0,s}$ and $T_{0,d}$ are due to the steady and damping basic load distributions, respectively.

It is also convenient to separate the apparent mass terms (L_l , M_l and Δp_l) into damping and steady components. This is achieved by recognizing that time-rate-of-change of the quasi-steady damping and steady component each produce an apparent mass term. Thus, L_l can be written as

$$\frac{L_l}{qc} \equiv C_{L,l} = K_{1,s}\beta' + K_{1,d}\beta'' \quad (2.63)$$

where from Eq. (2.9)

$$\begin{aligned} K_{1,s} &\equiv \frac{1}{qc} \frac{dL_l}{d\beta'} = \frac{\pi}{4} (2\bar{A}_{0,s} + \bar{A}_{2,s}) \\ K_{1,d} &\equiv \frac{1}{qc} \frac{dL_l}{d\beta''} = \frac{\pi}{4} (2\bar{A}_{0,d} + \bar{A}_{2,d}) \end{aligned} \quad (2.64)$$

$K_{l,s}$ can be physically interpreted as the apparent mass lift due to the time-rate-of-change of $\gamma_{0,s}$. Similarly, $K_{l,d}$ can be physically interpreted as the apparent mass lift due to the time-rate-of-change of $\gamma_{0,d}$. Because $\gamma_{0,d}$ depends on β' , $L_{l,d}$ is a function of β'' . Like L_l , M_l can be written as

$$\frac{M_l}{qc^2} \equiv C_{M,1} = J_{1,s}\beta' + J_{1,d}\beta'' \quad (2.65)$$

where from Eq. (2.13)

$$\begin{aligned} J_{1,s} &\equiv \frac{1}{qc^2} \frac{dM_l}{d\beta'} = -\frac{\pi}{32} (4\bar{A}_{0,s} + \bar{A}_{1,s} + 2\bar{A}_{2,s} - \bar{A}_{3,s}) \\ J_{1,d} &\equiv \frac{1}{qc^2} \frac{dM_l}{d\beta''} = -\frac{\pi}{32} (4\bar{A}_{0,d} + \bar{A}_{1,d} + 2\bar{A}_{2,d} - \bar{A}_{3,d}) \end{aligned} \quad (2.66)$$

Likewise, Δp_l can be written as

$$\begin{aligned} \frac{\Delta p_l(\theta)}{q} &= \Delta C_{p,1} = \frac{d\Delta p_l}{d\beta'} \beta' + \frac{d\Delta p_l}{d\beta''} \beta'' \\ &= T_{1,s}(\theta)\beta' + T_{1,d}(\theta)\beta'' \end{aligned} \quad (2.67)$$

where from Eq. (2.27)

$$\begin{aligned} T_{1,s} &\equiv \frac{1}{q} \frac{d\Delta p_l}{d\beta'} = 2\bar{A}_{0,s} \sin \theta - \bar{A}_{1,s} \theta + \frac{1}{2} \int_0^\theta T_{0,s}(\theta) \sin \theta d\theta \\ T_{1,d} &\equiv \frac{1}{q} \frac{d\Delta p_l}{d\beta''} = 2\bar{A}_{0,d} \sin \theta - \bar{A}_{1,d} \theta + \frac{1}{2} \int_0^\theta T_{0,d}(\theta) \sin \theta d\theta \end{aligned} \quad (2.67b)$$

The first term in Eq. (2.67) is the steady apparent mass term ($\Delta p_{l,s}$), which is due to the time-rate-of-change of $\gamma_{0,s}$, and the second term is the damping term ($\Delta p_{l,d}$), which is due to the time-rate-of-change of $\gamma_{0,d}$.

Collecting the terms defined in this section for the quasi-steady and apparent contributions to the lift, quarter-chord pitching moment, and load distribution, the following equations can be written

$$\boxed{C_L = K_{0,s}\beta + (K_{0,d} + K_{1,s})\beta' + K_{1,d}\beta'' + C_{L,2}} \quad (2.68)$$

$$\boxed{C_M = J_{0,s}\beta + (J_{0,d} + J_{1,s})\beta' + J_{1,d}\beta''} \quad (2.69)$$

$$\boxed{\Delta C_p = [\bar{A}_{0,s}\chi(\theta) + T_{0,s}(\theta)]\beta + [\bar{A}_{0,d}\chi(\theta) + T_{0,d}(\theta) + T_{1,s}(\theta)]\beta' + T_{1,d}(\theta)\beta'' + \Delta C_{p,2}} \quad (2.70)$$

where the wake-effect components ($C_{L,2}$ and $\Delta C_{p,2}$) depend on the time variation of β . For transient variations of β , $C_{L,2}$ can be written from Eqs. (2.32) and (2.59) as follows

$$C_{L,2}(\tau) = (K_{0,s} \Delta\beta(\tau_0) + K_{0,d} \Delta\beta'(\tau_0))\phi(s) + \int_{\tau_0}^{\tau} (K_{0,s} \beta'(\sigma) + K_{0,d} \beta''(\sigma))\phi(\tau - \sigma) d\sigma \quad (2.71)$$

For sinusoidal variations of β , $C_{L,2}$ can be written from Eqs. (2.43) and (2.59) as follows

$$C_{L,2} = [C(k) - 1](K_{0,s} \beta + K_{0,d} \beta') \quad (2.72)$$

For both of these cases $\Delta C_{p,2}$ can be written as

$$\Delta C_{p,2}(\tau) = \frac{\chi(\theta)}{2\pi} C_{L,2}(\tau) \quad (2.73)$$

where χ was defined in Eq. (2.62b). Applying Eq. (2.72) for a sinusoidal β will be the topic of the next section.

Two simple but important camberline motions, pitch and heave, provide a good example of determining the parameters defined in this section. For an airfoil pitching around an axis x_a (measured from the leading edge), the shape function ψ from Eq. (2.55) is

$$\begin{aligned} \psi &= x_a - x \\ &= x_a - (c/2)(1 - \cos \theta) \end{aligned} \quad (2.74)$$

For a heaving airfoil, ψ is written simply as

$$\psi = 1 \quad (2.75)$$

Tables 2.1 and 2.2 present the parameters defined in this section for the pitch and heave cases, which were obtained by applying Eqs. (2.56) and (2.57) to Eqs. (2.58-2.67). The complete lift, pitching moment, and load distribution equations (Eqs. (2.68-2.70)) resulting from these values can be shown to agree with the well known result (pp. 262-272 of Bisplinghoff, *et al.*, [1955]).

Table 2.1: Lift and pitching moment parameters for a pitching and heaving airfoil

	Pitch (about x_a)	Heave
$K_{0,s}$	2π	0
$K_{0,d}$	$2\pi(3/4 - x_a)$	-2π
$K_{1,s}$	$\pi/2$	0
$K_{1,d}$	$(\pi/2)(1/2 - x_a)$	$-\pi/2$
$J_{0,s}$	0	0
$J_{0,d}$	$-\pi/8$	0
$J_{1,s}$	$-\pi/8$	0
$J_{1,d}$	$-(\pi/2)(5/8 - x_a)$	$\pi/8$

Table 2.2: Load distribution parameters for a pitching and heaving airfoil

	Pitch (about x_a)	Heave
$A_{0,s}$	1	0
$A_{0,d}$	$1/2 - x_a$	-1
$T_{0,s}$	0	0
$T_{0,d}$	$2 \sin \theta$	0
$T_{1,d}$	$(1/2)(2 - 4x_a - \cos \theta) \sin \theta$	$-2 \sin \theta$

2.6 The Unsteady Aerodynamics for a Sinusoidal β

Section 2.4 briefly discussed the application of Theodorsen's function to a sinusoidal oscillation of L_0 . This section will generalize this result by applying the separation of “steady” and “damping” terms defined in Section 2.5 to a sinusoidal oscillation of β . Expressions will be obtained for the entire lift, pitching moment, and load distribution.

Consider a time-varying β defined as follows

$$\begin{aligned}\beta &= \bar{\beta} e^{i\bar{k}\tau} \\ &= \bar{\beta} [\cos(\bar{k}\tau) + i \sin(\bar{k}\tau)]\end{aligned}\quad (2.76)$$

where $\bar{\beta}$ is the magnitude of the oscillation and

$$\bar{k} = \frac{\omega c}{U_\infty} \quad (2.77)$$

$$\tau = \frac{U_\infty t}{c} \quad (2.78)$$

Note that \bar{k} is defined differently than the classically defined k , where $\bar{k} = 2k$. From Eqs. (2.68) and (2.72), the total unsteady lift coefficient can be written as

$$C_L(\tau) = K_{0,s}\beta + (K_{0,d} + K_{1,s})\beta' + K_{1,d}\beta'' + [C(k) - 1](K_{0,s}\beta + K_{0,d}\beta') \quad (2.79)$$

where $C(k)$ is Theodorsen's function defined in Eq. (2.44). Substituting Eq. (2.76) into (2.79) and keeping only the real part results in

$$\begin{aligned}C_L(\tau, \bar{k}) &= -[K_{1,d}\bar{k}^2 - K_{0,s}F + K_{0,d}\bar{k}G]\bar{\beta} \cos(\bar{k}\tau) \\ &\quad - [K_{1,s}\bar{k} + K_{0,s}G + K_{0,d}\bar{k}F]\bar{\beta} \sin(\bar{k}\tau)\end{aligned}\quad (2.80)$$

It will later be convenient to write this equation as

$$C_L(\tau, \bar{k}) = Z_1(\bar{k})\bar{\beta} \cos(\bar{k}\tau) + Z_2(\bar{k})\bar{\beta} \sin(\bar{k}\tau) \quad (2.81)$$

where Z_1 and Z_2 are defined as

$$\begin{aligned} Z_1(\bar{k}) &= -[K_{1,d}\bar{k}^2 - K_{0,s}F + K_{0,d}\bar{k}G] \\ Z_2(\bar{k}) &= -[K_{1,s}\bar{k} + K_{0,s}G + K_{0,d}\bar{k}F] \end{aligned} \quad (2.82)$$

Obtained in the same manner, the equation for the quarter-chord pitching moment (C_M) can be written as

$$C_M(\tau) = -(J_{1,d}\bar{k}^2 - J_{0,s})\bar{\beta} \cos(\bar{k}\tau) - (J_{0,d} + J_{1,s})\bar{k}\bar{\beta} \sin(\bar{k}\tau) \quad (2.83)$$

where recall that the wake-effect term is zero. As for C_L , it will be convenient to define C_M as

$$C_M(\tau, \bar{k}) = Y_1(\bar{k})\bar{\beta} \cos(\bar{k}\tau) + Y_2(\bar{k})\bar{\beta} \sin(\bar{k}\tau) \quad (2.84)$$

where Y_1 and Y_2 are defined as

$$\begin{aligned} Y_1(\bar{k}) &= -(J_{1,d}\bar{k}^2 - J_{0,s}) \\ Y_2(\bar{k}) &= -(J_{0,d} + J_{1,s})\bar{k} \end{aligned} \quad (2.85)$$

From Eqs. (2.70) and (2.73), the load distribution can be written as

$$\begin{aligned} \Delta C_p(\theta, \tau) &= (\bar{A}_{0,s}\chi(\theta) + T_{0,s}(\theta))\beta(t) + (\bar{A}_{0,d}\chi(\theta) + T_{0,d}(\theta) + T_{1,s}(\theta))\beta'(t) \\ &+ T_{1,d}(\theta)\beta''(t) + [C(k) - 1] \left[(K_{0,s}\beta + K_{0,d}\beta') \frac{\chi(\theta)}{2\pi} \right] \end{aligned} \quad (2.86)$$

Substituting Eqs. (2.44) and (2.76) into this equation and keeping only the real part results in the following expression for the unsteady load distribution

$$\begin{aligned} \Delta C_p(\theta, \tau) &= \left[\bar{A}_{0,s}\chi(\theta) + T_{0,s}(\theta) - T_{1,d}(\theta)\bar{k}^2 + \frac{\chi(\theta)}{2\pi} (K_{0,s}F - K_{0,s} - \bar{k}K_{0,d}G) \right] \bar{\beta} \cos(\bar{k}\tau) \\ &- \left[(\bar{A}_{0,d}\chi(\theta) + T_{0,d}(\theta) + T_{1,s}(\theta))\bar{k} + \frac{\chi(\theta)}{2\pi} (K_{0,s}G + \bar{k}K_{0,d}F - \bar{k}K_{0,d}) \right] \bar{\beta} \sin(\bar{k}\tau) \end{aligned} \quad (2.87)$$

Again, it will be convenient to define ΔC_p as

$$\Delta C_p(\tau, \theta, \bar{k}) = \Pi_1(\bar{k}, \theta)\bar{\beta} \cos(\bar{k}\tau) + \Pi_2(\bar{k}, \theta)\bar{\beta} \sin(\bar{k}\tau) \quad (2.88)$$

where Π_1 and Π_2 are defined as

$$\begin{aligned} \Pi_1(\bar{k}, \theta) &= \left[\bar{A}_{0,s}\chi(\theta) + T_{0,s}(\theta) - T_{1,d}(\theta)\bar{k}^2 + \frac{\chi(\theta)}{2\pi} (K_{0,s}F - K_{0,s} - \bar{k}K_{0,d}G) \right] \\ \Pi_2(\bar{k}, \theta) &= - \left[(\bar{A}_{0,d}\chi(\theta) + T_{0,d}(\theta) + T_{1,s}(\theta))\bar{k} + \frac{\chi(\theta)}{2\pi} (K_{0,s}G + \bar{k}K_{0,d}F - \bar{k}K_{0,d}) \right] \end{aligned} \quad (2.89)$$

The equations developed in this section will be applied in the later chapters.

Some interesting features regarding the aerodynamic forces for low-frequency oscillations can be seen by investigating Eqs. (2.80) and (2.88) in the limit as \bar{k} approaches zero. Substituting the limiting form of F and G (Eq. (2.45)) into Eq. (2.80) allows C_L to be written as

$$\begin{aligned}
C_L(\tau, \bar{k}) = & K_{0,s} \left(1 - \frac{\pi}{4} \bar{k} \right) \bar{\beta} \cos(\bar{k} \tau) \\
& - \left[K_{1,s} \bar{k} + K_{0,s} \frac{\bar{k}}{2} \left(\gamma + \ln \frac{\bar{k}}{4} \right) + K_{0,d} \bar{k} \right] \bar{\beta} \sin(\bar{k} \tau) + O(\bar{k}^2 \ln \bar{k})
\end{aligned} \tag{2.90}$$

For comparison, the result of steady thin airfoil theory (i.e. the quasi-steady terms) can be written from Eq. (2.90) as follows

$$C_{L,0}(\tau, \bar{k}) = K_{0,s} \bar{\beta} \cos(\bar{k} \tau) - K_{0,d} \bar{k} \bar{\beta} \sin(\bar{k} \tau) \tag{2.91}$$

Examining Eqs. (2.90) and (2.91) it is seen that $C_{L,0}$ is accurate to $O(\bar{k}^2 \ln \bar{k})$ if both $K_{0,s}$ and $K_{1,s}$ are equal to zero. Because of the logarithmic term in Eq. (2.90), if $K_{0,s}$ is *not* equal to zero, $C_{L,0}$ is only accurate to $O(\bar{k} \ln \bar{k})$, independent of $K_{1,s}$. From Table 2.1 it is seen that $K_{0,s}$ and $K_{1,s}$ are equal to zero for a heaving airfoil, but not for a pitching airfoil. Thus, for a pitching airfoil (and most camberline deformations) the quasi-steady approximation, even if the apparent mass term ($K_{1,s}$) is included, is not very accurate. A similar discussion was presented by Miles [1949], who also pointed out that the logarithmic term in Eq. (2.90) will reverse the sign of C_L from the quasi-steady value for small values of \bar{k} (< 0.2). For dynamic stability calculations, Miles [1950] mentioned that it is very important to keep all the terms in brackets in Eq. (2.90) because these forces act out-of-phase with the aircraft inertia, which dominates the high order in-phase aerodynamic forces. Goland [1950] presented an alternative method to previous methods of approximating low-frequency stability derivatives (White and Klampe [1945] and Jones and Cohen [1941]), where past methods had made the mistake of setting $G=0$ when making the low frequency approximation. This resulted in the absence of the logarithmic term, and as a result certain stability derivatives did not have the correct sign, as identified by Miles.

2.7 The Equivalence of $T_{1,s}$ and $T_{0,d}$

A useful relationship between $T_{1,s}$ (the apparent mass term due to the time-rate-of-change of $\gamma_{0,s}$) and $T_{0,d}$ (the damping basic load distribution) can be shown to exist. This relationship states that, surprisingly, the two terms are exactly equal if w_s and w_d can be represented by Eqs. (2.56) and (2.57). There are two significant consequences of this relationship. The first is that the integral in Eq. (2.67b) can be avoided for $T_{1,s}$. This integration is difficult because it requires the integration of $T_{0,s}$, which can be quite a complicated function. Furthermore, if there is no camberline acceleration, then $T_{1,d}$ does not have to be determined and therefore only the Fourier coefficient $A_{3,s}$ must be calculated beyond what is required for the quasi-steady terms. The

second important consequence of this relationship is that it proves that the pitching moment terms $J_{0,d}$ and $J_{1,s}$ are equal. This is true because $T_{0,d}$ is responsible for the entire $J_{0,d}$ term.

The proof of this relationship begins by recognizing the following identity

$$\frac{\partial \psi}{\partial x} = \frac{2}{c \sin \theta} \frac{\partial \psi}{\partial \theta} \quad (2.92)$$

From Eqs. (2.62b) and (2.67b), $T_{1,s}$ can be written as

$$T_{1,s} = 2\bar{A}_{0,s} \sin \theta - \bar{A}_{1,s} \theta + \frac{2}{\pi} \int_0^\theta \int_0^\pi \frac{\frac{\partial \psi}{\partial x}(\theta_0, t) \sin \theta}{\cos \theta_0 - \cos \theta} d\theta_0 \sin \theta d\theta \quad (2.93)$$

The integral in this equation may be evaluated by reversing the order of integration, which leads to the following

$$\begin{aligned} & \frac{4}{\pi} \int_0^\pi \frac{\partial \psi}{\partial x}(\theta_0, t) \int_0^\theta \frac{\sin \theta}{\cos \theta_0 - \cos \theta} \sin \theta d\theta d\theta_0 \\ &= \frac{4}{\pi} \int_0^\pi \frac{\partial \psi}{\partial x}(\theta_0, t) \left[\theta \cos \theta_0 + \ln \left[\frac{\sin\left(\frac{\theta_0 - \theta}{2}\right)}{\sin\left(\frac{\theta_0 + \theta}{2}\right)} \right] \sin \theta_0 + \sin \theta \right] d\theta_0 \end{aligned} \quad (2.94)$$

The first and last terms in brackets in Eq. (2.94) can be shown to cancel the first two terms in brackets in Eq. (2.93). Thus, $T_{1,s}$ can be written as

$$T_{1,s} = \frac{2}{\pi} \int_0^\pi \frac{\partial \psi}{\partial x}(\theta_0, t) \ln \left[\frac{\sin\left(\frac{\theta_0 - \theta}{2}\right)}{\sin\left(\frac{\theta_0 + \theta}{2}\right)} \right] \sin \theta_0 d\theta_0 \quad (2.95)$$

Applying Eq. (2.92), Eq. (2.95) can be written as

$$T_{1,s} = \frac{2}{\pi c} \int_0^\pi \frac{2}{\sin \theta} \frac{\partial \psi}{\partial \theta_0}(\theta_0, t) \ln \left[\frac{\sin\left(\frac{\theta_0 - \theta}{2}\right)}{\sin\left(\frac{\theta_0 + \theta}{2}\right)} \right] \sin \theta_0 d\theta_0 \quad (2.96)$$

Integrating by parts, the following expression is obtained

$$T_{1,s} = \frac{2}{\pi c} \left\{ 2\psi(\theta_0, t) \ln \left[\frac{\sin\left(\frac{\theta_0 - \theta}{2}\right)}{\sin\left(\frac{\theta_0 + \theta}{2}\right)} \right] \Big|_{\theta_0=0}^{\theta_0=\pi} + \int_0^\pi \psi(\theta_0, t) \left[\cot\left(\frac{\theta_0 + \theta}{2}\right) - \cot\left(\frac{\theta_0 - \theta}{2}\right) \right] d\theta_0 \right\} \quad (2.97)$$

For all ψ functions of interest, the first term in this equation vanishes. Also, Allen [1943] points out the following trigonometric identity

$$\cot\left(\frac{\theta_0 + \theta}{2}\right) - \cot\left(\frac{\theta_0 - \theta}{2}\right) = 2 \frac{\sin \theta}{\cos \theta_0 - \cos \theta} \quad (2.98)$$

so that Eq. (2.97) can be written as

$$T_{1,s} = \frac{4}{\pi c} \int_0^\pi \frac{\psi(\theta_0, t) \sin \theta}{\cos \theta_0 - \cos \theta} d\theta_0 \quad (2.99)$$

which is exactly equal to $T_{0,d}$ from Eq. (2.62b), so that the relationship is proved. One may wonder if there is a simpler way to show this equivalence. Other than the fact that $T_{1,s}$ and $T_{0,d}$ both depend on β' , there does not seem to be any obvious connection between the two terms. Also, it is likely that past researchers have not observed this relationship because it requires both the Fourier series representation of γ_0 and the separation of steady and damping terms to be recognized. This relationship can be shown to imply the following

$$\begin{array}{l} J_{0,d} = J_{1,s} \\ \bar{A}_{1,d} = \frac{1}{4}(2\bar{A}_{0,s} + \bar{A}_{2,s}) \\ \bar{A}_{2,d} = \frac{1}{8}(\bar{A}_{3,s} - \bar{A}_{1,s}) \end{array} \quad (2.100)$$

which will be used in Chapter 3.

Chapter 3

Application of the Theory to a General Deforming Camberline

3.1 Introduction

The majority of past research on the theoretical unsteady aerodynamics of deforming airfoils in incompressible flow has been concerned with harmonically oscillating trailing edge flaps. Theodorsen's [1935] result, which is summarized in Bisplinghoff *et al.* [1955], is the most widely recognized result for lift and pitching moment characteristics. Although Theodorsen presented results for the flap hinge moments, no results were given for the load distribution. Postel and Leppert [1948], along with a number of German researchers (Dietze, [1939, 1941, and 1951], Jaekel [1939], Schwarz [1940 and 1951], and Sohngen [1940 and 1951]), determined the load distribution on a harmonically oscillating airfoil. Recently, Mateescu and Abdo [2003] obtained both the unsteady forces and the load distribution using the method of velocity singularities. Narkiewicz *et al.* [1995] solved a similar problem which allowed for arbitrary flap and airfoil oscillations. Lieshman [1994] and Hariharan and Lieshman [1996] considered arbitrary flap deflections using indicial concepts, although both focused mainly on the compressible flow case.

Although there has been considerable research on the theoretical unsteady aerodynamics of a trailing edge flap, there has been little research concerning other deforming camberline shapes. Schwarz [1940 and 1951] studied an oscillating parabolic control surface. This shape was meant to account for the viscous effects of a conventional flap by smoothing out the hinge line. Recent interest in morphing aircraft has created interest in this parabolic, or conformal flap, for use as a hingless control surface (Sanders *et al.* [2003], Forster *et al.* [2003], Johnston [2003]).

Unfortunately, the previous work of Schwarz has gone unnoticed in the English-speaking literature except for the brief mention by Garrick [1957] and the discussion in the translated article by Schwarz [1951]. Spielberg [1953] studied the unsteady aerodynamics of an airfoil with an oscillating parabolic camberline. This study was restricted to a circular arc parabolic camberline, which was meant to represent chordwise aeroelastic deformations. Mesaric and Kosel [2004] determined the lift and pitching moment for cubic polynomial camberlines. No mention was made of the load distribution. Singh [1996] and Maclean [1994] presented a numerical model for the unsteady aerodynamics of deforming airfoils, although they did not discuss the agreement of their methods with theory. Another application of modeling deforming camberlines is for the study of sails and membrane airfoils. Llewelyn [1964] and Boyd [1963a, 1963b, and 1964] discuss the application of steady thin airfoil theory to various single-segment polynomial camberlines. The unsteady case was not discussed.

This chapter applies the unsteady thin airfoil theory method developed in Chapter 2 to a general deforming camberline. The camberline will be defined by two quadratic curves with arbitrary coefficients (a_1, b_1, \dots, c_2). Changing these coefficients allows for a wide range of time-varying camberlines to be modeled. This is especially advantageous because configurations with known solutions, such as a trailing edge flap, may be modeled with the correct choice of the coefficients and therefore the general solution may be validated. The unsteady lift, pitching moment, and pressure distribution will be derived for the general camberline and the equations presented. It is felt that the results of this derivation are easier to understand graphically, and therefore many plots will be presented and discussed. The resulting lift and pitching moment characteristics will be presented in terms of the K and J values defined in Section 2.5.

3.2 Camberline Representation

Consider a general camberline consisting of two quadratic segments, which can be written as

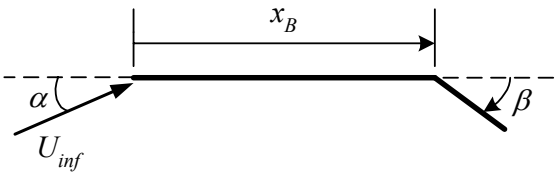
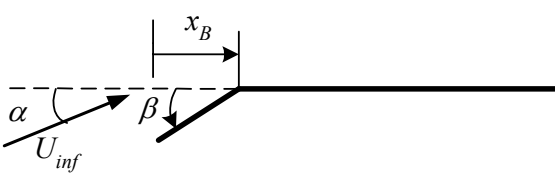
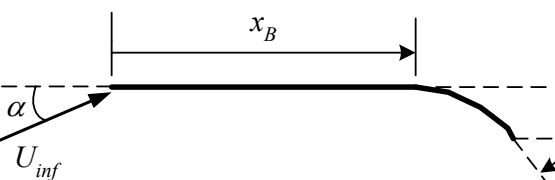
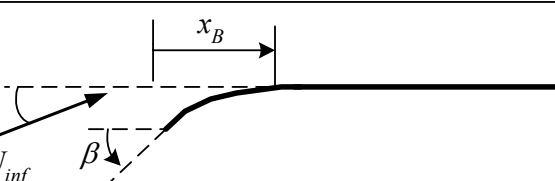
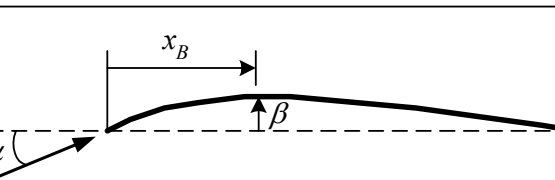
$$\begin{aligned} z_{c,1} &= \beta(\tau)(a_1x^2 + b_1x + c_1), & 0 \leq x \leq x_B \\ z_{c,2} &= \beta(\tau)(a_2x^2 + b_2x + c_2), & x_B \leq x \leq c \end{aligned} \quad (3.1)$$

where x_B is location at which the two segments connect and β is the control parameter that is a function of the nondimensional time (τ) defined in Eq. (2.52). Table 3.1 shows the five basic camberline shapes represented by Eq. (3.1) and their corresponding coefficients. Through linear superposition of these basic shapes, the majority of practical camberlines may be modeled.

Table 3.1: Geometric Coefficients for Specific Camberlines Represented by Eq. (3.1)

	a_1	b_1	c_1	a_2	b_2	c_2
(a) Trailing-Edge (TE) Flap	0	0	0	0	-1	x_B
(b) Leading-Edge (LE) Flap	0	1	$-x_B$	0	0	0
(c) Conformal TE Flap	0	0	0	$\frac{1}{2(x_B - 1)}$	$\frac{x_B}{(1 - x_B)}$	$\frac{x_B^2}{2(x_B - 1)}$
(d) Conformal LE Flap	$-\frac{1}{2x_B}$	1	$-\frac{x_B}{2}$	0	0	0
(e) NACA 4-digit	$-\frac{1}{x_B^2 c^2}$	$\frac{2}{x_B c}$	0	$\frac{-1}{(1 - x_B)^2 c^2}$	$\frac{2x_B}{(1 - x_B)^2 c^2}$	$\frac{(1 - 2x_B)}{(1 - x_B)^2}$

Table 3.2: Camberlines Represented by Eq. (3.1) and Table 3.1

(a) TE Flap	
(b) LE Flap	
(c) Conformal TE Flap	
(d) Conformal LE Flap	
(e) NACA 4-digit	

Eq. (3.1) has the form of Eq. (2.55); therefore the boundary condition may be separated into steady and damping components by Eqs. (2.56) and (2.57). This leads to the following equations for w_s and w_d

$$w_{s,n} = \beta(\tau)(2a_n x + b_n) \quad (3.2)$$

$$w_{d,n} = \frac{\beta'(\tau)}{c}(a_n x^2 + b_n x + c_n) \quad (3.3)$$

where $n = 1, 2$ corresponding to $z_{c,1}$ and $z_{c,2}$ in Eq. (3.1). Applying the transformation of Eq. (2.1) to Eqs. (3.2) and (3.3) results in the following

$$w_{s,n} = \beta(\tau)(H_n \cos \theta + I_n) \quad (3.4)$$

$$w_{d,n} = \frac{\beta'(\tau)}{c}(E_n \cos^2 \theta + F_n \cos \theta + G_n) \quad (3.5)$$

where

$$\begin{aligned} H_n &= -a_n \\ I_n &= a_n + b_n \end{aligned} \quad (3.6)$$

$$\begin{aligned} E_n &= a_n / 4 \\ F_n &= -a_n / 2 - b_n / 2 \\ G_n &= a_n / 4 + b_n / 2 + c_n \end{aligned} \quad (3.7)$$

Eqs. (3.4 – 3.7) provide a compact method of representing the camberlines of Table 3.1 in terms of the polar coordinates of Eq. (2.1). The next section will apply these equations to the unsteady thin airfoil method developed in Chapter 2.

3.3 The Quasi-Steady Load Distribution and Force Coefficients

Having defined the steady and damping components of w in Eqs. (3.4) and (3.5), the quasi-steady load distribution and force coefficients may be calculated using the method presented in Chapter 2. The main challenge in obtaining the load distribution is evaluating the integral for the basic load distribution (Eq. (2.62b)). The details of these integrations can be found in Appendix A. Substituting Eqs. (3.4) and (3.5) into Eq. (2.62b) results in the following two equations for the steady and damping components of the nondimensional basic load distribution

$$T_{0,s}(\theta) = \frac{2}{\pi} \left\{ \begin{aligned} & \left[2(I_1 - I_2) + 2(H_1 - H_2) \cos \theta \right] \ln \left(\frac{\sin \theta \tan(\theta_B / 2) - \cos \theta + 1}{\sin \theta \tan(\theta_B / 2) + \cos \theta - 1} \right) \\ & + 2[\theta_B H_1 + (\pi - \theta_B) H_2] \sin \theta \end{aligned} \right\} \quad (3.8)$$

$$T_{0,d}(\theta) = \frac{2}{\pi} \left\{ \begin{aligned} & \left[2(G_1 - G_2) + 2(F_1 - F_2) \cos \theta + (E_1 - E_2)(1 + \cos 2\theta) \right] \ln \left(\frac{\sin \theta \tan(\theta_B / 2) - \cos \theta + 1}{\sin \theta \tan(\theta_B / 2) + \cos \theta - 1} \right) \\ & + 2[\theta_B (F_1 + E_1 \cos \theta) + (\pi - \theta_B)(F_2 + E_2 \cos \theta) + (E_1 - E_2) \sin \theta_B] \sin \theta \end{aligned} \right\} \quad (3.9)$$

Eq. (3.8) was validated for a conventional TE flap by comparing with Spence's [1958] result and for a conformal TE flap by comparing with Johnston's [2003] result. For the NACA case, Eq. (3.8) can be shown to compare well with Pinkerton's [1936] approximate result. Figures 3.1 – 3.4 illustrate Eqs. (3.8) and (3.9) for the various camberlines shown in Table 3.1. Figures 3.1 and 3.2 show the difference between the LE and TE configurations as well as the difference between the conventional and conformal flaps. Because w_s is not discontinuous at x_B for the conformal case, unlike the conventional case there is no singularity in $T_{0,s}$ at x_B . For the $T_{0,d}$ terms in Figure 3.2, w_d is continuous for both the conventional and conformal cases (see Figure 2.3 and 2.4) so that there are no singularities in $T_{0,d}$. One may notice the similarity between $T_{0,s}$ for the conformal flap in Figure 3.1 and $T_{0,d}$ for the conventional flap in Figure 3.2. In fact, these two terms are exactly the same shape, although of different magnitudes. The magnitudes of these two components are equivalent through the relationship

$$T_{0,s \text{ conformal}} = (1 - x_B / c) T_{0,d \text{ conventional}} \quad (3.10)$$

This equivalence is apparent by considering the fact that the x -derivative of the quadratic conformal camberline is linear in x (so w_s is linear) and that the time-derivative of the conventional flap is also linear in x (so w_d is linear).

An interesting feature of Figure 3.1 is the similarity between the LE and TE flaps of $T_{0,s}$. In other words, the LE flap creates a $T_{0,s}$ that has the same shape and magnitude but is reversed from that of the TE flap. This indicates that in steady theory, the difference in the load distribution between “mirror image” camberlines (for example, the difference between a LE and TE flap or between an NACA camberline with $x_B = 0.3$ and 0.7) is captured entirely by the $A_{0,s}$ Fourier coefficient (see Eq. (2.62)). This conclusion could have also been reached by considering the simple analysis presented by Abzug [1955], which showed that a LE edge flap is just a TE flap on an airfoil at negative angle of attack. In contrast to $T_{0,s}$, Figures 3.2 and 3.4 show that the $T_{0,d}$ produced by LE and TE flaps are equal in magnitude but opposite in sign.

Figures 3.1 and 3.2 show that a conformal flap is less effective than a conventional flap. This is a result of the definition of β in Table 3.2. The angle β is defined as the angle at the trailing edge (or leading edge) of the conformal flap, which means that the rest of the control surface is at a smaller angle.

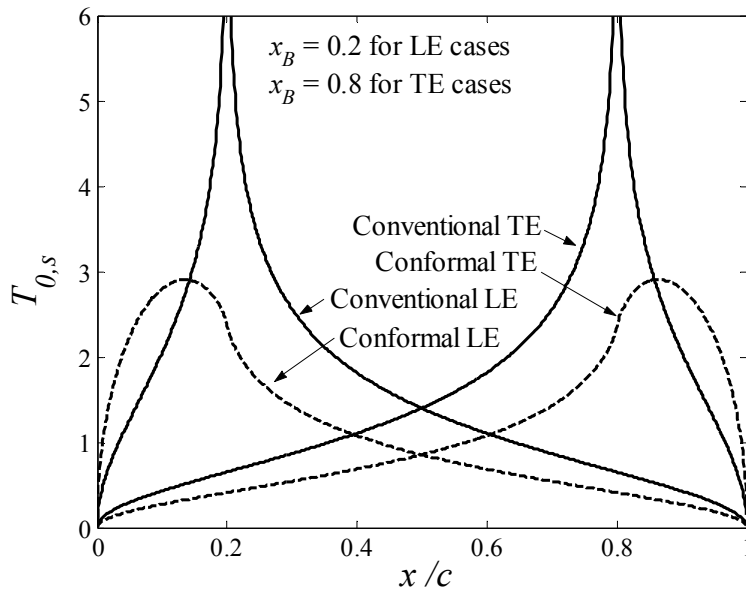


Figure 3.1: Steady component of the basic load distribution for various flap configurations

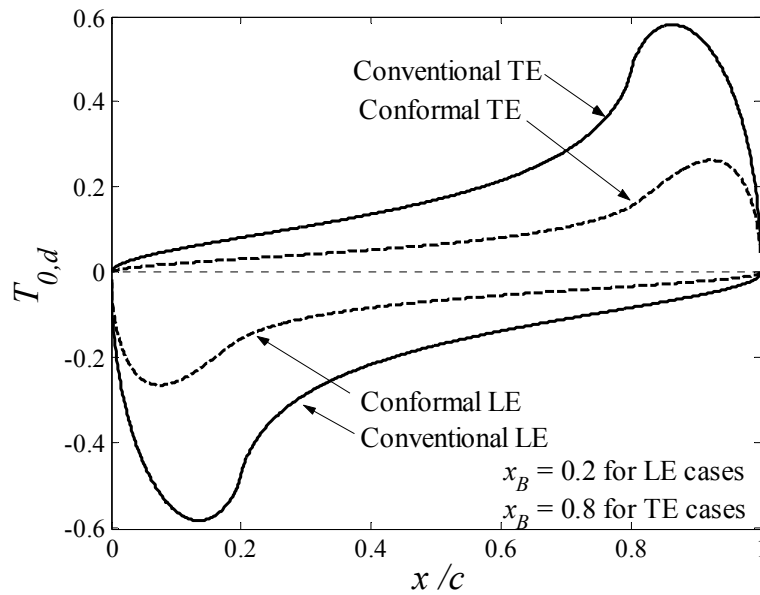


Figure 3.2: Damping component of the basic load distribution for various flap configurations

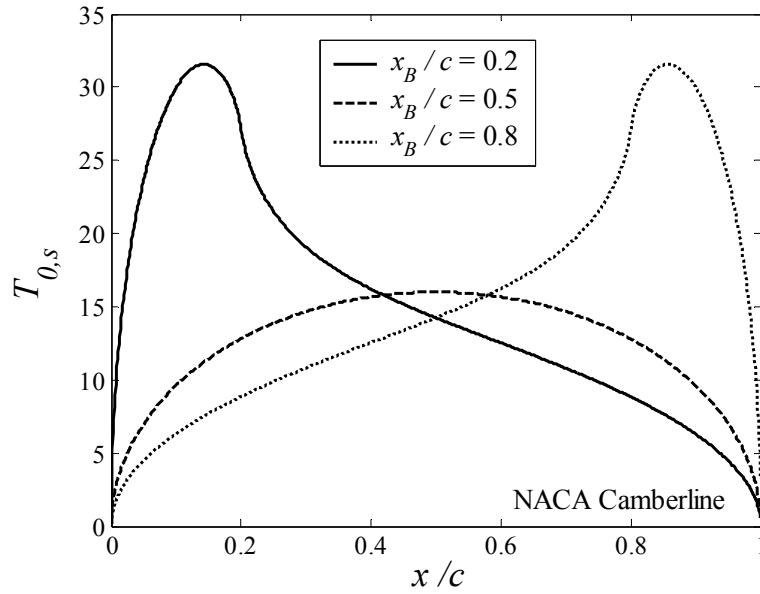


Figure 3.3: Steady component of the basic load distribution for various NACA camberlines

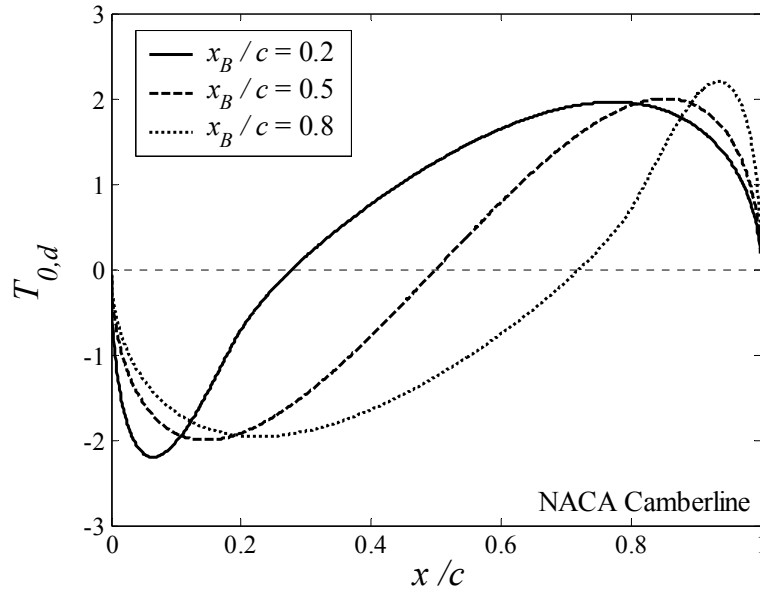


Figure 3.4: Damping component of the basic load distribution for various NACA camberlines

As shown in Eq. (2.62), the component of the quasi-steady load distribution *not* dependent on $T_{0,s}$ or $T_{0,d}$ is only dependent only on $\bar{A}_{0,s}$ and $\bar{A}_{0,d}$. This component of the load distribution, called the additional load distribution, has the shape of an angle of attack produced load distribution (represented by ψ). Equations (2.59) and (2.61) show that the quasi-steady lift and moment

coefficients depend on the first three Fourier coefficients (the fourth coefficient $\bar{A}_{3,s}$, is calculated as well to determine $\bar{A}_{2,d}$ from Eq. (2.100)). From Eqs. (3.4) and (2.59), the steady coefficients evaluate to the following

$$\begin{aligned}
\bar{A}_{0,s} &= -\frac{1}{\pi} [I_2(\pi - \theta_B) + I_1\theta_B + (H_1 - H_2)\sin\theta_B] \\
\bar{A}_{1,s} &= \frac{1}{\pi} [H_2(\pi - \theta_B) + H_1\theta_B + (2(I_1 - I_2) + (H_1 - H_2)\cos\theta_B)\sin\theta_B] \\
\bar{A}_{2,s} &= \frac{2}{3\pi} [3(I_1 - I_2)\cos\theta_B + (H_1 - H_2)(2 + \cos 2\theta_B)]\sin\theta_B \\
\bar{A}_{3,s} &= \frac{1}{3\pi} [6(H_1 - H_2)\cos^3\theta_B\sin\theta_B + 2(I_1 - I_2)\sin 3\theta_B]
\end{aligned} \tag{3.11}$$

For a TE flap, these coefficients can be shown to agree with Glauert's [1947] or Allen's [1938] result. For the damping quasi-steady terms, only $\bar{A}_{0,d}$ must be determined because of the relationships for $\bar{A}_{1,d}$ and $\bar{A}_{2,d}$ given in Eq. (2.70). In the next section, $\bar{A}_{3,d}$ will be required for the apparent mass pitching moment coefficient, so it calculated here as well. From Eqs. (3.6) and (2.59), $\bar{A}_{0,d}$ and $\bar{A}_{3,d}$ evaluate to the following

$$\begin{aligned}
\bar{A}_{0,d} &= -\frac{1}{2\pi} [(E_2 + 2G_2)\pi + (E_1 - E_2 + 2G_1 - 2G_2)\theta_B + (2F_1 - 2F_2 + (E_1 - E_2)\cos\theta_B)\sin\theta_B] \\
\bar{A}_{3,d} &= \frac{1}{60\pi} [30(E_1 - E_2 + 4(F_1 - F_2)\cos^3\theta_B)\sin\theta_B + 20(E_1 - E_2 + 2G_1 - 2G_2)\sin 3\theta_B + 6(E_1 - E_2)\sin 5\theta_B]
\end{aligned} \tag{3.12}$$

Figures 3.5 and 3.6 show $\bar{A}_{0,s}$ and $\bar{A}_{0,d}$ from Eqs. (3.11) and (3.12) plotted as a function of x_B . Note that x_B is defined in Table 3.2 so that for the LE flap configurations, x_B is equal to the flap-to-chord ratio (c_f/c), but for TE configurations, $x_B = 1 - c_f/c$. Figure 3.5 shows that $\bar{A}_{0,s}$ is of opposite sign for LE and TE cases of the same c_f/c . The negative value of $\bar{A}_{0,s}$ for leading edge configurations indicates the well-known superior control effectiveness of TE configurations in steady airfoil theory. Similarly, Figure 3.5 shows that it is more effective to place the location of maximum camber on an NACA camberline aft of $x = 0.5$. Figure 3.6 shows that, in contrast to $T_{0,d}$, $\bar{A}_{0,d}$ has the same sign for LE and TE configurations of identical c_f/c . Because for the LE configuration, $T_{0,s}$ and $\bar{A}_{0,s}$ as well as $T_{0,d}$ and $\bar{A}_{0,d}$ have opposite signs (but the same magnitude as for the TE case), the quasi-steady lift effectiveness is always less for a LE flap configuration (relative to a TE configuration with the same c_f/c).

Figures 3.5 and 3.6 present values for the NACA camberline for values of x_B ranging from 0.1 to 0.9. Unlike the LE and TE configurations, the values of $\bar{A}_{0,s}$ and $\bar{A}_{0,d}$ for the NACA case do not asymptote to finite values at x_B equal to zero or one. This is because, as defined in Table 3.2, β represents the magnitude of maximum camber; which is a distance instead of an angle. Thin airfoil theory assumes small angles, which is violated as x_B approaches zero or one with a fixed and finite β .

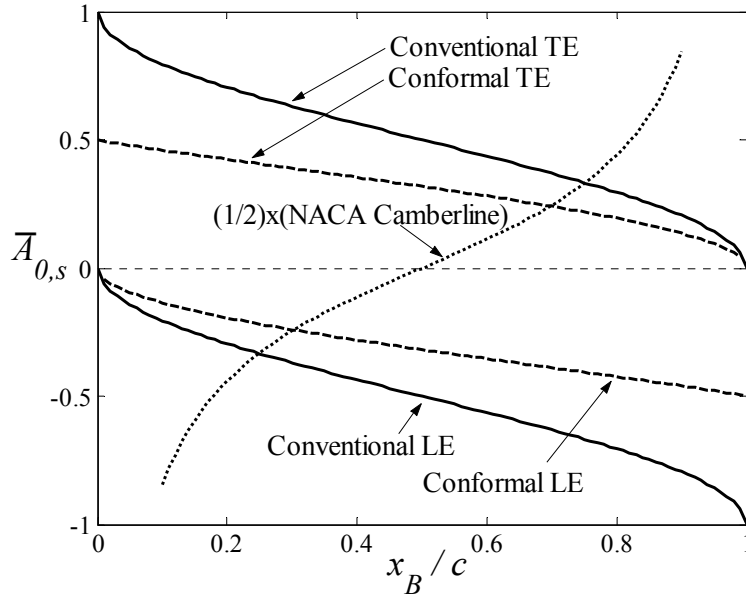


Figure 3.5: Steady component of A_0 for various flap configurations

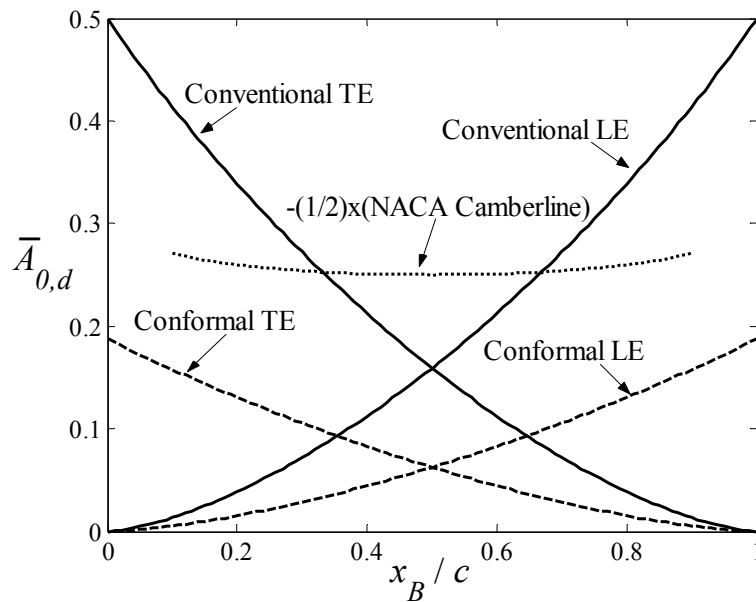


Figure 3.6: Damping component of A_0 for various flap configurations

Figures 3.7 through 3.9 confirm the previous discussion on the lift effectiveness of the various configurations. Recall the definitions of the K -values given in Eq. (2.59). The $K_{0,s}$ values in Figures 3.7 and 3.8 show that, as mentioned previously, the TE configurations produce significantly more lift per-unit β than the LE configurations. Similarly, the $K_{0,d}$ values indicate that the TE configurations produce significantly more lift per-unit $d\beta/d\tau$ than the LE configurations. Figure 3.9 shows that although the steady lift effectiveness increases for an NACA camberline as x_B is shifted aft, the damping lift becomes more negative.

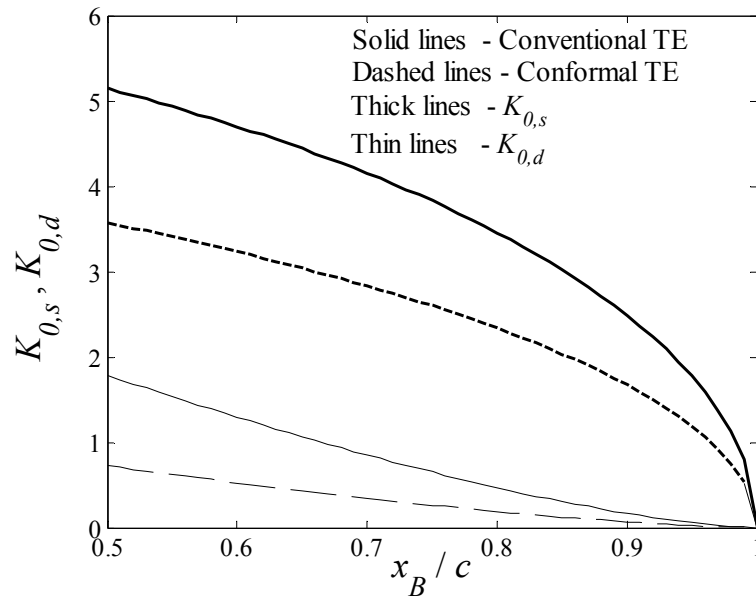


Figure 3.7: Effect of the trailing edge flap size on the steady flap effectiveness for lift

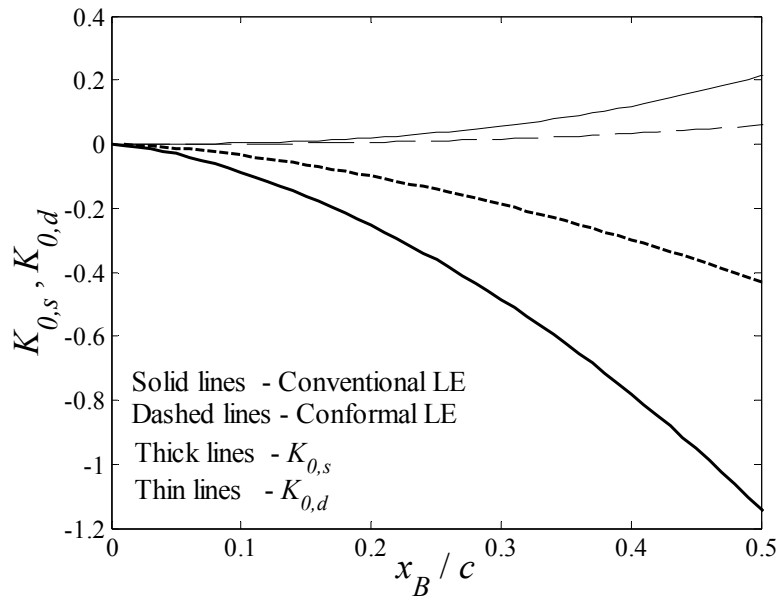


Figure 3.8: Effect of the leading edge flap size on the steady flap effectiveness for lift

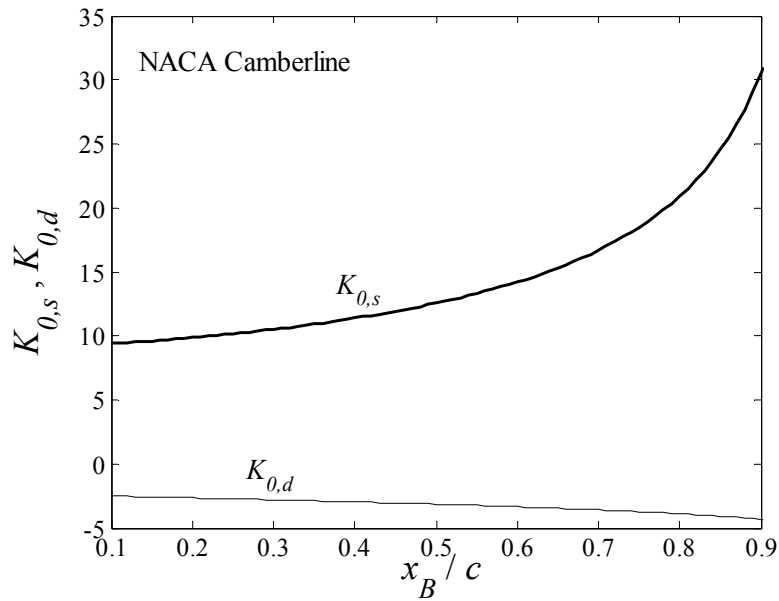


Figure 3.9: Effect of the maximum camber location on the steady camber effectiveness for lift

Figures 3.10 – 3.12 show the influence of x_B on the quarter-chord pitching moment parameters defined in Eq. (2.61). An important concept to keep in mind when examining the effect of the camberline on the quarter-chord pitching moment is that the additional load distribution, which is

proportional to $\bar{A}_{0,s}$ and $\bar{A}_{0,d}$, has no influence. Thus, only the effect of the camberline on the basic load distribution ($T_{0,s}$ and $T_{0,d}$) needs to be considered. Figures 3.10 and 3.11 show that $J_{0,s}$ is negative for both the LE and TE configurations. Figure 3.12 shows that the same is true for the NACA case. Unlike $J_{0,s}$, the value of $J_{0,d}$ is negative for the TE case and positive for the LE case. This difference in sign is due to the difference in sign between the LE and TE flap $T_{0,s}$ and $T_{0,d}$ distributions as shown in Figures 3.1 and 3.2. Figure 3.12 shows that the $J_{0,d}$ approaches zero for the NACA case as x_B approaches one. This figure also shows, as for the TE cases, $J_{0,s}$ and $J_{0,d}$ have the same sign for any x_B .

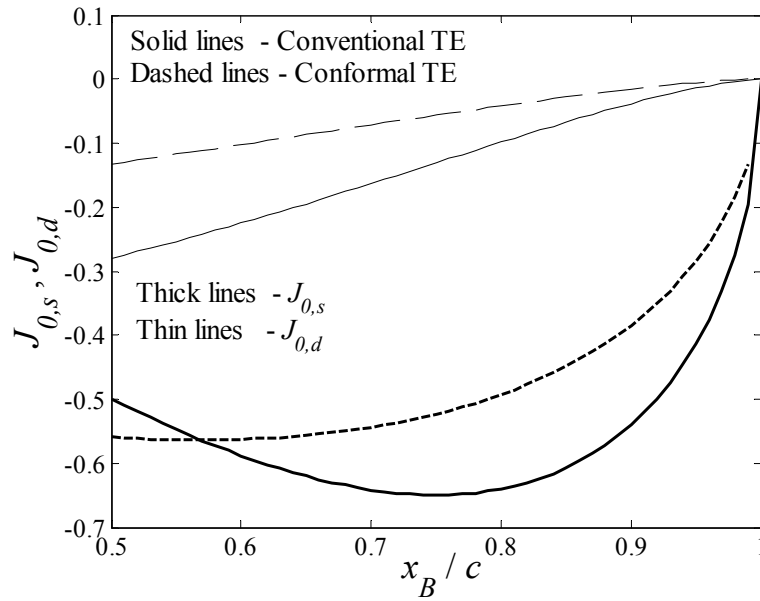


Figure 3.10: Effect of the trailing edge flap size on the steady flap effectiveness of the quarter chord pitching moment

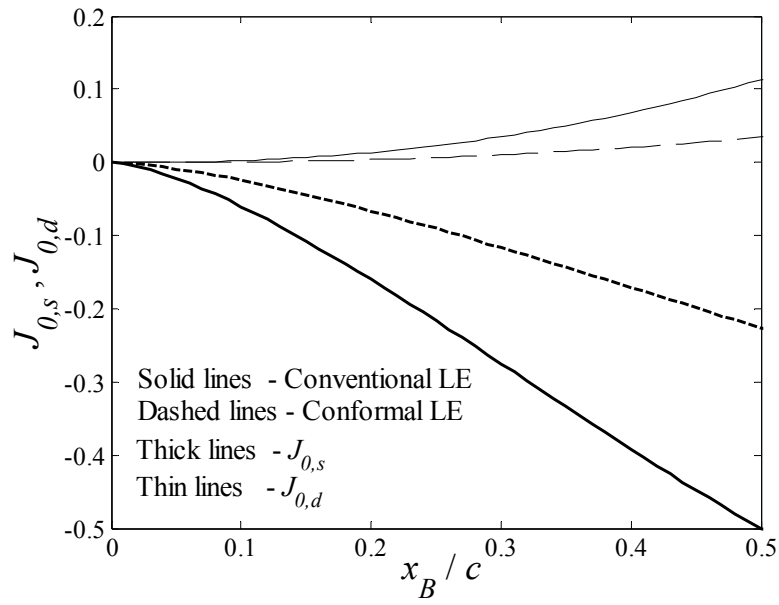


Figure 3.11: Effect of the leading edge flap size on the steady flap effectiveness of the quarter chord pitching moment

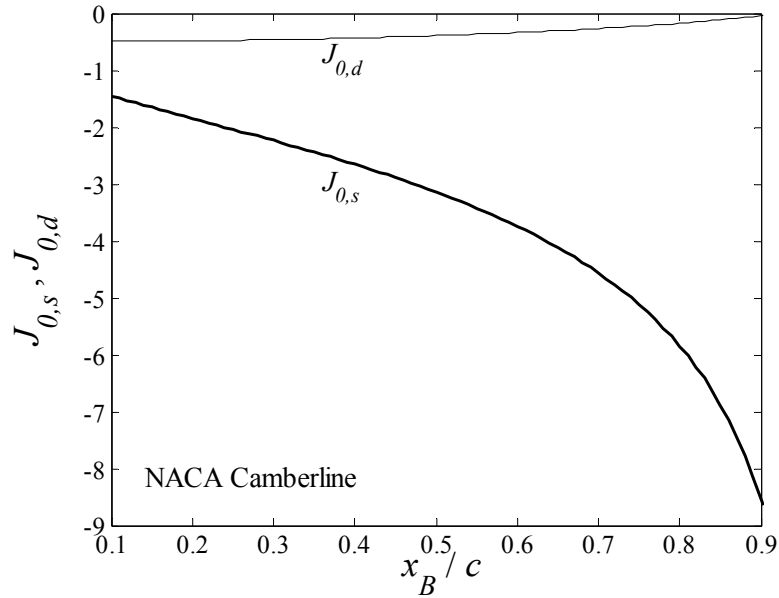


Figure 3.12: Effect of the maximum camber location on the steady camber effectiveness for the quarter chord pitching moment

3.4 The Apparent Mass Load Distribution and Force Coefficients

Examining Eq. (2.67) for the apparent mass load distribution ($\Delta C_{p,l}$) it is clear that the only component not yet known is the integral term (the Fourier coefficients were required for the quasi-steady terms). Furthermore, $T_{l,s}$ does not need to be determined because it was shown in Section 2.7 that this is equal to $T_{0,d}$. Thus, the only required integration is the following

$$\int_0^{\theta} T_{0,d}(\theta) \sin \theta d\theta = \frac{1}{3\pi} \left[\begin{aligned} & [(3E + 12G) \cos \theta_B + 3(F) \cos 2\theta_B + E \cos 3\theta_B] \ln \left[\frac{\sin\left(\frac{\theta_B + \theta}{2}\right)}{\sin\left(\frac{\theta_B - \theta}{2}\right)} \right] \\ & - [(3E + 12G) \cos \theta + 3(F) \cos 2\theta + E \cos 3\theta] \ln \left[\frac{\sin\left(\frac{\theta_B + \theta}{2}\right)}{\sin\left(\frac{\theta_B - \theta}{2}\right)} \right] \\ & + (4E + 12G + 6F \cos \theta_B) \theta \sin \theta_B + 2E \theta \cos 2\theta_B \sin \theta_B + 6F \sin \theta_B \sin \theta \\ & + 4E \cos \theta_B \sin \theta_B \sin \theta + E \sin \theta_B \sin 2\theta + 3(E_2(\pi - \theta_B) + E_1 \theta_B) \sin \theta \\ & + 6(F_2(\pi - \theta_B) + F_1 \theta_B + E \sin \theta_B)(\theta - \cos \theta \sin \theta) - (E_2(\pi - \theta_B) + E_1 \theta_B) \sin 3\theta \end{aligned} \right] \quad (3.13)$$

where the terms E , F , and G represent $E_1 - E_2$, $F_1 - F_2$, and $G_1 - G_2$, respectively. Applying Eqs. (3.11), (3.12) and (3.13) to Eq. (2.67) allows $T_{l,d}$ to be determined. Note that this term is proportional to the acceleration of the camberline deformation (β''). The apparent mass load distribution for the conventional TE flap case can be shown to agree with the result obtained by Postel and Leppert [1948]. Figure 3.13 shows $T_{l,d}$ for the LE and TE configurations shown in Table 3.2. This figure shows that LE and TE flaps with the same c_f/c have equivalent load distributions. Figure 3.14 shows that $T_{l,d}$ is also equivalent for the NACA camberline with the maximum camber located at equal distances from the airfoil center. In contrast, from Figures 3.2 and 3.4 it is seen that $T_{0,d}$ ($=T_{l,s}$) changes sign for equivalent configurations.

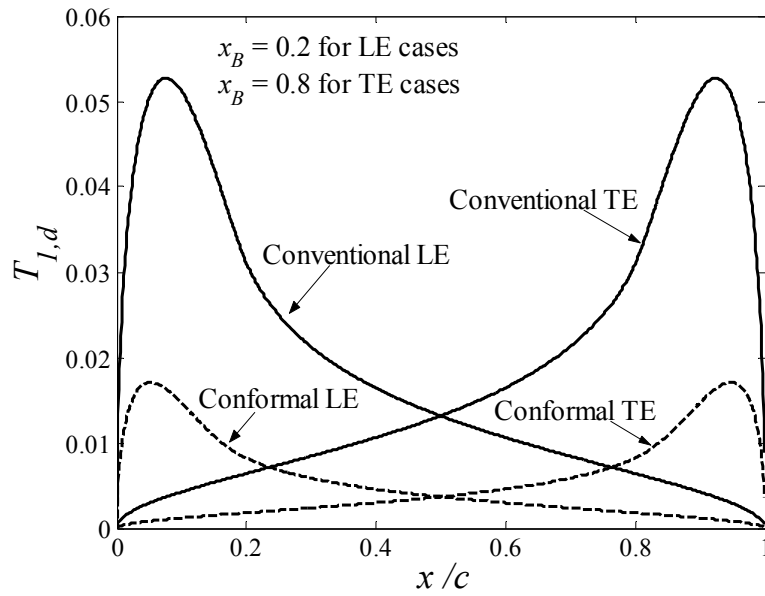


Figure 3.13: Damping apparent mass load distribution for various flap configurations

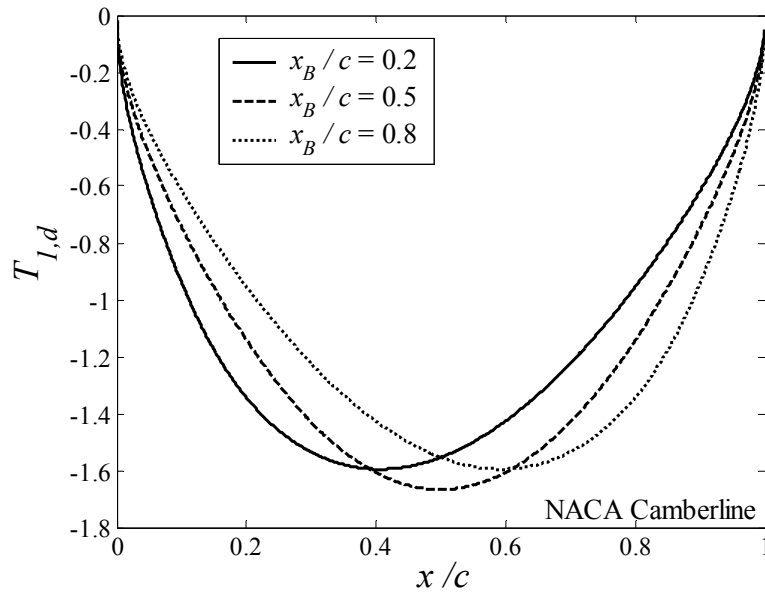


Figure 3.14: Damping apparent mass load distribution for various NACA camberlines

The Fourier coefficients required by Eqs. (2.64) and (2.66) for the apparent mass lift and pitching moment coefficients were presented in Eqs. (3.11) and (3.12). Figures 3.15 through 3.17 present the $K_{l,s}$ and $K_{l,d}$ values defined in Eq. (2.64). These results agree with Theodoresen's [1935] result for a conventional TE flap.

Figures 3.18 through 3.20 present the value $J_{l,d}$ defined in Eq. (2.66) for the various camberline configurations. These figures show the expected variation with x_B .

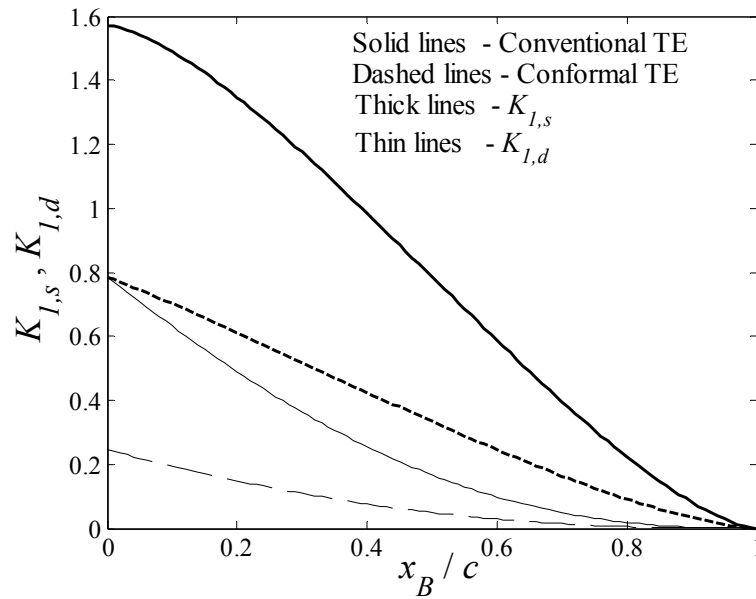


Figure 3.15: Effect of the trailing edge flap size on the steady apparent mass lift

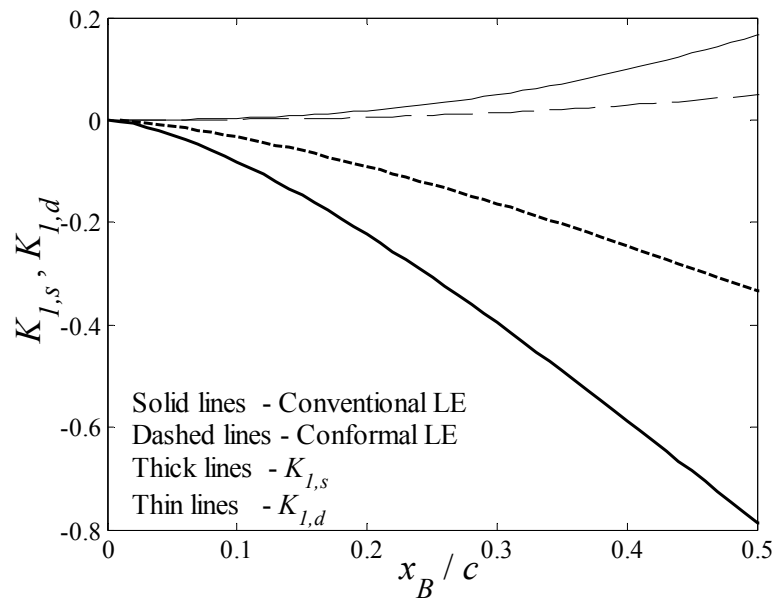


Figure 3.16: Effect of the leading edge flap size on the steady apparent mass lift

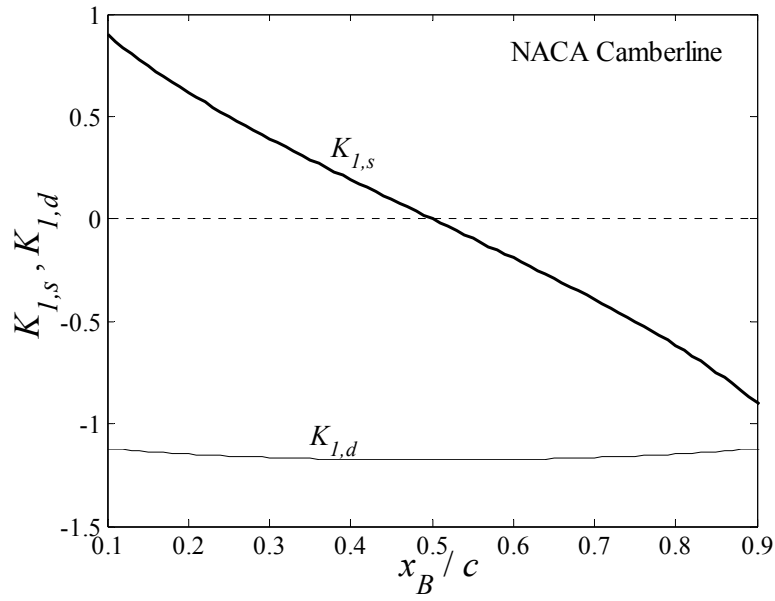


Figure 3.17: Effect of the maximum camber location on the steady apparent mass lift

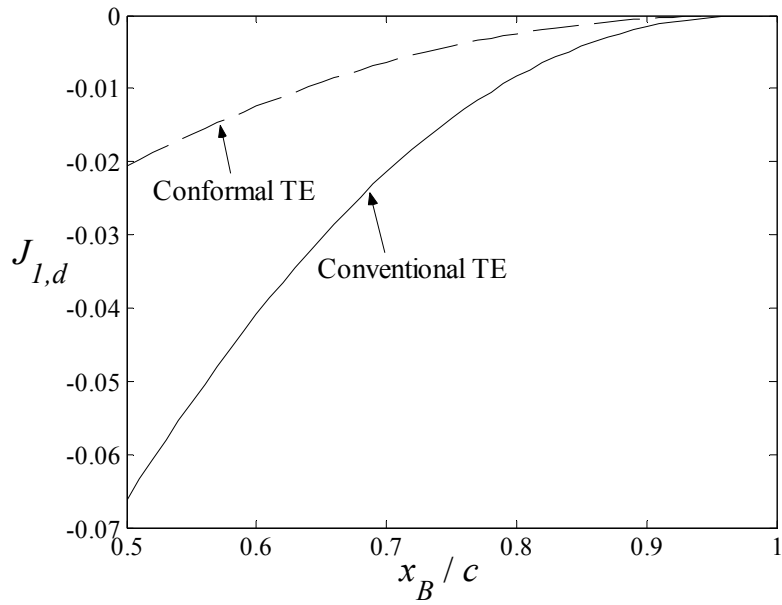


Figure 3.18: Effect of the trailing edge flap size on the damping apparent mass quarter-chord pitching moment

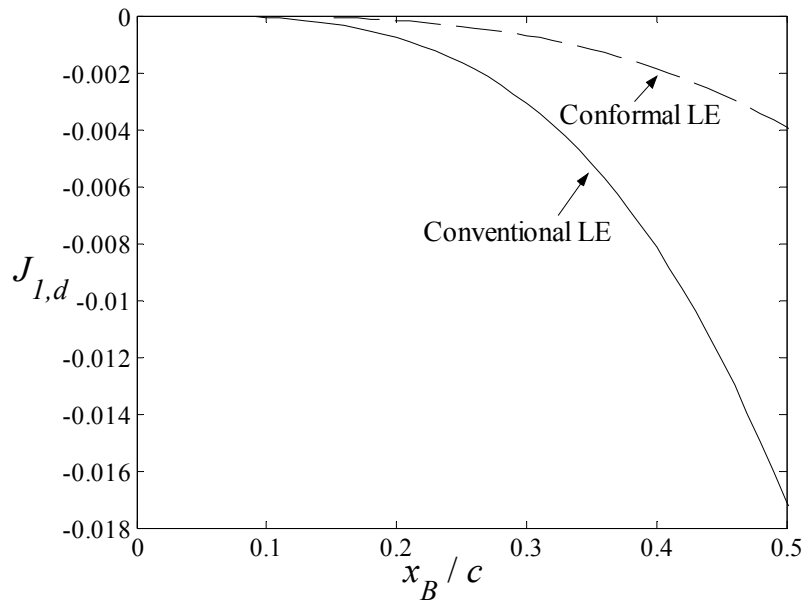


Figure 3.19: Effect of the leading edge flap size on the damping apparent mass quarter-chord pitching moment

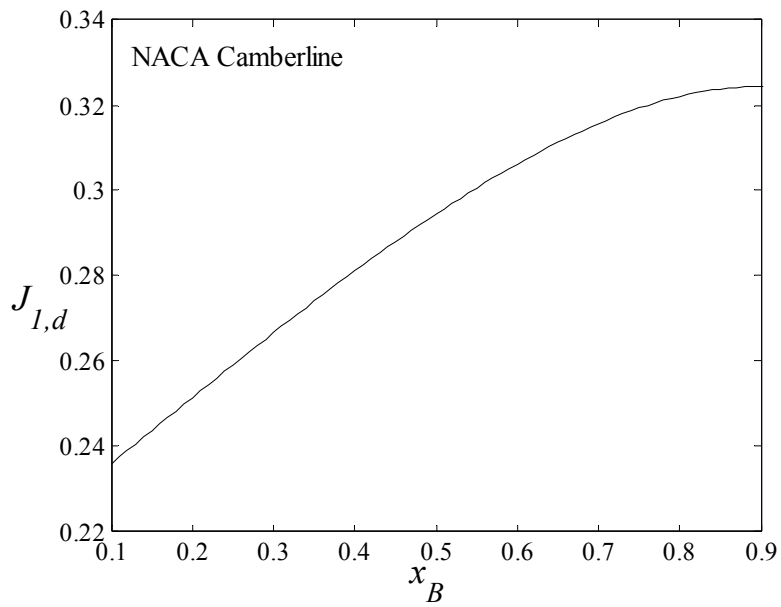


Figure 3.20: Effect of the maximum camber location on the damping apparent mass quarter-chord pitching moment

3.5 A Variable-Camber Problem

Consider the two variable-camber configuration shown in Figure 3.31. Configuration *A* is exactly the NACA camberline presented in Tables 3.1 and 3.2. Configuration *B* is a combination of the conformal LE and TE flaps presented in Tables 3.1 and 3.2 and has the same w_s as configuration *A*. The only difference between these two configurations is w_d . In fact, w_d for configuration *B* is a combination of the w_d for configuration *A* along with a heaving motion. How do the unsteady characteristics differ for these cases?

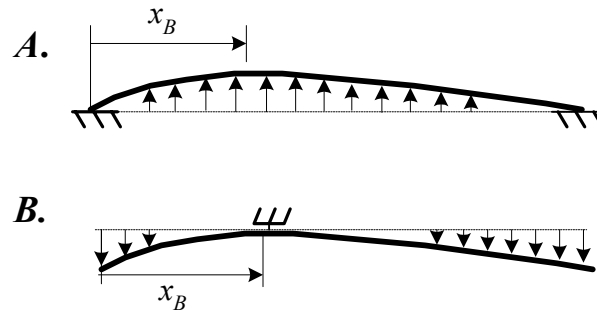


Figure 3.21: Two different variable-camber configurations of the same camberline

This problem is greatly simplified by using the relationship between $T_{l,s}$ and $T_{0,d}$ presented in Section 2.7. Before this done though, it must be recognized that because w_s is identical between the two cases, then $T_{0,s}$ and $T_{l,s}$ are identical. It then follows from Section 2.6 that $T_{0,d}$ is also the same. So, in the absence of camberline acceleration (meaning that $T_{l,d}$ is not considered), the only difference between the two configurations is the magnitude of the damping additional load distribution (more specifically the difference is in $\bar{A}_{0,d}$). This implies that the quarter chord pitching moment is the same for both cases.

As mentioned previously, configuration *B* can be modeled from the LE and TE conformal flaps shown in Table 3.1. For these cases, β represents the angle of either the leading or trailing edge. To compare with configuration *A*, in which case β represents the camber at x_B , the following relationships may be applied

$$\beta_{LE} = 2 \frac{\beta_A}{x_B} \tag{3.14}$$

$$\beta_{TE} = 2 \frac{\beta_A}{1-x_B}$$

where β_A is the maximum camber of configuration A and β_{LE} and β_{TE} are the equivalent leading and trailing deflections for configuration B . With Eq. (3.14), the results of Section 3.3 may be used to compare $\bar{A}_{0,d}$ between the two configurations. Figure 3.32 presents this comparison and shows that the sign of $\bar{A}_{0,d}$ is different between the two configurations.

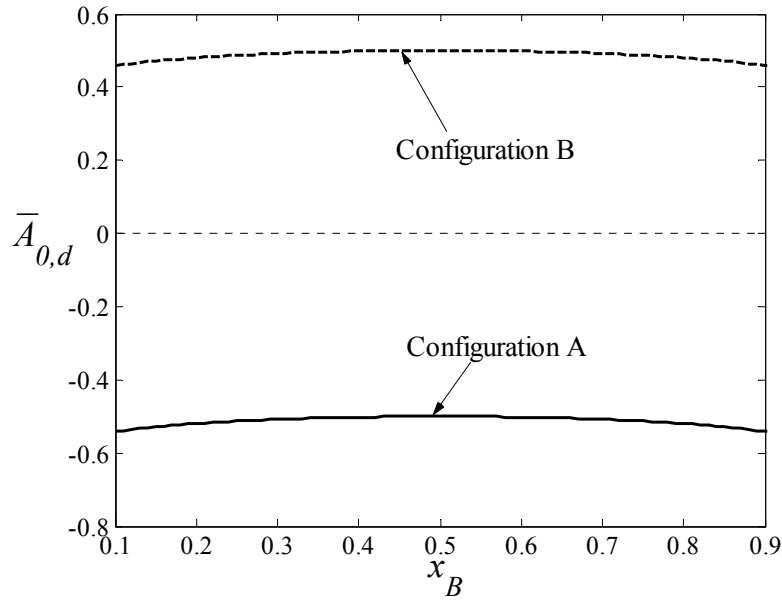


Figure 3.22: The difference between configuration A and B if there are no acceleration terms

To put the difference in $\bar{A}_{0,d}$ shown in Figure 3.32 in perspective, Figure 3.33 compares the lift due to $d\beta/d\tau$ (which from Eq. (2.68) is $K_{0,d}+K_{l,s}$). The sign difference between the two cases is significant because it implies that for a positive change in lift (meaning a positive $d\beta/d\tau$), the $d\beta/d\tau$ terms produce positive lift for configuration B and negative lift for configuration A . Although this component of lift acts only during the motion of the camberline, it could have a significant effect on the maneuverability of the vehicle. Determining which configuration is favorable would require that the maneuver and vehicle be specified.

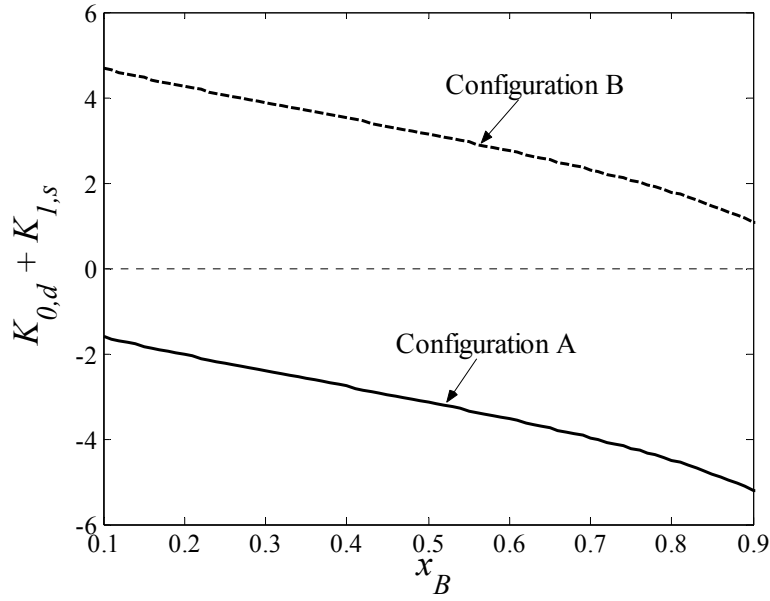


Figure 3.23: The difference in the lift due to $d\beta/dt$ between configuration A and B

3.6 The Load Distribution and Force Coefficients for a Sinusoidal β

Combining the lift, pitching moment, and pressure distribution parameters determined in Sections 3.3 and 3.4 for a general camberline with the equations derived in Section 2.6 for a sinusoidal β , the influence of \bar{k} on the lift, pitching moment, and pressure distribution of various camberline configurations may be determined.

It is convenient to present the lift and pitching moment in terms of a magnitude and phase angle. From Eqs. (2.81) and (2.82), this is written as follows for the lift coefficient

$$C_L(\tau, \bar{k}) = \bar{C}_L \bar{\beta} \cos(\bar{k}\tau + \phi_L) \quad (3.15)$$

where

$$\begin{aligned} \bar{C}_L &= \sqrt{Z_1^2 + Z_2^2} \\ \phi_L &= \tan^{-1}\left(-\frac{Z_2}{Z_1}\right) \end{aligned} \quad (3.16)$$

The terms Z_1 and Z_2 were defined in Eq. (2.82) as follows

$$\begin{aligned} Z_1(\bar{k}) &= -[K_{1,d}\bar{k}^2 - K_{0,s}F + K_{0,d}\bar{k}G] \\ Z_2(\bar{k}) &= -[K_{1,s}\bar{k} + K_{0,s}G + K_{0,d}\bar{k}F] \end{aligned} \quad (3.17)$$

The pitching moment is represented analogously in terms of \bar{C}_M and ϕ_M , where Y_1 and Y_2 are substituted for the Z_1 and Z_2 in Eqs. (3.16) and (3.17). The terms Y_1 and Y_2 were defined in Eq. (2.85) as

$$\begin{aligned} Y_1(\bar{k}) &= -(J_{1,d}\bar{k}^2 - J_{0,s}) \\ Y_2(\bar{k}) &= -(J_{0,d} + J_{1,s})\bar{k} \end{aligned} \quad (3.18)$$

The load distribution will be presented in terms of Π_1 and Π_2 defined as follows in Eq. (2.89)

$$\begin{aligned} \Pi_1(\bar{k}, \theta) &= \left[\bar{A}_{0,s}\chi(\theta) + T_{0,s}(\theta) - T_{1,d}(\theta)\bar{k} + \frac{\chi(\theta)}{2\pi}(K_{0,s}F - K_{0,s} - \bar{k}K_{0,d}G) \right] \\ \Pi_2(\bar{k}, \theta) &= - \left[(\bar{A}_{0,d}\chi(\theta) + T_{0,d}(\theta) + T_{1,s}(\theta))\bar{k} + \frac{\chi(\theta)}{2\pi}(K_{0,s}G + \bar{k}K_{0,d}F - \bar{k}K_{0,d}) \right] \end{aligned} \quad (3.19)$$

where

$$\Delta C_p(\tau, \theta, \bar{k}) = \Pi_1(\bar{k}, \theta)\bar{\beta} \cos(\bar{k}\tau) + \Pi_2(\bar{k}, \theta)\bar{\beta} \sin(\bar{k}\tau) \quad (3.20)$$

The components Π_1 and Π_2 are the same as the real and *negative* imaginary components that are sometimes presented in the literature (this is also true for the Z and Y terms). The unsteady load distribution is sometimes presented in terms of a magnitude and phase angle, which are functions of x . This representation is used mostly for studying the unsteady Kutta condition (Satyanarayana and Davis [1978], and Ardonceau [1989]).

a) TE Configurations

Figures 3.24 through 3.29 present the results for the conventional and conformal TE flaps. The lift coefficient magnitude divided by the quasi-steady lift coefficient ($K_{0,s}$) is presented in Figure 3.24 for both the conventional and conformal cases with different flap sizes. Note that $K_{0,s}$ is different for each case, as shown in Figure 3.7, but is used here to normalize each case to the same oscillation in the steady-state C_L . Figure 3.25 presents the phase angle for the lift for each case. Figures 3.24 and 3.24 indicate that for a given oscillation of the steady-state lift coefficient, the larger flap sizes have a larger C_L magnitude and phase angle. This is due mainly to the larger value of $K_{0,d}$, which is shown in Figure 3.7. For the same reason, the conventional flap has a larger C_L magnitude than the conformal flap.

Figures 3.26 and 3.27 present the magnitude and phase angle for the quarter-chord pitching moment (C_M). The C_M magnitude is normalized by the absolute value of the quasi-steady

pitching moment coefficient ($J_{0,s}$) presented in Figure 3.10. Note that, as shown in Eq. (3.18), C_M is independent of the Theodorsen function, which explains the simpler dependence shown of \bar{C}_M on \bar{k} . Like for C_L , the larger flap sizes have a larger C_M magnitude due to the larger values of $J_{0,d}$ and $J_{1,d}$ shown in Figures 3.10 and 3.18. The phase angle is 180 degrees out-of-phase for \bar{k} equal to zero because $J_{0,s}$ is negative.

Figures 3.28 and 3.29 show the in-phase (real) and out-of-phase (negative imaginary) components of the load distribution for the conventional and conformal TE flap configurations of various flap sizes. These distributions are shown for a \bar{k} equal to 2 and each case is normalized by $K_{0,s}$. The conventional flap cases can be shown to agree with the equations developed by Postel and Leppert [1948]. For a \bar{k} equal to 0.48 or 0.68, the present method does not completely agree with the results presented by Mateescu and Abdo [2003] for the conformal flap. Their values are larger near the middle of the airfoil. The reason for this is not clear.

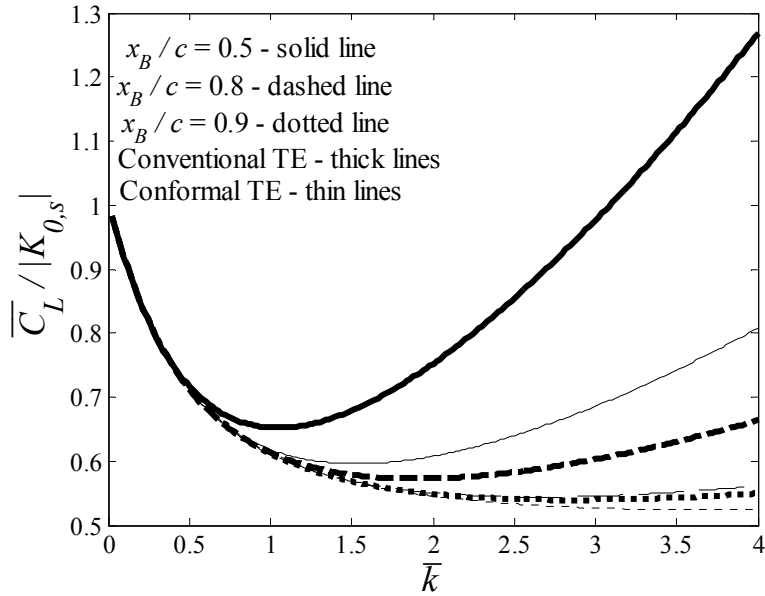


Figure 3.24: The lift coefficient amplitude for TE configurations

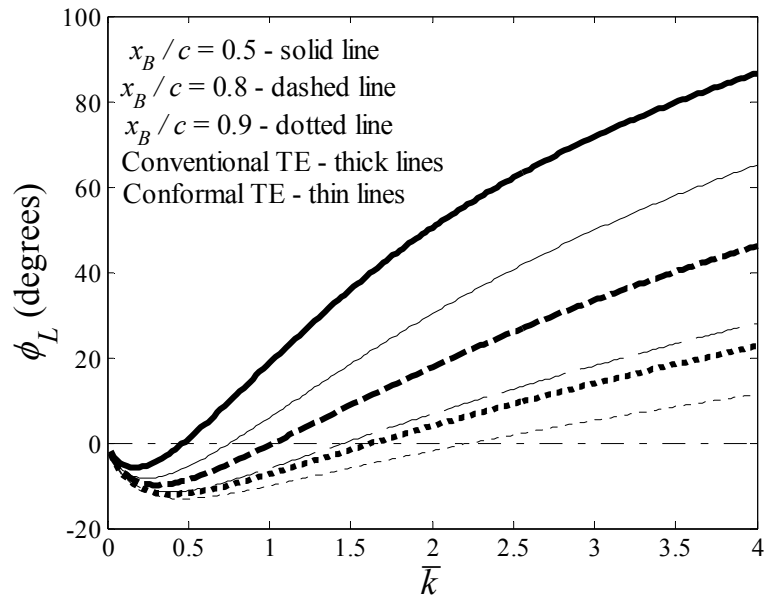


Figure 3.25: The lift coefficient phase angle for TE configurations

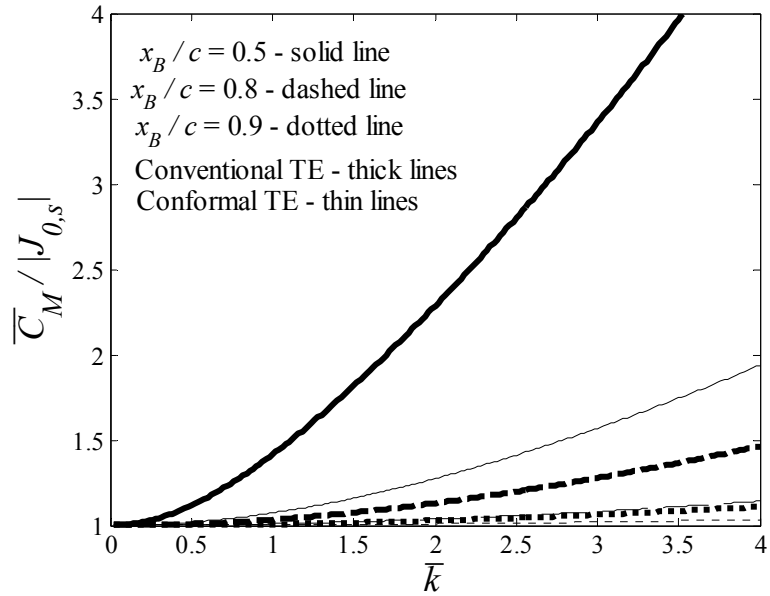


Figure 3.26: The quarter-chord pitching moment amplitude for TE configurations

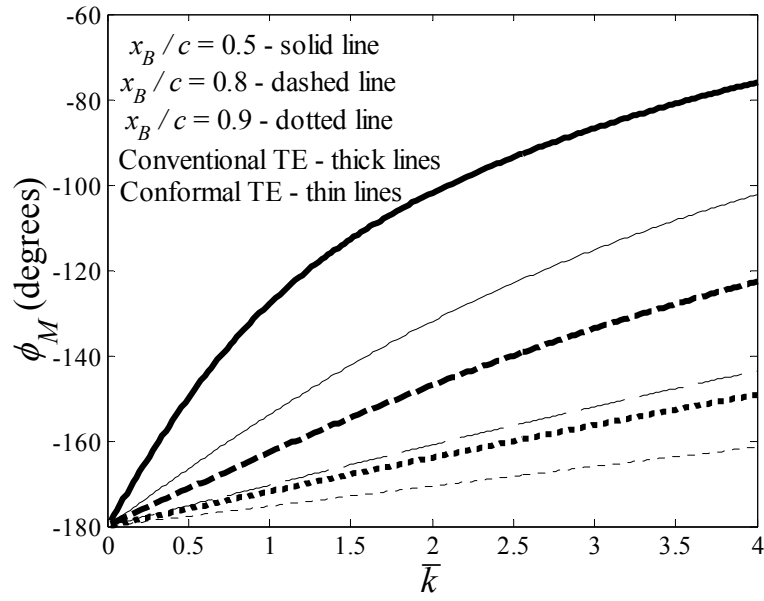


Figure 3.27: The quarter-chord pitching moment phase angle for TE configurations

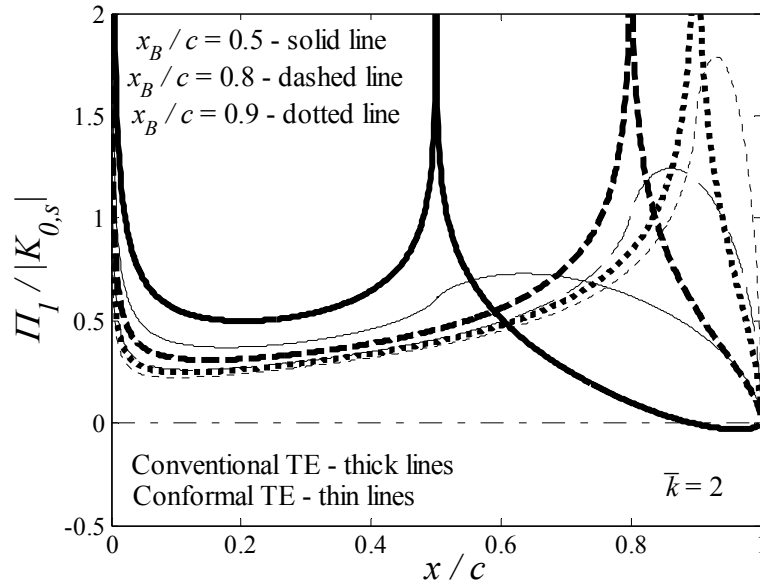


Figure 3.28: The in-phase component of the load distribution for TE configurations

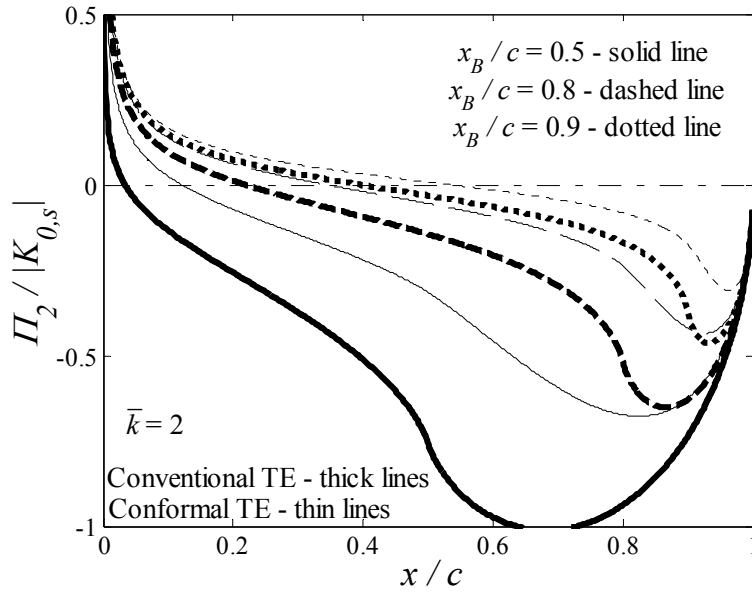


Figure 3.29: The out-of-phase component of the load distribution for TE configurations

b) LE Configurations

Figures 3.30 through 3.35 present the results of Eq. (3.15-3.20) for the conventional and conformal LE flaps. Figure 3.30 shows that the smaller flap sizes have a larger normalized lift magnitude, which is opposite of the TE case. The various cases appear to be similar in Figure 3.30 compared to the TE cases in Figure 3.28. Notice that at \bar{k} equal to 4, the lift magnitudes are approximately 3.75 times the quasi-steady value, which are significantly different than the values for the TE cases. Figure 3.31 shows that ϕ_L is 180 degrees out-of-phase with the flap deflection at \bar{k} equal to zero and increases with increasing \bar{k} . The trends shown Figures 3.32 and 3.33 for the pitching moment amplitude and phase angle are similar to those shown for the TE configurations. Figures 3.34 and 3.35 show the in-phase and out-of-phase components of the load distribution for a \bar{k} of 2. The large gradient near the leading edge of the in-phase components shown in Figure 3.34 indicate that the thin airfoil theory prediction is not likely to be accurate. This large gradient is present for small flap sizes because of the combination of $T_{0,s}$ and χ in Eq. (3.19). Past theoretical or experimental studies on oscillating leading edge flaps could not be found by the author.

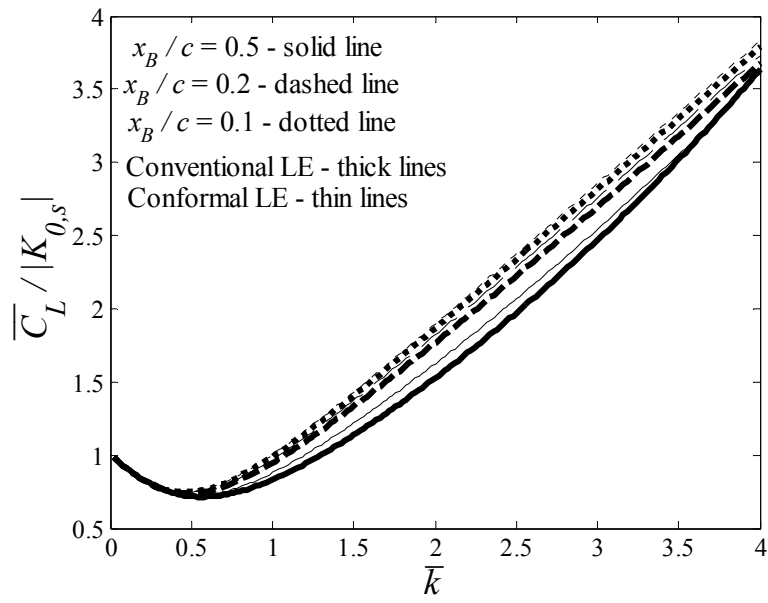


Figure 3.30: The lift coefficient amplitude for LE configurations

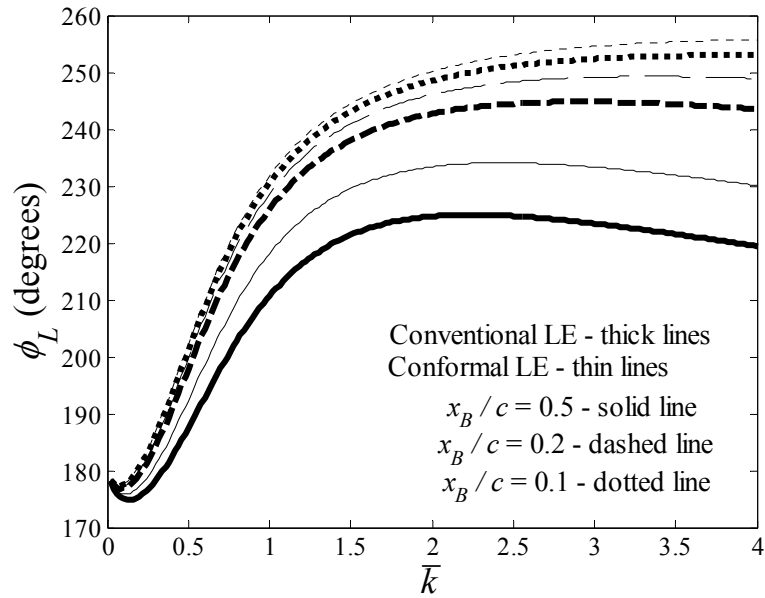


Figure 3.31: The lift coefficient phase angle for LE configurations

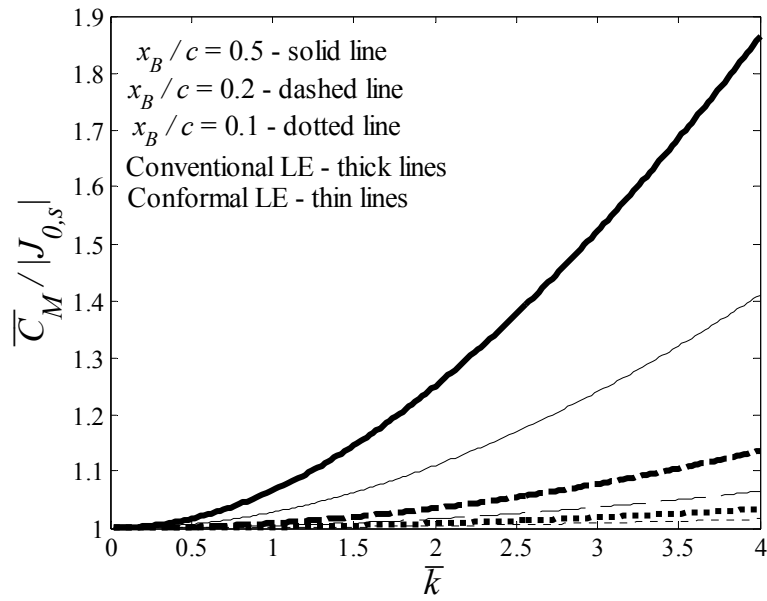


Figure 3.32: The quarter-chord pitching moment amplitude for LE configurations

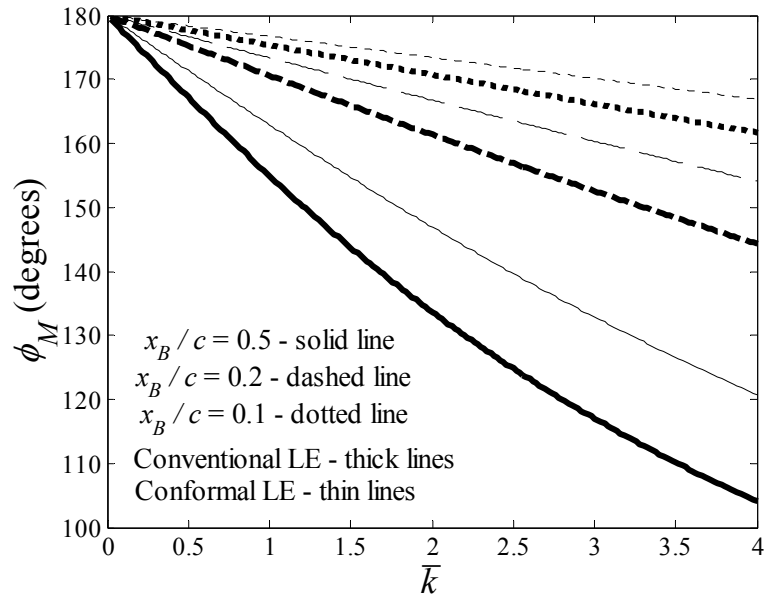


Figure 3.33: The quarter-chord pitching moment phase angle for LE configurations

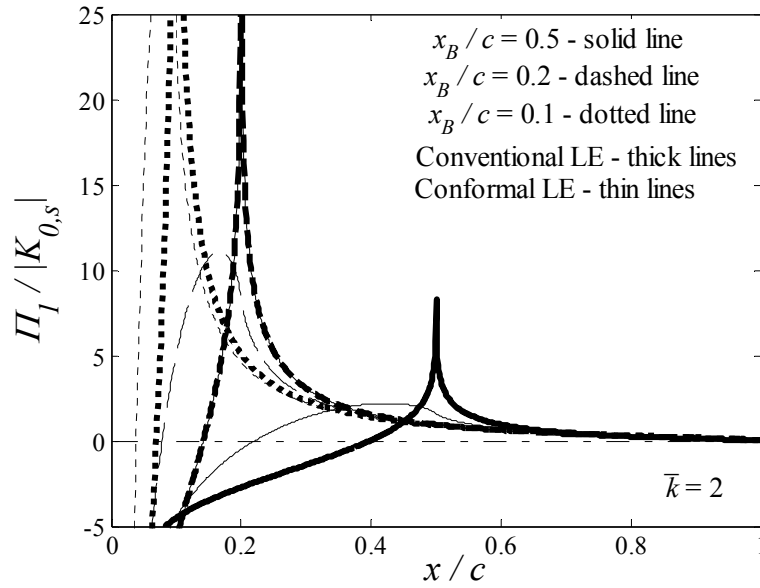


Figure 3.34: The in-phase component of the load distribution for LE configurations

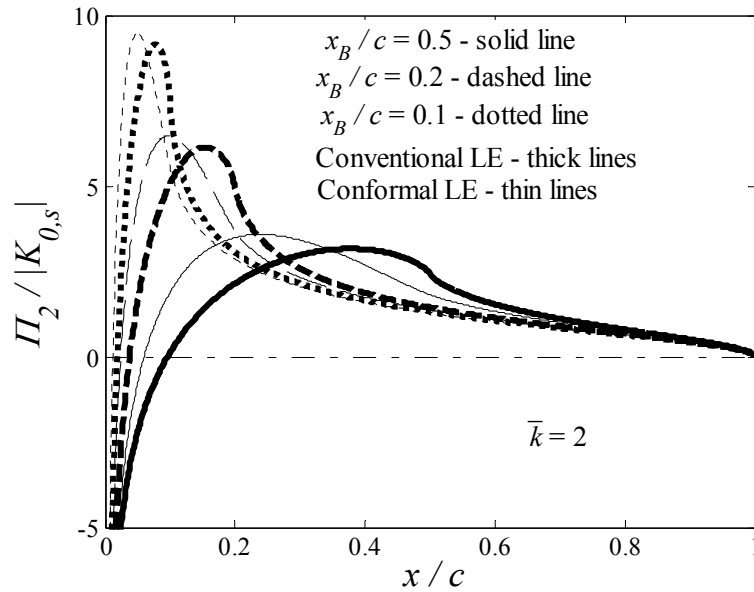


Figure 3.35: The out-of-phase component of the load distribution for LE configurations

b) NACA Configurations

Figures 3.36 through 3.41 present the results of Eq. (3.15-3.20) for the NACA configurations discussed in Section 3.5. These results have never been presented in the literature. The comparison between configurations A and B is interesting because both configurations (with the

same x_B) have the same $K_{0,s}$ and $J_{0,s}$ value. As mentioned previously, configuration B can be obtained by superimposing a heaving motion onto configuration A. The effect of maximum camber location (x_B) is seen to have a similar effect for both cases. Figures 3.36 and 3.38 show that both the magnitude of lift and pitching moment are significantly larger for configuration A. Figures 3.37 and 3.39 show that both phase angles vary more for configuration B. In particular, Figure 3.37 shows that the phase angle for lift becomes large and positive for configuration B while it remains negative for configuration A. The load distributions for both configurations are shown in Figures 3.40 and 3.41 for a \bar{k} of 2. Figure 3.40 shows that the in-phase components are similar in shape for the two configurations. On the other hand, the out-of-phase components, shown in Figure 3.41, are very dissimilar in shape. A significant difference is the leading edge singularity, which is of opposite sign for the two configurations. It is interesting to note that the out-of-phase load distribution for configuration B is equal to zero at three locations along the chord.

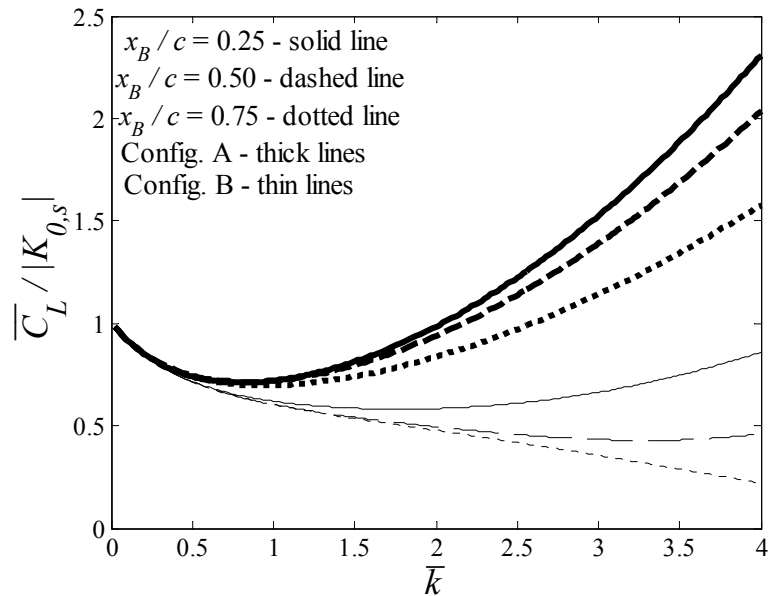


Figure 3.36: The lift coefficient amplitude for NACA configurations

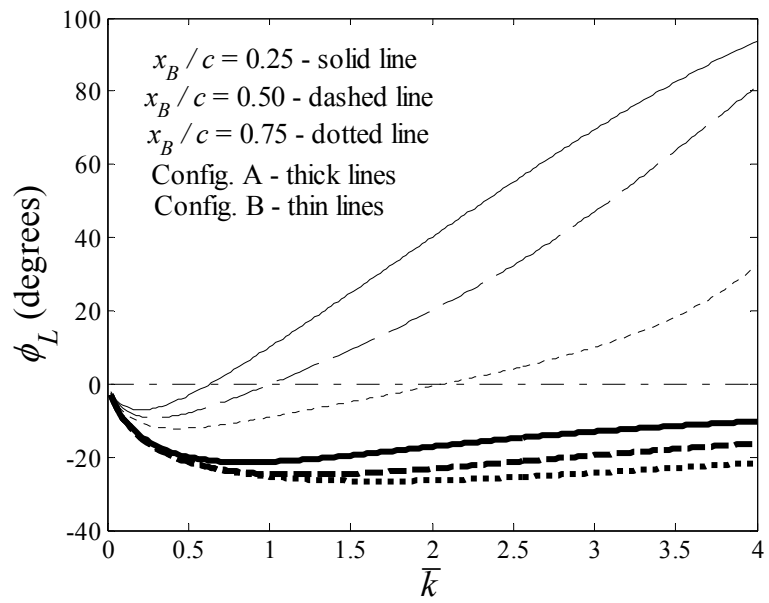


Figure 3.37: The lift coefficient phase angle for NACA configurations

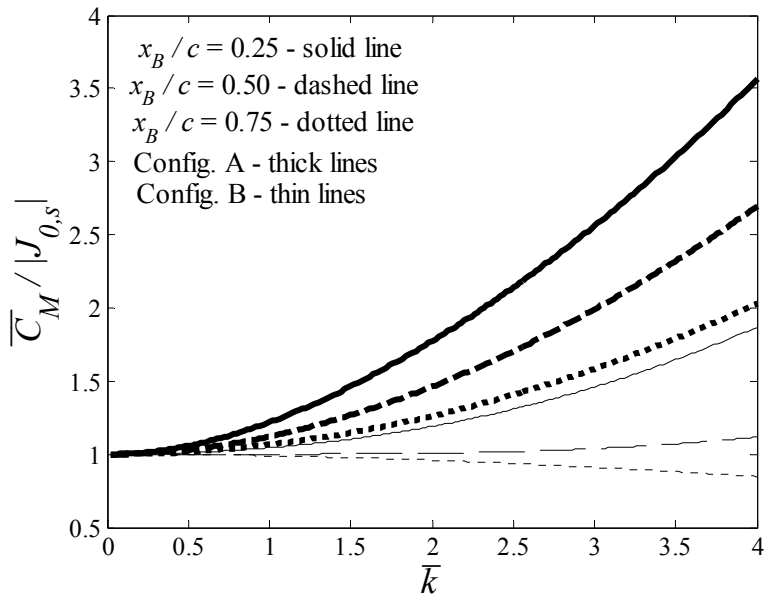


Figure 3.38: The quarter-chord pitching moment amplitude for NACA configurations

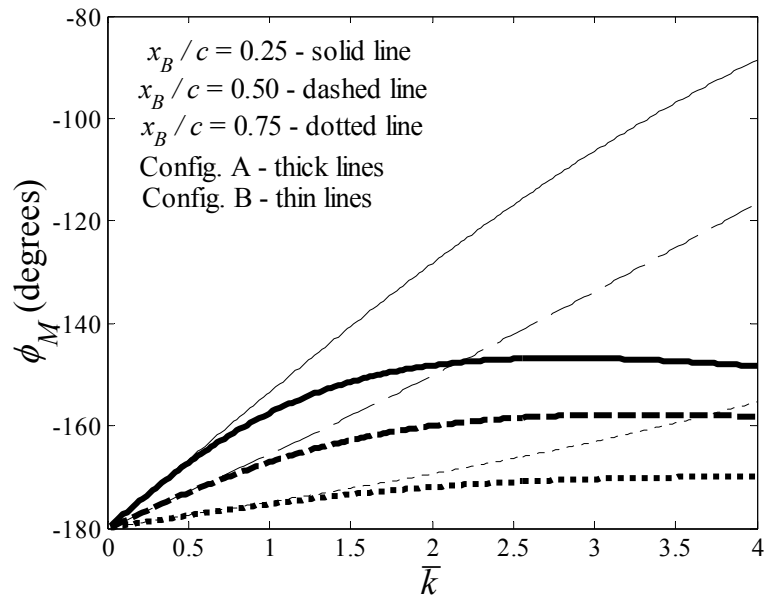


Figure 3.39: The quarter-chord pitching moment phase angle for NACA configurations

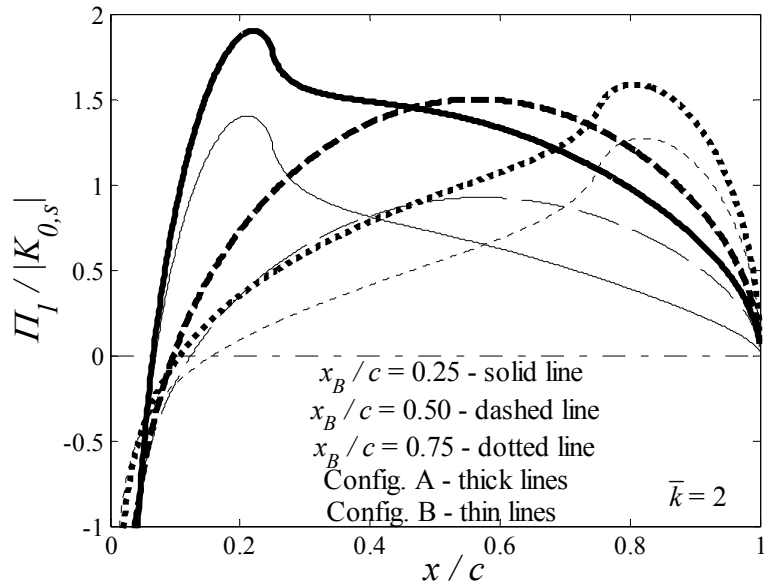


Figure 3.40: The in-phase component of the load distribution for NACA configurations

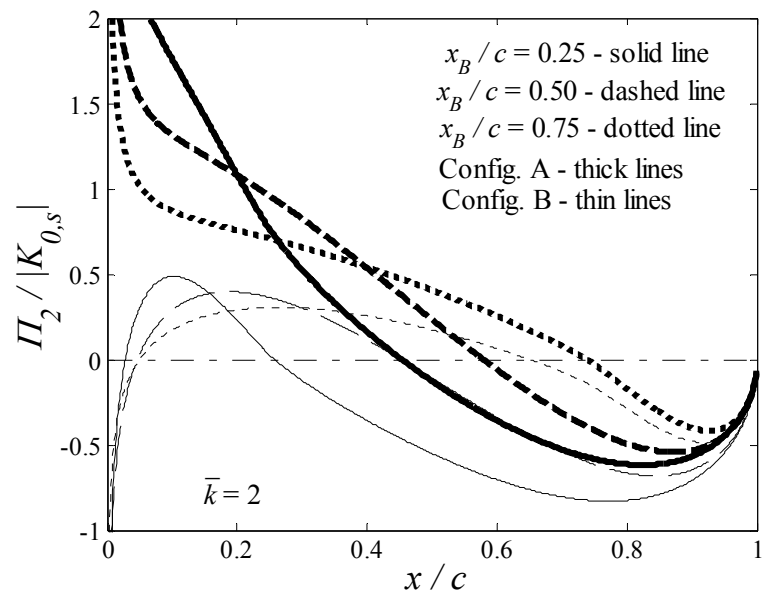


Figure 3.41: The out-of-phase component of the load distribution for NACA configurations

Chapter 4

Drag in Unsteady Thin Airfoil Theory

4.1 Introduction

This chapter presents a method of calculating the drag on an unsteady thin airfoil. In particular, the calculation of the drag on airfoils with deforming camberlines will be discussed. A clear presentation of the transient drag calculation on deforming airfoils seems to be absent from the literature. Although the transient drag for an oscillating flat plate and an airfoil with a trailing edge flap have been studied, the focus has been on rotorcraft (Lieshman [1991, 2000] and Li, *et al.* [1990, 1991]), bird flight (Garrick [1936]), and fish propulsion (Wu [1961, 1971]) applications. Past discussions on transient drag (von Karman and Burgers [1935], Garrick [1957], Leishman [1988, 2000], and Weihs and Katz [1986]) are not directly applicable to general deforming camberline shapes. A discussion of the lack of drag in steady flow will be presented in the first section of this chapter in hopes of clarifying some of the subtleties which may confuse the unsteady drag calculation. The drag equation for unsteady flow will be derived and applied to various airfoil configurations. In addition, it will be shown that the transient drag on a suddenly accelerated thin airfoil with a given steady state lift is independent of the camberline shape and angle of attack. The drag for an oscillating camberline will be derived and the asymptotic limits for large and small reduced frequencies will be examined.

4.2 The Lack of Drag in Steady Thin Airfoil Theory

It is well known that in 2D steady, unbounded, incompressible airfoil theory there is no drag component acting on the airfoil. This fact is proved easily by considering an energy balance for the system. With no wake trailing from a steadily moving airfoil, there is no place for the energy

created from the combination of drag and free-stream velocity to go. Hence, the presence of drag is impossible. Of course in reality, because of the vorticity created in the boundary layer, there is a wake shed from a steadily moving airfoil. Thus, the presence of drag on a steadily moving airfoil in a real fluid is justified.

The aerodynamic forces acting on a flat plate in steady flow are shown in Figure 4.1. The leading-edge thrust coefficient (C_a) is a result of the leading-edge singularity in the pressure distribution. It is defined as [Garrick 1957]

$$C_a = \frac{\pi}{8} \lim_{x \rightarrow 0} \{ \Delta C_p^2(x)x \} \quad (4.1)$$

From Eq. (2.5) (note $\Delta C_p = 2\gamma$), the ΔC_p for a flat plate at angle of attack can be written as

$$\Delta C_p(\theta) = 4\alpha \frac{1 + \cos \theta}{\sin \theta} \quad (4.2)$$

Substituting Eqs. (4.2) into (4.1) and taking the limit as θ goes to zero results in the following

$$C_a = 2\pi\alpha^2 \quad (4.3)$$

It is well known from steady thin airfoil theory that the normal force coefficient (C_n) may be written as

$$C_n \cong C_l = 2\pi\alpha \quad (4.4)$$

Taking the forces acting in the direction opposite of the free-stream velocity in Figure 4.1, the drag force can be written as

$$C_d = C_n \sin \alpha - C_a \cos \alpha \quad (4.5)$$

Substituting Eqs. (4.3) and (4.4) into Eq. (4.5) and assuming small angles results in the following

$$\begin{aligned} C_d &= (2\pi\alpha)(\alpha) - (2\pi\alpha^2)(1) \\ &= 0 \end{aligned} \quad (4.6)$$

which is the expected (and required) result.

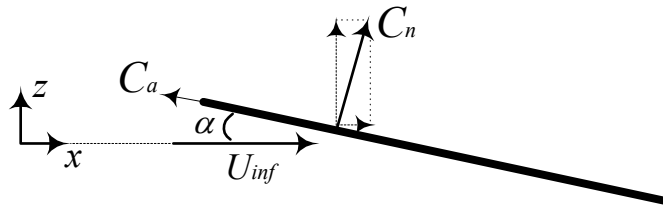


Figure 4.1: The aerodynamic forces acting on a flat plate in steady flow

What if we add a trailing-edge flap of length a to the airfoil in Figure 1? Now the camberline is not a straight line, so C_n is inclined to the free-stream by α and the camberline slope. Therefore, Eq. (4.5) cannot be directly applied. Instead, a more general expression for C_d is used, which can be written as

$$C_d = \int_0^c \Delta C_p(x) \left[-\frac{dz}{dx}(x) \right] dx - C_a \quad (4.7)$$

where the free-stream velocity is defined to lie along the x -axis as shown in Figure 4.1 and 4.2. Therefore, the drag is parallel to the x -axis and the lift is perpendicular. In Chapter 3, the function $z(x)$ was defined for a general airfoil camberline with zero angle of attack. For a flapped airfoil, the ΔC_p distribution is obtained from Eqs. (3.8), (3.11), and Table 3.1, which results in

$$\Delta C_p(\theta) = 4 \left\{ \left[\alpha + \beta \left(1 - \frac{\theta_B}{\pi} \right) \right] \left[\frac{1 + \cos \theta}{\sin \theta} \right] + \frac{1}{\pi} \ln \left(\frac{\sin \theta \tan(\theta_B / 2) - \cos \theta + 1}{\sin \theta \tan(\theta_B / 2) + \cos \theta - 1} \right) \right\} \quad (4.8)$$

where β is the flap deflection angle and θ_B is the location of the hinge line. Eq. (4.8) contains an angle of attack term which is not present in the equations developed in Chapter 3. Note that the 2nd term in Eq. (4.8) does not contain a leading edge singularity. Using Eq. (4.8), the integral in Eq. (4.7) may be evaluated and shown to cancel C_a , which results in zero drag as it should. It is helpful to see how the integral in Eq. (4.7) cancels C_a . Consider first the flapped airfoil at zero degrees angle of attack. The integral in Eq. (4.7) reduces to the following

$$\begin{aligned} & \int_{\theta_B}^{\pi} 2\beta^2 \left\{ \left(1 - \frac{\theta_B}{\pi} \right) \left[\frac{1 + \cos \theta}{\sin \theta} \right] + \frac{1}{\pi} \ln \left(\frac{\sin \theta \tan(\theta_B / 2) - \cos \theta + 1}{\sin \theta \tan(\theta_B / 2) + \cos \theta - 1} \right) \right\} \sin \theta d\theta \\ & = \frac{2\beta^2}{\pi} (\pi^2 - 2\pi\theta_B + \theta_B^2) \end{aligned} \quad (4.9)$$

which represents the normal force on the flap in the direction parallel to the free-stream. According to Eq. (4.7), this force should be balanced by the leading edge suction, which from Eq. (4.1) is found to equal

$$C_a = 2\pi\beta^2 \left(1 - 2\frac{\theta_B}{\pi} + \frac{\theta_B^2}{\pi^2} \right) \quad (4.10)$$

Eqs. (4.9) and (4.10) show that the two forces do cancel each other. Note that the direction of the leading edge suction for cambered airfoils is not important (the only significant component will be drag). This is because any lift component from the leading edge suction is third order in the camberline slope, which is beyond the order of accuracy of thin airfoil theory.

We have shown examples of the absence of drag for a flat plate at angle of attack and a flapped airfoil at zero degrees angle of attack. What about a combination of flap deflection and angle of attack? The drag is not linear and is therefore not simply the addition of the two separate cases. There is coupling between the two cases, meaning the pressure distribution due to the flap deflection acts on the flat plate at angle of attack and the pressure distribution due to angle of attack acts on the flap. This coupling is obvious if the pressure distribution due to both the flap deflection and angle of attack (Eq. 4.8) is substituted into Eq. (4.7). The streamwise force caused by the flapped airfoil pressure distribution acting on the flat plate at angle of attack is

$$\int_0^\pi 2\beta\alpha \left\{ \left(1 - \frac{\theta_B}{\pi}\right) \left[\frac{1 + \cos\theta}{\sin\theta} \right] + \frac{1}{\pi} \ln \left(\frac{\sin\theta \tan(\theta_B/2) - \cos\theta + 1}{\sin\theta \tan(\theta_B/2) + \cos\theta - 1} \right) \right\} \sin\theta d\theta \quad (4.11)$$

$$= 2\beta\alpha(\pi - \theta_B + \sin\theta_B)$$

The streamwise force caused by the flat-plate-at-angle-of-attack pressure distribution acting on the flapped airfoil is

$$\int_{\theta_B}^\pi 2\beta\alpha \left[\frac{1 + \cos\theta}{\sin\theta} \right] \sin\theta d\theta \quad (4.12)$$

$$= 2\beta\alpha(\pi - \theta_B - \sin\theta_B)$$

Adding Eqs. (4.11) and (4.12) results in the streamwise force that must be balanced by the leading edge suction in order for the drag to be zero. From Eqs. (4.7) and (4.1) the leading edge suction can be written as

$$C_a = 2\pi \left[\alpha + \beta \left(1 - \frac{\theta_B}{\pi}\right) \right]^2 \quad (4.13)$$

$$= 2\pi \left[\alpha^2 + \beta^2 \left(1 - \frac{\theta_B}{\pi}\right)^2 + 2\beta\alpha \left(1 - \frac{\theta_B}{\pi}\right) \right]$$

The first two terms in Eq. (4.13) cancel the angle of attack only (Eq. 4.9) and flap only (Eq. 4.4) terms shown in the previous two examples. The last term in Eq. (4.13) is the coupled term that must cancel the sum of Eqs. (4.11) and (4.12), which it does.

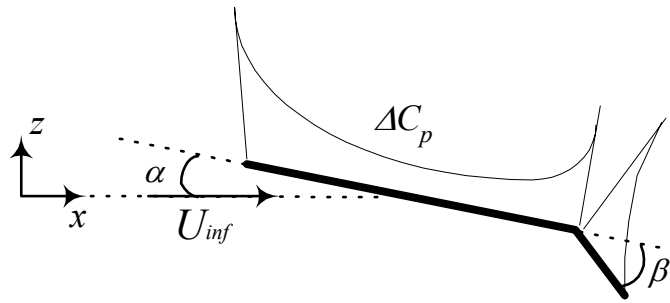


Figure 4.2: Airfoil with a flap showing the load distribution

4.3 The Presence of Drag in Unsteady Thin Airfoil Theory

This section will develop an expression for the inviscid drag on a deforming thin airfoil. This derivation is general to both an airfoil with a deforming camberline and/or an airfoil undergoing pitch/plunge motions. Chapter 3 derived the equations for the lift, pitching moment, and pressure distribution caused by the unsteady motion of the general camberline defined in Tables 3.1 and 3.2. The effect of pitch and plunge motions was not discussed because the results are well known and may simply be added to the deforming camberline results. Unlike the lift, pitching moment, and pressure distribution, which are linear with respect to the airfoil geometry and motion, the unsteady drag is quadratic. Therefore, the influence of general time-varying pitch and plunge motions cannot simply be added to the drag expression for the deforming camberline. But, pitch and plunge motions can be added to the deforming camberline results if the time variation of the pitch and plunge motion is the same as the time variation of the camberline deformation. This allows the general motion of the airfoil and camberline to remain a function of one time-varying parameter (β) and therefore Eq. (2.48) still applies. This approach requires that the appropriate terms be added to the coefficients in Table 3.1 to account for the pitch and plunge motions. From Eq. (2.70), the unsteady load distribution can be written as

$$\Delta C_p(\theta, t) = \alpha_{un}(t)\chi(\theta) + (\bar{A}_{0,s}\chi(\theta) + T_{0,s}(\theta))\beta(t) + (\bar{A}_{0,d}\chi(\theta) + T_{0,d}(\theta) + T_{1,s}(\theta))\beta'(t) + T_{1,d}(\theta)\beta''(t) \quad (4.14)$$

where the α_{un} component represents $\Delta C_{p,2}$ and is defined as

$$\alpha_{un}(t) = \frac{L_2(t)}{2\pi q c} \quad (4.15)$$

An important property of the T terms in Eq. (4.14) is that they do not contain leading edge singularities; hence they do not contribute to the leading edge thrust (Leishman [2000]). From Eqs. (4.1) and (4.14), the leading edge thrust can be written as

$$C_a(t) = 2\pi \left[\bar{A}_{0,s}\beta(t) + \bar{A}_{0,d}\beta'(t) + \alpha_{un}(t) \right]^2 \quad (4.16)$$

Substituting Eqs. (4.14) and (4.16) into (4.1) results in the following equation for the unsteady drag

$$C_d = \int_0^\pi \left\{ \alpha_{un}\chi(\theta) + (\bar{A}_{0,s}\chi(\theta) + T_{0,s}(\theta))\beta + (\bar{A}_{0,d}\chi(\theta) + T_{0,d}(\theta) + T_{1,s}(\theta))\beta' + T_{1,d}(\theta)\beta'' \right\} \left[-\frac{\partial z}{\partial x}(\theta) \right] \frac{1}{2} \sin \theta d\theta - 2\pi \left[\bar{A}_{0,s}^2 \beta^2 + \bar{A}_{0,d}^2 \beta'^2 + \alpha_{un}^2 + 2\bar{A}_{0,d}\beta'\alpha_{un} + 2\bar{A}_{0,d}\bar{A}_{0,s}\beta'\beta + 2\bar{A}_{0,s}\beta\alpha_{un} \right] \quad (4.17)$$

Eq. (4.17) may be simplified by recalling the cancellation of drag that occurs in steady airfoil theory. In terms of the present notation, the cancellation of the steady drag can be written as

$$\beta \int_0^\pi \{A_{0,s} \chi(\theta) + T_{0,s}(\theta)\} \left[-\frac{\partial z}{\partial x} \right] \frac{1}{2} \sin \theta d\theta - 2\pi \bar{A}_{0,s}^2 \beta^2 = 0 \quad (4.18)$$

Substituting Eq. (4.18) into Eq. (4.17) results in the following

$$C_d = \int_0^\pi \left\{ \alpha_{un} \chi(\theta) + (\bar{A}_{0,d} \chi(\theta) + T_{0,d}(\theta) + T_{1,s}(\theta)) \beta' + T_{1,d}(\theta) \beta'' \right\} \left[-\frac{\partial z}{\partial x}(\theta) \right] \frac{1}{2} \sin \theta d\theta \quad (4.19)$$

$$- 2\pi \left[\bar{A}_{0,d}^2 \beta'^2 + \alpha_{un}^2 + 2\bar{A}_{0,d} \beta' \alpha_{un} + 2\bar{A}_{0,d} \bar{A}_{0,s} \beta' \beta + 2\bar{A}_{0,s} \beta \alpha_{un} \right]$$

This equation can be further simplified by recognizing the following relationships

$$\int_0^\pi \chi(\theta) \left[-\frac{\partial z}{\partial x} \right] \frac{1}{2} \sin \theta d\theta = 2\pi \left(\bar{A}_{0,s} - \frac{1}{2} \bar{A}_{1,s} \right) \beta \quad (4.20)$$

$$K_{0,s} = \pi (2\bar{A}_{0,s} + \bar{A}_{1,s}) \beta \quad (4.21)$$

which reduces Eq. (4.19) to the following

$$C_d = -K_{0,s} \beta (\bar{A}_{0,d} \beta' + \alpha_{un}) + \int_0^\pi \left\{ (T_{0,d}(\theta) + T_{1,s}(\theta)) \beta' + T_{1,d}(\theta) \beta'' \right\} \left[-\frac{\partial z}{\partial x}(\theta) \right] \frac{1}{2} \sin \theta d\theta \quad (4.22)$$

$$- 2\pi (\bar{A}_{0,d} \beta' + \alpha_{un})^2$$

Eq. (4.22) is relatively complicated and deserves some explanation. First of all, this drag is not totally “induced” drag. The induced drag components are the components depending on α_{un} , meaning the downwash from the wake is responsible for the drag (as in classical incompressible 3-D wing theory). In addition to the induced drag, there is apparent mass and aerodynamic damping drag. The apparent mass drag is a result of the apparent mass force contributing to the normal force but not contributing to the leading edge thrust. The damping drag is a result of the aerodynamic damping forces being caused by a fictitious camberline, meaning you could draw a camberline in Figure 2.3 that resulted in the same steady boundary condition. But for an actual camberline, the normal force would be inclined from the camberline slope (as in Figure 4.2). As shown in the previous section, there is a balance between the camberline slope, leading edge thrust, and load distribution so that the drag is always zero in steady theory. The fact that the damping load distribution is not caused by an actual camberline slope, but instead by camberline motion (as shown in Figure 2.4), disrupts the balance between the camberline slope, leading edge thrust, and load distribution and drag (or thrust) therefore results.

4.4 The Drag for a Suddenly Accelerated Flat Plate

The simplest example of unsteady drag is the drag acting on a suddenly accelerated flat plate. Because the acceleration is sudden, the apparent mass acts only at $t = 0$ and the damping terms are zero; hence the drag for the motion after $t = 0$ is all induced drag. For this case, the drag expression in Eq. (4.22) reduces to the following

$$C_d(\tau) = -(K_{0,s}\beta + 2\pi\alpha_{un}(\tau))\alpha_{un}(\tau) + \delta(\tau) \int_0^\pi T_{1,s}(\theta) \left[-\frac{\partial z}{\partial x}(\theta) \right] \frac{1}{2} \sin \theta d\theta \quad (4.23)$$

where the Dirac delta function on the last term represents the infinite apparent mass term acting at $t = 0$. This equation was presented by Lomax [1960], although he used a different approach to obtain it. The theoretical result obtained Chuen and Huang [1982] agrees with Eq. (4.23), except they do not include the infinite term at $t = 0$. Equation (4.23) shows that it does not matter whether we are dealing with a suddenly accelerated flat plate or suddenly accelerated cambered airfoil, as long the steady lift ($K_{0,s}\beta$) is the same. Stated another way, this says that the chordwise load distribution does not affect the induced drag as long as the total integrated force is the same. This is not an obvious point and has apparently not been recognized in past literature. It is interesting to note that Munk's stagger theorem (Munk [1923]) states an analogous result for the induced drag of steady three dimensional wings. Figure 4.3 shows a comparison of Eq. (4.23) and the numerical computation of Katz and Plotkin [2001] (the infinite value at $t = 0$ is not shown). The present method may be considered exact under the linearized assumptions of thin airfoil theory. Katz and Plotkin obtain their results through a discrete "time-stepping" method. Because there are time-derivative terms in the unsteady force calculation, discrete time steps introduce noticeable error in regions of rapid change. This explains the difference between the two methods shown in Figure 4.3 and emphasizes the benefit of the present analytic representation of the unsteady aerodynamic forces. It should be mentioned that the result shown in Figure 4.3 for $t = 0$ does not agree with the result of Weihs and Katz [1986], who propose a value of C_d at $t = 0$ that is twice as large as that shown (ignoring the infinite term). Their approach is unconventional and only deals with the value of C_d at $t = 0$. The discrepancy between their method and the method presented here seems to be the enforcement of the Kutta condition. Weihs and Katz model the airfoil at the very beginning of motion with a vortex of equal strength but opposite direction at the leading and trailing edge. Because a vortex is placed at the trailing edge, the Kutta condition is not satisfied. Therefore the forces on the airfoil will be different than those predicted by the present method, which requires that the vorticity is zero at the trailing edge.

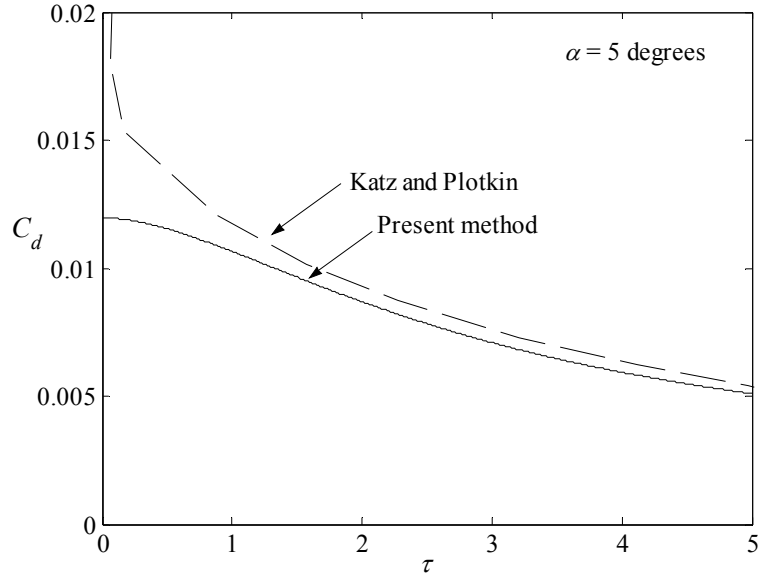


Figure 4.3: Transient induced drag for a suddenly accelerated flat plate

For airfoils with finite accelerations, the statement that the *induced* drag does not depend on chordwise load distribution remains true. But, in these cases the induced drag component is not the only component of inviscid drag. The finite acceleration causes the apparent mass to be finite, which as seen in Eq. (4.22), contributes to the drag through $T_{l,s}$ (there are still no damping terms for these cases). For these cases, Eq. (4.22) reduces to the following

$$C_d(\tau) = -(K_{0,s}\beta + 2\pi\alpha_{un})\alpha_{un} + \int_0^\pi T_{l,s}(\theta) \left[-\frac{\partial z}{\partial x}(\theta) \right] \frac{1}{2} \sin\theta d\theta \quad (4.24)$$

If it was desired to calculate the camberline shape and angle of attack for minimum drag for a given final value of lift, then only the last two terms in Eq. (4.24) need to be considered. Thus, our “stagger theorem” simplifies the problem considerably. It should be mentioned that for an accelerated airfoil, α_{un} may be calculated using the Duhamel integral as discussed in Section 2.4. This fact which was proved by Ashley *et al.* [1952]. Note that for this case Eq. (2.49) and (2.50) are written as

$$w_s = \frac{U(\tau)}{U_{ref}} \frac{\partial \psi}{\partial x} \beta \quad (4.25)$$

$$w_d = 0 \quad (4.26)$$

where U_{ref} is the reference velocity used to nondimensionalize the force coefficients.

4.5 A Comparison Drag for a ΔC_l

This section will compare the drag on an airfoil as the lift is changing in unaccelerated motion. Three different lift changing devices, a pitching flat plate, flapped airfoil, and parabolic camber airfoil will be compared with each being subject to a ramp input. If it was desired to compare the drag for a sudden change in lift, the results of a sudden acceleration from the previous section would apply. Note that the drag goes as $1/\tau$ as τ approaches infinity. This will be of great significance in Chapter 5.

Figure 4.4 shows the time-history of the drag coefficient for the three configurations mentioned above. Each configuration is subject to a ramp (linear) input of β so that when $\tau = 1$ the control input corresponds to a steady state C_l of 0.1. For the control input stage ($\tau < 1$), apparent mass, damping, and wake-effect forces are all acting on the airfoil and contribute to the drag as shown in Eq. (4.22). When the control input stage is complete ($\tau > 1$), the damping and apparent mass forces immediately terminate. In this stage only the wake effect term contributes to the drag.

The pitching flat plate case (x_a is the location of the axis of rotation) is seen in Figure 4.4 to have the greatest drag during the control input stage. This is because of the large damping force created by the pitching plate. At the very beginning of motion, the pitching flat plate actually produces thrust instead of drag, although only for a very short period of time. The variable camber case (x_B indicates the location of maximum camber) produces a larger amount of thrust than the pitching plate case. The $x_B = 0.5$ case is seen to have the largest drag in the stage after the motion while the $x_B = 0.3$ case has the smallest drag. This shows the importance of the location of maximum camber on the unsteady aerodynamic characteristics of a variable camber airfoil.

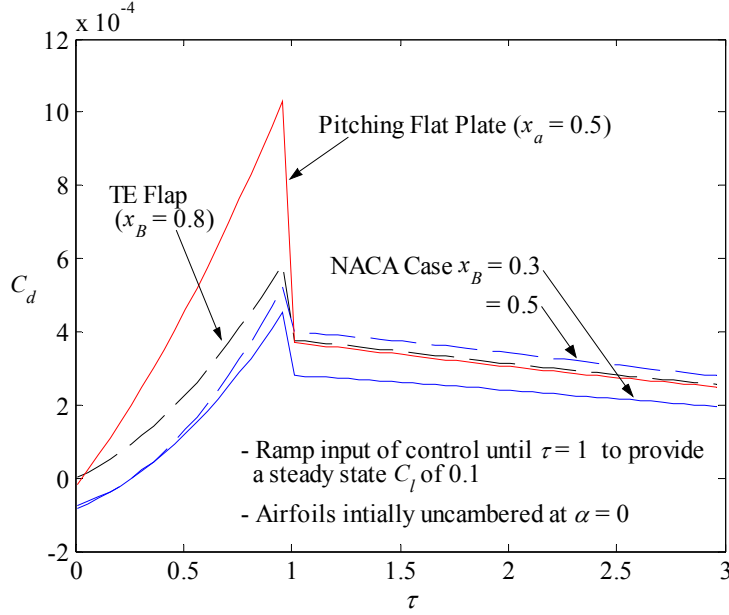


Figure 4.4: Drag for various configurations subject to a ramp input of control command

4.6 The Drag on an Airfoil with a Sinusoidal β

In Section 2.6, the lift, pitching moment, and load distribution of an airfoil with an oscillating β were determined. Chapter 3 determined the aerodynamic characteristics for a general two-segment camberline where β could represent a variety of camberline shapes. This section will apply the general camberline solution of Chapter 3 and the equations presented in Section 2.6 to determine the drag acting on an airfoil with an oscillating β . Some interesting discussions on determining the drag on an oscillating airfoil through a wake analysis are given by Weihs [1972] and Michelson [1963].

Applying the results of Section 3.6, the drag can be written from Eq. (4.22) as follows

$$C_d = -K_{0,s} \bar{\beta}^2 \cos(\bar{k}\tau) \left(-\bar{A}_{0,d} \bar{k} \sin(\bar{k}\tau) + \alpha_{un} \right) - \int_0^\pi \left\{ \begin{array}{l} (T_{0,d}(\theta) + T_{1,s}(\theta)) \bar{k} \sin(\bar{k}\tau) \\ + T_{1,d}(\theta) \bar{k}^2 \cos(\bar{k}\tau) \end{array} \right\} \left[-\frac{\partial \psi}{\partial x}(\theta) \cos(\bar{k}\tau) \right] \frac{\bar{\beta}^2}{2} \sin \theta d\theta - 2\pi \bar{\beta}^2 \left(-\bar{A}_{0,d} \bar{k} \sin(\bar{k}\tau) + \alpha_{un} \right)^2 \quad (4.27)$$

where α_{un} is the wake effect term, which is written as

$$\alpha_{un}(\tau) = \alpha_A \bar{\beta} \cos(\bar{k}\tau) + \alpha_B \bar{\beta} \sin(\bar{k}\tau) \quad (4.28)$$

$$\alpha_A(\tau) = \frac{1}{2\pi} [K_{0,s}(F-1) - K_{0,d}\bar{k}G]$$

$$\alpha_B(\tau) = \frac{1}{2\pi} [-K_{0,s}G - K_{0,d}\bar{k}(F-1)]$$

For most practical purposes we are interested in the average value of drag over one cycle, which will be defined as

$$\bar{C}_d = \frac{\bar{k}}{2\pi} \int_0^{2\pi/\bar{k}} C_d(\tau) d\tau \quad (4.29)$$

From (4.27) and (4.29), the average drag evaluates to

$$\bar{C}_d = \frac{\bar{\beta}^2}{2} \left[\begin{array}{l} -K_{0,s}\alpha_A + \frac{\bar{k}^2}{2} \int_0^\pi T_{1,d}(\theta) \frac{\partial \psi}{\partial x}(\theta) \sin \theta d\theta \\ -2\pi \left((\alpha_B - \bar{A}_{0,d}\bar{k})^2 + \alpha_A^2 \right) \end{array} \right] \quad (4.30)$$

which from Eq. (4.28) can be written as

$$\bar{C}_d = -\frac{\bar{\beta}^2}{4\pi} \left[\begin{array}{l} K_{0,s} [K_{0,s}(F-1) - K_{0,d}\bar{k}G] - \pi \bar{k}^2 \int_0^\pi T_{1,d}(\theta) \frac{\partial \psi}{\partial x}(\theta) \sin \theta d\theta \\ + [-K_{0,s}G - K_{0,d}\bar{k}(F-1) - 2\pi \bar{A}_{0,d}\bar{k}]^2 + [K_{0,s}(F-1) - K_{0,d}\bar{k}G]^2 \end{array} \right] \quad (4.31)$$

After some cancellations, the final equation for average drag is written as

$$\bar{C}_d = -\frac{\bar{\beta}^2}{4\pi} \left[\begin{array}{l} K_{0,s} [K_{0,s}(F-1) - K_{0,d}\bar{k}G] - \pi \bar{k}^2 \int_0^\pi T_{1,d}(\theta) \frac{\partial \psi}{\partial x}(\theta) \sin \theta d\theta \\ + [-K_{0,s}G - K_{0,d}\bar{k}(F-1) - 2\pi \bar{A}_{0,d}\bar{k}]^2 + [K_{0,s}(F-1) - K_{0,d}\bar{k}G]^2 \end{array} \right] \quad (4.32)$$

Applying the asymptotic form of the Theodorsen function for small values of \bar{k} given in Eq. (2.45), Eq. (4.32) reduces to the following

$$\bar{C}_d = \frac{(K_{0,s}\bar{\beta})^2}{16\pi} \left[\pi \bar{k} - (\bar{k} \ln \bar{k})^2 \right] + O(\bar{k}^2 \ln \bar{k}) \quad (4.33)$$

which shows that the average drag tends to zero like \bar{k} as $\bar{k} \rightarrow 0$. It is interesting to note that, as determined by Wu [1961], the instantaneous drag (C_d) tends to zero like $\bar{k} \log \bar{k}$ as $\bar{k} \rightarrow 0$. But, the $\bar{k} \log \bar{k}$ term does not contribute to the *average* drag. To determine the behavior of the average drag for large values of \bar{k} , Eq. (2.46) is substituted into Eq. (4.32) and terms of $O(1)$ retained. After some algebra, the following equation is obtained

$$\bar{C}_d = -\frac{\bar{\beta}^2}{4\pi} \left\{ \left[-\pi \int_0^\pi T_{1,d}(\theta) \frac{\partial \psi}{\partial x}(\theta) \sin \theta d\theta - 2\pi K_{0,d} A_{0,d} + \frac{K_{0,d}^2}{4} + 4\pi^2 A_{0,d}^2 \right] \bar{k}^2 \right. \\ \left. - \frac{K_{0,s}^2}{4} + \frac{K_{0,s} K_{0,d}}{4} - \frac{3K_{0,d}^2}{16} + \pi K_{0,d} A_{0,d} - \pi K_{0,s} A_{0,d} \right\} + \mathcal{O}\left(\frac{1}{\bar{k}^2}\right) \quad (4.34)$$

This equation shows that the average drag behaves like \bar{k}^2 as $\bar{k} \rightarrow \infty$. This agrees with Wu's result for C_d for large values of \bar{k} .

Chapter 5

Aerodynamic Work and Actuator Energy Concepts

5.1 Introduction

Recent interest in morphing aircraft (Stanewsky [2000 and 2001]) has initiated research concerning the characteristics of unconventional aerodynamic control devices. These unconventional, or morphing, devices are meant to provide an alternative to conventional hinged-flap configurations. For the design of a morphing device, it is desired to determine the change in wing shape that most efficiently produces the necessary change in the aerodynamic forces. Thus, understanding the process of producing a change in wing shape is of fundamental importance for morphing aircraft. One of the main design issues related to understanding this process is avoiding the weight penalty for unnecessary actuator capability. For a requested change in wing shape, the actuators on the wing must provide the work required to deform the wing while being acted on by the aerodynamic forces. Determining the change in wing shape that requires the minimum actuator work allows the morphing device to operate efficiently and with minimum actuator weight (Forester *et al.* [2003a and 2003b], Gern *et al.* [2002], Pettit *et al.* [2001], Prock *et al.* [2002], Sanders *et al.* [2003]).

This chapter presents a theoretical study of the relationship between the change in camberline shape of a two-dimensional thin airfoil and the resistance of the aerodynamic forces to this change. This resistance will be represented by the work required from the actuators on the airfoil to overcome the aerodynamic forces while producing a change in camberline shape. The relationship between the output work produced by the actuators and the required input energy will

be discussed and shown to affect the optimal changes in wing shape. A general actuator model will be presented and used throughout the analysis. The method of unsteady thin airfoil theory presented in the previous chapters will be used to determine the aerodynamic forces. This method allows the aerodynamic load distribution to be represented analytically, which provides insight into the work calculation. The energy required to produce a change in lift for a pitching flat plate will be thoroughly analyzed. The minimum energy pitching axes will be determined for various cases. The analysis of the pitching flat plate is applicable to variable twist morphing concepts. A comparison and analysis of the actuator energy cost for a conventional flap, conformal morphing flap, and two variable camber configurations will be presented. The analytic nature of this study clarifies the fundamental issues involved with the process of producing a change in airfoil shape.

5.2 The Aerodynamic Energy Balance and Actuator Energy Cost

For a wing moving in an inviscid potential flow, energy transfer between the wing and the fluid is achieved through the mechanical work required to produce wing motion or deformation while overcoming the fluid forces. This energy balance is stated mathematically through the following equation for conservation of energy (Karman and Burgers [1935]),

$$P + DU = E \quad (5.1)$$

where P is the rate of work done by the wing against the fluid forces in a direction normal to the oncoming flow, D is the drag force, U is the free-stream velocity of the oncoming flow, and E is the kinetic energy dissipated to the flow per unit time. For a thin airfoil in incompressible potential flow, the first two of these components are defined as follows (Garrick [1936])

$$P(t) = -\int_0^c \Delta p(x, t) \left[\frac{\partial z_c}{\partial t}(x, t) \right] dx \quad (5.2)$$

$$D(t) = -\int_0^c \Delta p(x, t) \left[\frac{\partial z_c}{\partial x}(x, t) \right] dx - S(t) \quad (5.3)$$

where Δp is the pressure loading on the airfoil, z_c defines the camberline shape, and S is the leading-edge suction force. Viscous effects may be included in the energy balance (Eq. 5.1) by including the skin friction component of drag in D and viscous dissipation in E (Wu [1971]).

For the oscillatory motion of a thin airfoil, Wu [1961] shows that the average value of E over a period of oscillation is always positive. Wu [1972] later explains that this point is readily

apparent because in the frame of reference fixed to the undisturbed fluid, the kinetic energy of the basic flow is zero. Therefore, any unsteady motion of a body must increase the energy of the surrounding flow. It follows from Eq. (5.1) that for thrust to be generated from oscillatory airfoil motion, \bar{P} must be positive. The case of $\bar{P} < 0$ has a meaningful interpretation from two different points of view. The first point of view is that for an airfoil being propelled through a fluid. Although some energy is being taken from the flow (by definition of $\bar{P} < 0$), more energy is being supplied to propel the airfoil (because $\bar{E} < 0$, if $\bar{P} < 0$, then from Eq. (5.1) $\bar{D} > -\bar{P} > 0$). This case may be interpreted as flutter because the flow is supplying energy to the structure (Send [1992]). Patil [2003] points out that flutter analyses assume a constant flight speed, which is not practical because it implies that the aircraft propulsion system automatically accounts for the increase in drag caused by the unsteady wing motion. The second point of view is that of a fixed airfoil oscillating in an oncoming flow, which may be interpreted as the power extraction mode (Jones and Platzer [1997] and McKinney and Delaurier [1981]). The difference between this case and the flutter case is that here there is no energy spent on propulsion because the oncoming flow, such as naturally occurring wind, provides the $\bar{D}U$ component of energy. It should be mentioned that the flutter mode can also be interpreted as a power extraction mode if the structure is designed for the task. The drawback is that the power spent on propulsion due to the oscillations will always be greater than the harvested power because $\bar{E} < 0$.

For the transient motion or deformation of a thin airfoil, the consequences of the aerodynamic energy balance are significantly different from those of the oscillatory case discussed in the previous paragraph. The oscillatory case consists of a continuous motion that allows for a mean value over a period of oscillation to be defined. For the transient case, the unsteady motion ends at some prescribed time (t^*) while the aerodynamic forces continue to change. This means that P is zero after t^* , but the unsteady drag continues to act on the airfoil and therefore energy continues to be transferred to the wake. Notice that in the previous paragraph, no mention was made of the mean lift acting on the airfoil. This is because a constant aerodynamic force does not affect the mean energy balance of an oscillating airfoil (Wu [1971b]). For the transient case, though, a constant aerodynamic force component is significant. This significance is understood by recognizing that the energy required to produce a steady lifting flow from an initially non-lifting flow is infinite (Jones [1990]). The reason for this infinite energy is shown by Lomax [1960] to be a result of the $1/t$ dependence of the unsteady drag as t tends to infinity. With an initial value of lift acting on an airfoil during a transient motion, the flow has the ability to transfer some of the infinite energy present initially in the flow to the airfoil. If the initial lift on the airfoil is zero,

a result analogous to Wu's result that $\bar{E} > 0$ may be stated as follows: if the fluid is undisturbed at $t = 0$, then

$$\int_0^t E(t)dt > 0 \quad (5.4)$$

For an airfoil with a finite value of lift at $t = 0$, this inequality does not necessarily hold. Another consequence of the infinite energy required to produce a change in lift is that it makes any attempt to minimize the energy lost in the wake for a given change in lift invalid. Recognizing that an infinite amount of time is required for the unsteady drag to transfer the infinite energy to the flow, it becomes clear that the addition of a steady component of drag (e.g. viscous or 3-D induced drag) will also require an infinite amount of energy to overcome. Adding the practical consideration that these steady components of drag will overshadow the unsteady component of drag for most values of time, it becomes clear that the unsteady drag will be an insignificant component of the energy required by an aircraft propulsion system. On the other hand, the power required to overcome the aerodynamic forces and produce camberline deformations (P), which is finite, is not affected by the addition of steady drag components. Therefore, the component P drives the design of the actuation systems on an aircraft that produce camberline deformations. *The remainder of this paper will be concerned with the determination and minimization of the energy required to produce camberline deformations; with it being accepted from the practical standpoint mentioned above that the infinite energy required to overcome the unsteady component of drag is being ignored.*

Figure. 5.1 shows one way of allocating the total required actuator power (P_{out}) for a general airfoil control device. The structural forces would be present on any morphing-type device that must deform an outer skin. Frictional forces may also be grouped in the structural forces category, which would also apply to conventional hinged flaps. The inertial forces are present for any device, but are negligible compared to the aerodynamic and structural forces. As previously stated, the current study is concerned with the power required to overcome the aerodynamic forces (P), and therefore P_{out} is assumed to equal P in Figure. 5.1. For a prescribed change in camberline shape along a defined path between $t=0$ and $t=t^*$, the total energy required to overcome the aerodynamic forces is defined as

$$W = \int_0^{t^*} P(t)dt \quad (5.5)$$

The power required by the actuator to produce P is defined as P_a in Figure. 5.1. The corresponding energy input to the actuators for a prescribed camberline deformation is defined as

$$W_a = \int_0^{t^*} P_a(t) dt \quad (5.6)$$

Note that Eq. (5.5) and (5.6) are defined separately for each control surface or actuator on the airfoil. The value of P required for each control surface or actuator is distinguished by the dz_c/dt term in Eq. (5.2).

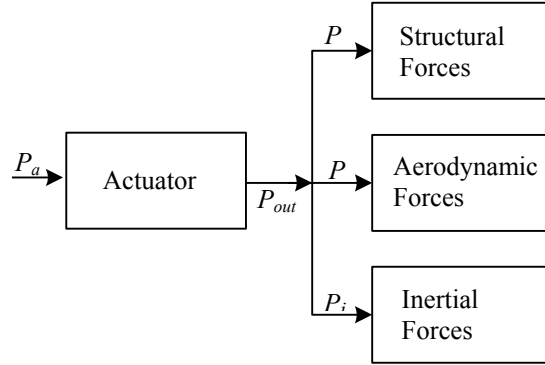


Figure 5.1: The distribution of the provided actuator power for a general configuration

To obtain the quantity P_a , knowledge of the actuator energetics and actuator placement is required. For the current study, which is intended to investigate the fundamentals of the actuator energy required to overcome the aerodynamic forces, a general model of the actuator energetics is proposed. The model is defined as follows

$$\begin{aligned} \text{for } P_{out} \geq 0, \quad P_a &= P_{out} \\ \text{for } P_{out} < 0, \quad P_a &= \eta |P_{out}| \end{aligned} \quad (5.7)$$

where η is a constant ranging from -1 to 1 depending on the actuator. A separate efficiency could be defined for positive values of P_{out} (so that 100% actuator efficiency is not assumed), although this implies just multiplying W_a by a constant (since η will change accordingly). This will not influence a comparison between different control surface configurations and is therefore not used for this analysis. Figure. 5.2 illustrates Eq. (5.7) for three key values of η . For $\eta = 1$, the actuator requires the same power input to produce negative values of P_{out} as it does to produce positive values. Recall that positive P_{out} values indicate that the actuator motion is resisted by the external forces while negative values indicate that the external forces act in the direction of actuator motion. For $\eta = 0$, the actuator requires no power input and allows no power to be extracted while producing negative values of P_{out} . This case is the most consistent with feedback controlled pneumatic (Fleischer [1995]) and hydraulic (Green [1985]) actuators, which require only the

controlled release of pressurized fluid to produce negative power. The neglecting of negative work values has also been considered for the energy-cost analysis of insect flight (Weis-Fogh [1973]) and human muscles (Abbot *et al.* [1952]). The $\eta = -1$ case allows the actuator to store the incoming energy associated with negative values of P_{out} to be used later to produce positive P_{out} values with 100% conversion efficiency. This value of η allows W_a to be negative and zero for certain cases. Negative values of η are possible for piezo-electric actuators due to their electro-magnetic coupling (Giurgiutiu *et al.* [1996]).

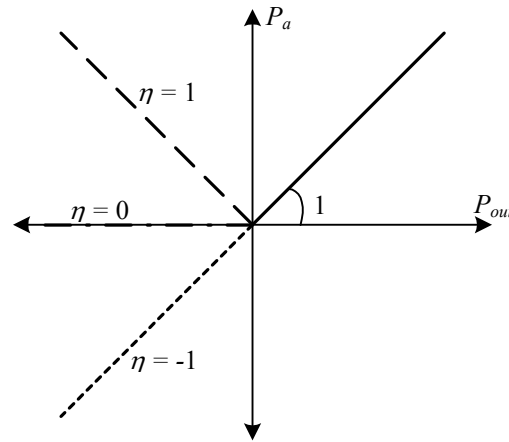


Figure 5.2: The relationship between P_{out} , the required rate of actuator work, and P_a , the rate of actuator energy, for the proposed general actuator model

Applying the general actuator model of Eq. (5.7) to Eq. (5.6), the equation for the total required actuator energy input can be written as

$$W_a = W_+ + \eta W_- \quad (5.8)$$

where W_+ and W_- are the absolute values of the positive and negative components of the integral in Eq. (5.6). An example of these components is shown in Figure. 5.3, where in this case W_+ is the integral of P from $t = 0$ to t_0 and W_- is the negative of the integral from t_0 to t^* .

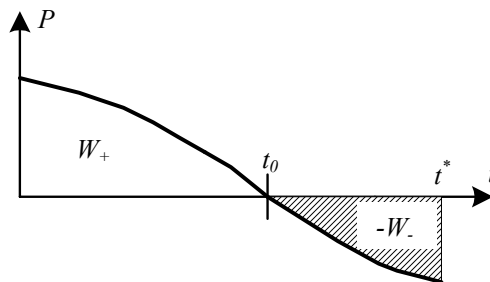


Figure 5.3: Example of the separation of W into W_+ and W_- terms for a given transient motion

5.3 The Aerodynamic Work for a Ramp Input of Control Deflection

For a camberline defined by Eq. (2.55), the time-dependence of the camberline deformation is defined entirely by the function β . This section will derive the aerodynamic work and power components discussed in Section 5.2 for the function β defined as a terminated ramp, which will be written as

$$\begin{aligned}\beta(\tau) &= \bar{\beta}_0, & -\infty < \tau < 0 \\ \beta(\tau) &= \bar{\beta}_0 + \frac{\tau}{\tau^*} \Delta\bar{\beta}, & 0 \leq \tau \leq \tau^* \\ \beta(\tau) &= \bar{\beta}_0 + \Delta\bar{\beta}, & \tau^* < \tau < \infty\end{aligned}\quad (5.9)$$

where $\bar{\beta}_0$ is the initial value of β , and $\Delta\bar{\beta}$ is the change in β between $\tau = 0$ and $\tau = \tau^*$. These terms are illustrated in Figure 5.4 along with the corresponding first and second derivatives of β . Notice that the second derivative is defined by two Dirac delta function impulses.

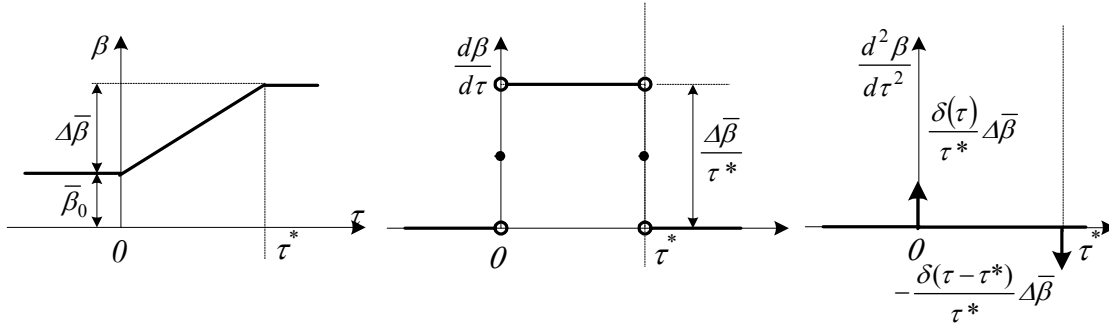


Figure 5.4: The specified time-history of the camberline deformation β and the corresponding time-derivatives

The power required to overcome the aerodynamic forces was defined in Eq. (5.2). It will be convenient to represent the power by the following nondimensional power coefficient (C_P)

$$\begin{aligned}C_P(\tau) &= \frac{P}{qUc} \\ &= -\frac{1}{c^2} \int_0^c \Delta C_p(x, \tau) \left[\frac{\partial z_c}{\partial \tau}(x, \tau) \right] dx\end{aligned}\quad (5.10)$$

From Eq. (2.70), ΔC_p may be written in terms of β as follows

$$\begin{aligned} \Delta C_p(x, t) = & \alpha_{un}(t) \chi(x) + (\bar{A}_{0,s} \chi(x) + T_{0,s}(x)) \beta(t) \\ & + (\bar{A}_{0,d} \chi(x) + T_{0,d}(x) + T_{1,s}(x)) \beta'(t) + T_{1,d}(x) \beta''(t) \end{aligned} \quad (5.11)$$

For the β defined in Eq. (5.9), the wake effect term, α_{un} , evaluates to the following

$$\alpha_{un}(\tau) = \frac{\Delta \bar{\beta}}{2\pi \tau^*} [K_{0,d} \phi_1(\tau) + K_{0,s} \phi_2(\tau)] \quad (5.12)$$

where

$$\begin{aligned} \phi_1(\tau) & \equiv \phi(\tau) \\ & = -0.165e^{-0.091\tau} - 0.335e^{-0.6\tau} \end{aligned} \quad (5.13)$$

$$\begin{aligned} \phi_2(\tau) & \equiv \int_0^\tau \phi(\tau - \sigma) d\sigma \\ & = -2.37152 + 0.55833e^{-0.6\tau} + 1.81319e^{-0.091\tau} \end{aligned} \quad (5.14)$$

Substituting ΔC_p from Eqs. (5.11 – 5.14) and z_c from Eqs. (2.55 and 5.9) into Eq. (5.10) allows the power coefficient for a single control surface to be written as

$$C_P = \frac{\Delta \bar{\beta}^2}{\tau^{*2}} [Q_1 \phi_1(\tau) + Q_2 \phi_2(\tau) + Q_3 \tau + Q_4 + (\delta(\tau) - \delta(\tau - \tau^*)) Q_5] + \frac{\Delta \bar{\beta} \bar{\beta}_0}{\tau^*} Q_3 \quad (5.15)$$

where the Q terms are defined as

$$Q_1 = -\frac{K_{0,d}}{2\pi} \int_0^c \psi(x) dx \quad (5.16)$$

$$Q_2 = -\frac{K_{0,s}}{2\pi} \int_0^c \psi(x) dx \quad (5.17)$$

$$Q_3 = -\int_0^c (\bar{A}_{0,s} \chi(x) + T_{0,s}(x)) \psi(x) dx \quad (5.18)$$

$$Q_4 = -\int_0^c (\bar{A}_{0,d} \chi(x) + 2T_{0,d}(x)) \psi(x) dx \quad (5.19)$$

$$Q_5 = -\frac{1}{2} \int_0^c T_{1,d}(x) \psi(x) dx \quad (5.20)$$

Note that the $\frac{1}{2}$ in the Q_5 equation is a result of the definition of $d\beta/d\tau$ at $\tau = 0$ and τ^* , which from Figure 5.4 can be written as

$$\begin{aligned} \frac{d\beta}{d\tau}(\tau = 0) & = -\frac{d\beta}{d\tau}(\tau = \tau^*) \\ & = \frac{1}{2} \frac{\Delta \bar{\beta}}{\tau^*} \end{aligned} \quad (5.21)$$

For linear camberline shapes, ψ is linear, and each term in Eq. (5.15) may be interpreted as a component of the dynamic hinge-moment coefficient multiplied by the flap deflection rate ($d\beta/d\tau$). The Q_1 and Q_2 terms are due to the wake effect forces, Q_3 is due to the quasi-steady forces, and Q_4 and Q_5 are due to the apparent mass forces. The Dirac delta functions in Eq. (5.15) are a result of the acceleration pulse of the camberline as shown in Figure 5.4.

Having obtained an expression for the output power required by an actuator to overcome the aerodynamic forces during a ramp input of camberline deformation, the input energy required by the actuator (W_a) may be calculated using Eqs. (5.6 - 5.8). The nondimensional input energy coefficient is defined as

$$C_{W_a} = \frac{W_a}{qc^2} = \int_0^{\tau^*} C_{P_a} d\tau \quad (5.22)$$

where C_{P_a} is defined through the general actuator model defined in Eq. (5.7), which can be written in terms of C_P as

$$\begin{aligned} \text{for } C_P \geq 0, \quad C_{P_a} &= C_P \\ \text{for } C_P < 0, \quad C_{P_a} &= \eta|C_P| \end{aligned} \quad (5.23)$$

From Eq. (5.23), the integration required by Eq. (5.22) for C_{W_a} can be separated into positive (C_{W+}) and negative (C_{W-}) components as follows

$$C_{W_a} = C_{W+} + \eta C_{W-} \quad (5.24)$$

which is equivalent to Eq. (5.8) and is illustrated in Figure. 5.3. Note that the two Dirac delta functions in Eq. (5.15) result in there always being both a component of C_{W+} and C_{W-} present. Assuming Q_5 is greater than zero, the impulses at $\tau = 0$ and $\tau = \tau^*$ provide components of C_{W+} and C_{W-} , respectively. These components can both be written as

$$C_{W,\delta} = \frac{\Delta\bar{\beta}^2}{\tau^{*2}} Q_5 \quad (5.25)$$

which represent the instantaneous transfer of energy from the airfoil to the surrounding fluid. Although this is an unrealistic concept, it is accepted because it simplifies the effect of camberline acceleration by concentrating it at the beginning and end of the unsteady motion.

The difficulty in applying Eq. (5.24) is that the integrations required for C_{W+} and C_{W-} can only be evaluated analytically for special cases. The reason for this is that τ_0 must be found and then used

as a limit of integration for the evaluation of C_{W+} and C_{W-} (τ_0 is equivalent to t_0 in Figure. 5.3). The analytic evaluation of τ_0 is made difficult by the exponentials present in Eqs. (5.13) and (5.14). For Eq. (5.24) to be evaluated analytically, τ_0 must be less than zero or greater than τ^* so that C_p remains either positive or negative throughout the deformation process. Details of these considerations are explained most effectively through an example, which is the focus of the next section.

5.4 Application to a Pitching Flat-Plate Airfoil

The application of the actuator energy theory developed in the previous sections to a pitching flat-plate identifies many of the interesting aspects of the theory. Consider the flat plate shown in Figure 5.5. The shape function of Eq. (2.55) is simply

$$\psi(x) = x_a - x \quad (5.26)$$

and the time dependent angle of attack, $\beta(\tau) = \alpha(\tau)$, is specified to be the ramp input defined in Eq. (5.9).

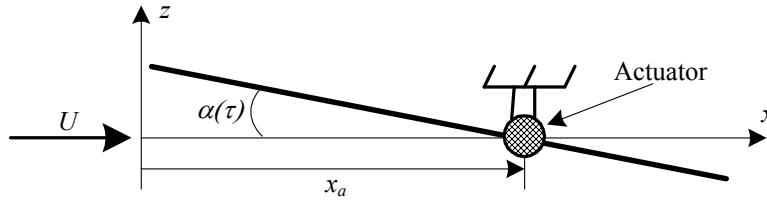


Figure 5.5: Definition of the geometry and actuator placement for a pitching flat plate

The Q terms from Eqs. (5.16 – 5.20) evaluate to the following

$$Q_1 = \pi \left(\frac{3}{8} - 2x_a + 2x_a^2 \right) \quad (5.27)$$

$$Q_2 = Q_3 = \frac{\pi}{2} (1 - 4x_a) \quad (5.28)$$

$$Q_4 = \pi \left(\frac{3}{4} - \frac{5}{2}x_a + 2x_a^2 \right) \quad (5.29)$$

$$Q_5 = \frac{\pi}{2} \left(\frac{9}{64} - \frac{1}{2}x_a + \frac{1}{2}x_a^2 \right) \quad (5.30)$$

Applying these functions to Eq. (5.15) for a value of $x_a/c = 0.5$, the time-history of C_p was determined for various values of τ^* and is plotted in Figure 5.6. The axes of Figure 5.6 are

normalized with τ^* to allow the various cases to be shown on the same figure. This figure shows that the required positive work (C_{W+}) decreases as τ^* increases, which is a result of reduced aerodynamic damping. Because the initial angle of attack (α_0) is zero for this case, Eq. (5.15) indicates that the value of τ at which C_P is zero (τ_0) is independent of τ^* (this is not obvious in Figure 5.6 because of the scaling of the axes).

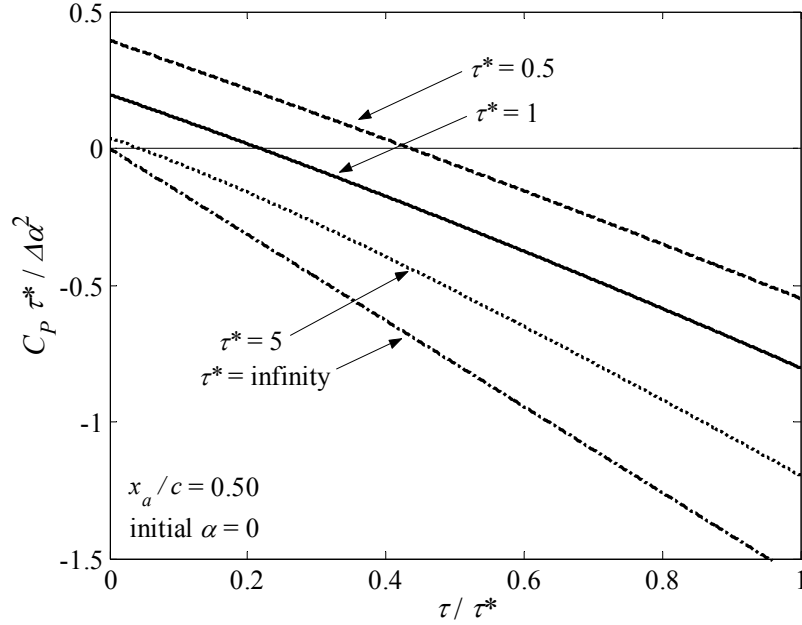


Figure 5.6: The time-history of the C_P for a ramp input of α for various values of τ^*

It turns out that this initially nonlifting case allows for the approximate analytic evaluation of C_{W+} and C_{W-} . This is possible because τ_0 may be determined analytically by making use of a few valid assumptions. The solution process for τ_0 is initiated by setting C_P from Eq. (5.15) equal to zero,

$$Q_1\phi_1(\tau_0) + Q_2\phi_2(\tau_0) + Q_3\tau_0 + Q_4 = 0 \quad (5.31)$$

where ϕ_1 and ϕ_2 are defined in Eqs. (5.38) and (5.39). It is observed in Figure 5.6 that τ_0 is less than one, which is true for values of $x_a/c > 0.45$. It is also observed from Eqs. (5.38) and (5.39) that the coefficients in the exponentials are less than one. From these observations it is concluded that ϕ_1 and ϕ_2 may be accurately approximated as follows using the first two terms of a Taylor series

$$\phi_1(\tau_0) = -0.5 + 0.216\tau_0 + O(\tau_0^2) \quad (5.32)$$

$$\phi_2(\tau_0) = -0.5\tau_0 + O(\tau_0^2) \quad (5.33)$$

Substituting these expansions into Eq. (5.31), τ_0 is found to equal

$$\tau_0 = \frac{0.5Q_1 - Q_4}{0.216Q_1 - 0.5Q_2 + Q_3} + \dots \quad (5.34)$$

From Figure 5.6, the limits of integration for C_{W+} and C_{W-} are identified, which allows the two terms to be written as

$$\begin{aligned} C_{W+} &= \int_0^{\tau_0} C_P(\tau) d\tau \\ &= \frac{\Delta\alpha^2}{\tau^{*2}} \left[Q_1\Phi_1(\tau_0) + Q_2\Phi_2(\tau_0) + Q_3 \frac{\tau_0^2}{2} + Q_4\tau_0 + Q_5 \right] \end{aligned} \quad (5.35)$$

$$\begin{aligned} C_{W-} &= \left| \int_{\tau_0}^{\tau^*} C_P(\tau) d\tau \right| \\ &= -\frac{\Delta\alpha^2}{\tau^{*2}} \left\{ Q_1[\Phi_1(\tau^*) - \Phi_1(\tau_0)] + Q_2[\Phi_2(\tau^*) - \Phi_2(\tau_0)] + Q_3 \frac{\tau^{*2} - \tau_0^2}{2} + Q_4[\tau^* - \tau_0] - Q_5 \right\} \end{aligned} \quad (5.36)$$

where

$$\Phi_1(\tau) = \int \phi_1(\tau) d\tau = -2.37152 + 0.55833e^{-0.6\tau} + 1.81319e^{-0.091\tau} \quad (5.37)$$

$$\Phi_2(\tau) = \int \phi_2(\tau) d\tau = 20.8755 - 2.37152\tau - 0.93055e^{-0.6\tau} - 19.945e^{-0.091\tau} \quad (5.38)$$

Applying the approximations of Eqs. (5.7 – 5.9), the expression for C_{W+} from Eq. (5.35) simplifies to the following

$$C_{W+} = \frac{\Delta\alpha^2}{\tau^{*2}} \left[-\frac{1}{2} \frac{(0.5Q_1 - Q_4)^2}{(0.216Q_1 + 0.5Q_3)} + Q_5 \right] \quad (5.39)$$

where the Taylor Series approximations of $\Phi_1(\tau_0)$ and $\Phi_2(\tau_0)$ are used. Similarly, the approximate equation for C_{W-} is written as

$$C_{W-} = -\frac{\Delta\alpha^2}{\tau^{*2}} \left\{ Q_1\Phi_1(\tau^*) + Q_2\Phi_2(\tau^*) + Q_3 \frac{\tau^{*2}}{2} + Q_4\tau^* - Q_5 + \frac{1}{2} \frac{(0.5Q_1 - Q_4)^2}{(0.216Q_1 + 0.5Q_3)} \right\} \quad (5.40)$$

where Eq. (5.37) and (5.38) are used for $\Phi_1(\tau^*)$ and $\Phi_2(\tau^*)$. These equations are valid for values of $x_a/c > 0.45$ and for $\tau^* > 0.1$. For values of $\tau^* < 0.1$, τ_0 is greater than τ^* so that the limits of integration in Eqs. (5.35) and (5.36) are no longer valid. The usefulness of these equations is that they accurately predict the value of x_a for the minimum C_{W_a} for any value of η and for values of $\tau^* > 0.1$. They also indicate that C_{W-} has a more complex functional dependence on τ^* than does

C_{W+} . Figure 5.7 presents the exact values of C_{W+} and C_{W-} , which were obtained by computing τ_0 and specifying the limits of integration for each case. The results of Eq. (5.39) for C_{W+} are shown as a dashed line for each case. It is seen that the results of Eq. (5.39) are indistinguishable from the exact result for $x_a/c > 0.45$ and become invalid as x_a/c approaches 0.25. The result of Eq. (5.40) is not shown in Figure 5.7, although it can be shown to be accurate for the same values of x_a as Eq. (5.39). This figure shows that C_{W+} and C_{W-} converge to the limit of $\tau^* = \text{infinity}$, which represents the results of steady airfoil theory. It also shows that, as expected from steady airfoil theory, C_{W+} is largest for $x_a/c < 0.25$ and C_{W-} is largest for $x_a/c > 0.25$. The pitching axis for minimum C_{W+} is found exactly from Eq. (5.39) to equal 0.572, which is independent of τ^* . Figure 5.7 verifies that this minimum is located within the range of x_a values where Eq. (5.39) is valid. From the C_{W-} plot in Figure 5.7 it is deduced that as η becomes nonzero and positive, the minimum C_{W+} pitching axis shifts towards the leading edge. Similarly, as η becomes negative, the optimal axis shifts to the trailing edge.

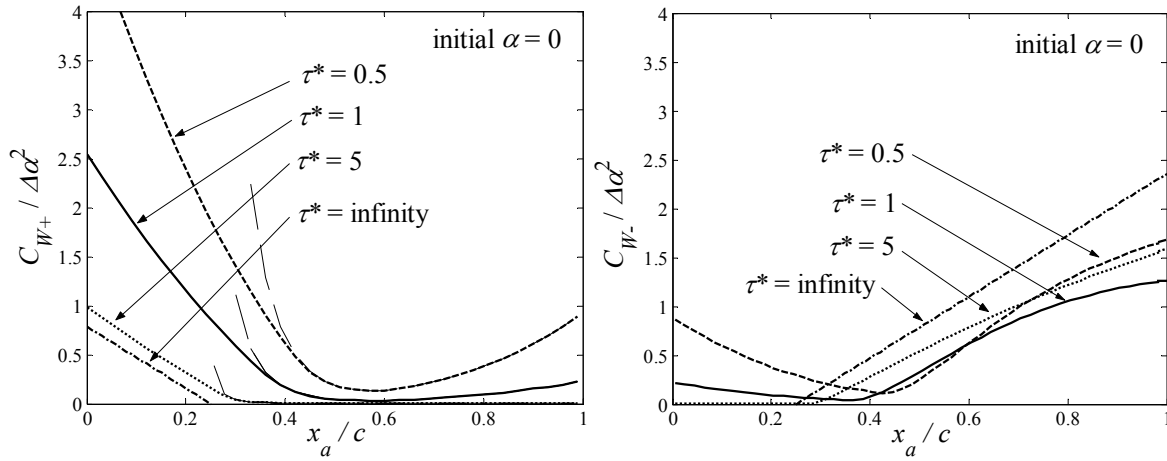


Figure 5.7: The variation of C_{W+} and C_{W-} with x_a/c and τ^* . The thin dashed lines in the C_{W+} plot represent the result of Eq. (5.39)

The cases shown in Figure 5.6 and discussed previously specified that the initial α , and therefore the initial lift, was zero. The effect of an initial lift will now be presented. From Eq. (5.40) it is seen that an initial angle of attack (α_0) only influences C_P through the last term, which contains Q_3 . Dividing this equation by $\Delta\alpha^2$ allows C_P to be written as follows

$$\frac{C_P}{\Delta\alpha^2} = \frac{1}{\tau^{*2}} [Q_1\phi_1(\tau) + Q_2\phi_2(\tau) + Q_3\tau + Q_4 + (\delta(\tau) - \delta(\tau - \tau^*))Q_5] + \frac{k}{\tau^*} Q_3 \quad (5.41)$$

where

$$k = \frac{\alpha_0}{\Delta\alpha} \quad (5.42)$$

The value k represents the initial lift divided by the change in steady state lift. Recognizing the term k in Eq. (5.41) is useful because it indicates that the normalized power coefficient ($C_P / \Delta\alpha^2$) is dependent only on the ratio of α_0 and $\Delta\alpha$, and not each term independently. The presence of k significantly complicates the problem of analytically determining C_{W+} and C_{W-} , although the approximate method discussed previously can be applied to certain values of k . The main effect of the initial lift is to vertically displace the C_P curves, such as those shown in Figure 5.6. This significantly changes τ_0 and therefore alters the allocation of C_W into C_{W+} and C_{W-} terms.

To gain some insight into the effect of k on C_{W_a} , the limiting cases of τ^* approaching zero and infinity will be examined. For τ^* approaching zero, the region of integration for C_{W+} is $0 \leq \tau < \tau^*$, and the C_{W-} component comes completely from the Dirac delta function at τ^* . From Eq. (5.41), the integration for C_{W_a} , with τ^* approaching zero, results in

$$\frac{C_{W_a}}{\Delta\alpha^2} = \frac{1}{\tau^*} \left[-\frac{1}{2} Q_1 + Q_4 \right] + \frac{(1+\eta)Q_5}{\tau^{*2}} + O(1) \quad (5.43)$$

which is independent of k . For $\eta > -1$, the Q_5 term is dominant. Thus, from Eq. (5.30) the pitching axis for minimum C_{W_a} is at the half chord. For $\eta = -1$, only the bracketed term remains in Eq. (5.43). Substituting Eqs. (5.27) and (5.29) into (5.43) and setting the derivative with respect to x_a equal to zero, the pitching axis for minimum C_{W_a} is found to be located at $x_a/c = 3/4$.

For τ^* approaching infinity, the region of integration for C_{W+} and C_{W-} depends upon k and x_a . This is seen by writing Eq. (5.41) in terms of its lowest order components for large values of τ^* . To determine the lowest order components, it is necessary to define τ as

$$\tau = \bar{\tau} \tau^* \quad (5.44)$$

where $0 < \bar{\tau} < 1$. Substituting this into Eq. (5.41), the lowest order equation for C_P is written as follows

$$\frac{C_P}{\Delta\alpha^2} = \frac{Q_3}{\tau^*} (\bar{\tau} + k) + O\left(\frac{\ln \tau^*}{\tau^{*2}}\right) \quad (5.45)$$

Note that, as pointed out by Lomax [1960], the asymptotic limits of ϕ_1 and ϕ_2 obtained from Eqs. (5.38) and (5.39) are incorrect. Therefore, the approximate Wagner function suggested by Garrick [1938] was used instead for obtaining Eq. (5.45). As expected, Eq. (5.45) represents the steady thin airfoil theory result. Equation (5.45) shows that, if k is less than -1 or greater than

zero, the lowest order component of C_{W_a} is composed entirely of either C_{W_+} or C_{W_-} . For these values of k , C_{W_a} , is written from Eq. (5.45) and (5.28) as follows

$$F(x_a, k) = \frac{\pi}{2} \left[\left(\frac{1}{2} + k \right) (1 - 4x_a) \right] + O\left(\frac{\ln \tau^*}{\tau^*} \right)$$

$$\text{if } F \geq 0, \quad \frac{C_{W_a}}{\Delta \alpha^2} = F(x_a, k) \quad (5.46)$$

$$\text{if } F < 0, \quad \frac{C_{W_a}}{\Delta \alpha^2} = \eta |F(x_a, k)|$$

For values of k between -1 and zero, τ_0 is determined by setting Eq. (5.45) equal to zero. This value of τ_0 is then used as a limit of integration for C_{W_a} , which from Eqs. (5.45) and (5.28) results in

$$\text{if } x_a < 1/4, \quad \frac{C_{W_a}}{\Delta \alpha^2} = \frac{\pi}{2} \left(\frac{1}{2} + k + \frac{k^2}{2} \right) (1 - 4x_a) + \eta \pi k^2 \left(\frac{1}{4} - x_a \right) + O\left(\frac{\ln \tau^*}{\tau^*} \right)$$

$$\text{if } x_a \geq 1/4, \quad \frac{C_{W_a}}{\Delta \alpha^2} = -\pi k^2 \left(\frac{1}{4} - x_a \right) - \eta \frac{\pi}{2} \left(\frac{1}{2} + k + \frac{k^2}{2} \right) (1 - 4x_a) + O\left(\frac{\ln \tau^*}{\tau^*} \right) \quad (5.47)$$

Table 5.1 presents the pitching axes for minimum C_{W_a} obtained from Eqs. (5.46) and (5.47) with the constraint that the axes remain within the chord. These results are intuitive from the elementary nature of a steady thin airfoil at an angle of attack.

Table 5.1: The minimum C_{W_a} pitching axes as τ^* approaches infinity

	$k < -1$	$-1 < k < -1/2$	$-1/2 < k < 0$	$k > 0$
$\eta = 1$	$x_a/c = 1/4$	$x_a/c = 1/4$	$x_a/c = 1/4$	$x_a/c = 1/4$
$\eta = 0$	$0 < x_a/c < 1/4$	$x_a/c = 1/4$	$x_a/c = 1/4$	$1/4 < x_a/c < 1$
$\eta = -1$	$x_a/c = 0$	$x_a/c = 0$	$x_a/c = 1$	$x_a/c = 1$

The limiting cases of τ^* discussed above allowed C_{W_a} to be obtained analytically, which allowed the optimal pitching axes to be determined analytically. For the $k \geq 0$ cases, the approximate approach presented in Eqs. (5.9 – 5.15), accounting for the k term in Eq. (5.41), is valid for a wide range of τ^* values. Where this approach is not valid, the integration for C_{W_a} is performed numerically from Eqs. (5.47), (5.23), and (5.41). Using a combination of analytic and numerical approaches, the minimum C_{W_a} pitching axes were obtained for $\eta = 0, 1,$ and -1 . Figure 5.9 shows the variation of the optimal pitching axis with τ^* for the $\eta = 0$ case for various k values. As determined previously, the axes are shown to approach $x_a/c = 0.5$ as τ^* approaches zero. It is seen in this figure that as k becomes large and positive, the optimal axis is located at $x_a/c = 0.5$ for most τ^* values. This is a result of C_{W_+} being composed of only the initial impulse, which is

smallest for the mid-chord axis. For negative k values, the optimal axis moves toward the leading edge as τ^* increases. Figure 5.9 shows the variation of the optimal pitching axis with τ^* for the $\eta = 1$ case and various k values. It is interesting to note that for this case, as was determined previously, the optimal axis at both τ^* equal to zero and infinity is independent of k . This explains the increased similarity between the optimal axes curves for various k values in Figure 5.9 when compared to Figure 5.8. For airfoils that must complete a cycle, meaning they produce a change in lift (positive k) and then later produce a negative change in lift to return to their initial state (negative k), the similarity in the optimal axes for negative and positive k values is advantageous. This is because a smaller compromise must be made, assuming the pitching axis remains fixed, when choosing the optimal pitching axis for the complete motion. For the majority of negative and positive combinations of k , the optimal axis for the combination is located between the two independent optimal points for a given τ^* . Thus, Figures 5.4 and 5.5 are very general and applicable to many practical cases. Figure 5.10 presents the variation of the optimal pitching axis with τ^* for the $\eta = -1$ case. It is seen that the difference between positive and negative k values is very large compared to Figures 5.4 and 5.5. The result of increasing k in Figure 5.10 is seen to be a decrease in the value of τ^* at which the optimal axis is the same as those shown in Table 5.1 for the τ^* equal to infinity case. The same conclusion can be stated from Figures 5.5. A similar result was reported by Yates [1986] for the minimum energy pitching axes of an oscillating flat plate intended to produce thrust.

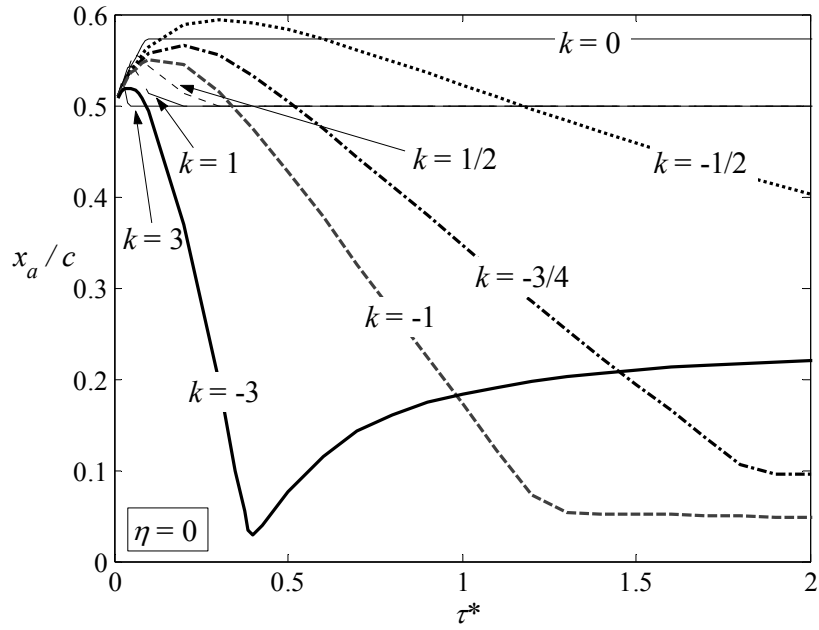


Figure 5.8: The $\eta = 0$ case for the variation of the minimum C_{wa} pitching axes with τ^* for various values of k

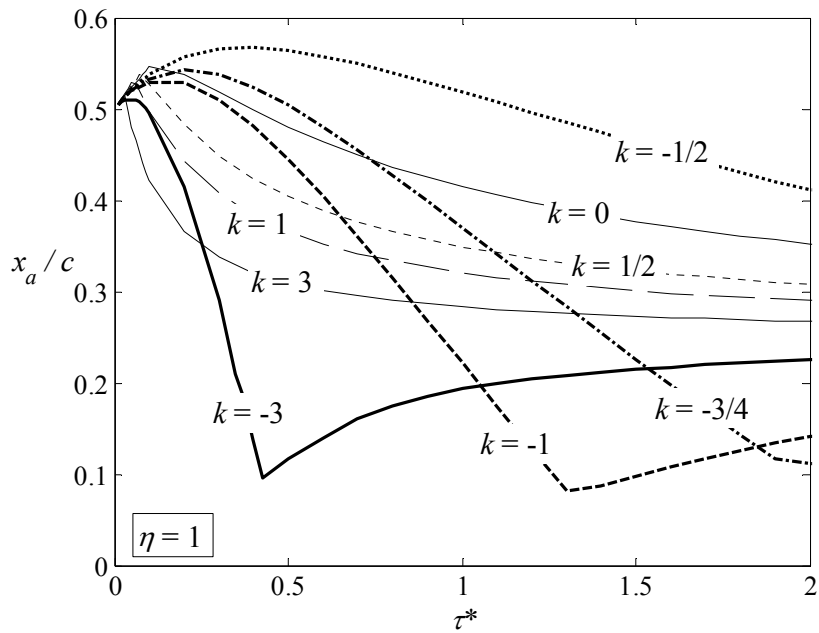


Figure 5.9: The $\eta = 1$ case for the variation of the minimum C_{wa} pitching axes with τ^* for various values of k

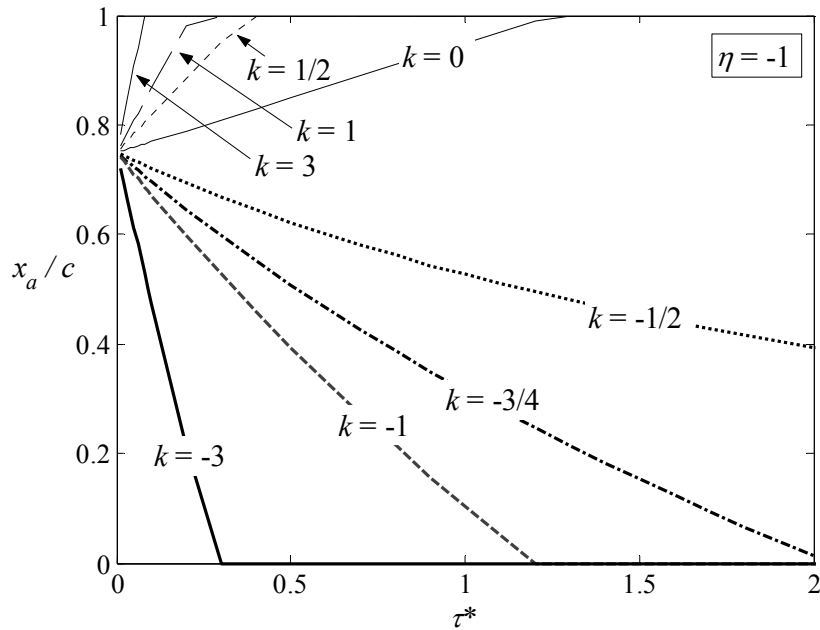


Figure 5.10: The $\eta = -1$ case for the variation of the minimum C_{wa} pitching axes with τ^* for various values of k

5.5 Application to Various Control Surface Configurations

This section describes the affect of various control surface shapes on the C_{wa} required for a given change in lift. The first two cases to be considered are shown in Figures 6.1 and 6.2. A conventional hinged flap is shown in Figure 5.11. The conformal control surface, shown in Figure 5.12, is a quadratic segment defined to have zero slope at x_b . The magnitude of the flap deflection (β) is defined in both cases as the angle at the trailing edge. The ramp input of β , defined in Eq. (5.34), will be used for this analysis. From the shape functions (ψ), which are shown for each case in Figures 6.1 and 6.2, the components of ΔC_p in Eq. (5.36) may be determined analytically from the equations of Section III. The resulting equations are relatively complex, and it is therefore convenient to perform the integrations required for the Q -terms defined in Eqs. (4.8 – 4.12) numerically.

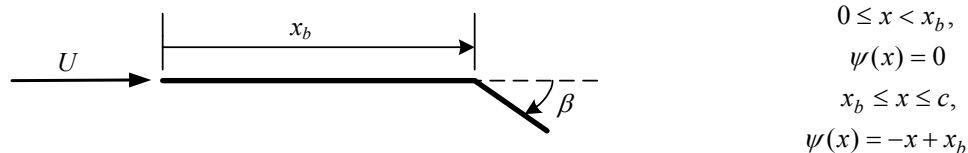


Figure 5.11: The camberline geometry for a conventional flap

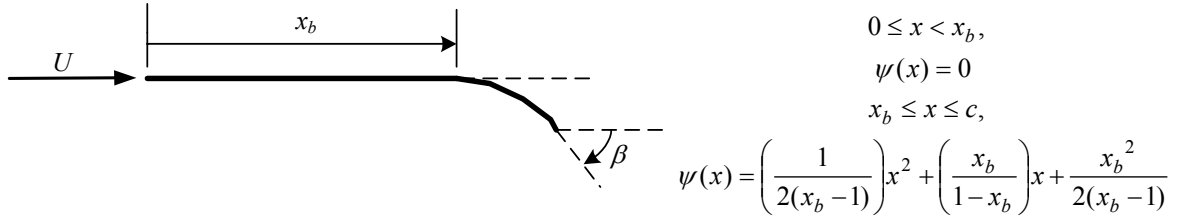


Figure 5.12: The camberline geometry for a conformal flap

Note that in the previous case of the pitching flat plate, the ΔC_L produced by a $\Delta\alpha$ was independent of the pitching axis. This meant that the C_{W_a} required for a given lift could be represented by $C_{W_a} / \Delta\alpha^2$. For comparing various control surface configurations, it is convenient to instead normalize C_P and C_{W_a} by the ΔC_L^2 . From Eq. (5.40), the normalized equation for C_P can then be written as

$$\frac{C_P}{\Delta C_L^2} = \frac{1}{\tau^{*2} K_{0,s}^2} [Q_1\phi_1(\tau) + Q_2\phi_2(\tau) + Q_3\tau + Q_4 + (\delta(\tau) - \delta(\tau - \tau^*))Q_5] + \frac{k}{\tau^* K_{0,s}} Q_3 \quad (5.48)$$

where

$$k = \frac{\bar{\beta}_0}{\Delta\beta} = \frac{C_{L,initial}}{\Delta C_L} \quad (5.49)$$

Recall that the quantity ΔC_L refers to the change in steady state lift, which from Eq. (3.7) is written as

$$\Delta C_L = K_{0,s} \Delta\bar{\beta} \quad (5.50)$$

Considering the conventional and conformal flap configurations, if k is greater than zero, then C_P remains positive throughout the ramp input of β . Therefore, C_{W+} is obtained by integrating Eq. (5.48) from $\tau = 0$ to τ^* and C_{W-} is obtained from Eq. (5.25). For small negative values of k , C_P changes from positive to negative and therefore τ_0 must be determined. For these cases, the process described with Eqs. (5.9 – 5.15) may be used. For large negative k values, C_P remains negative throughout the ramp input of β . Therefore, C_{W-} is obtained by integrating Eq. (5.48) from $\tau = 0$ to τ^* and C_{W+} is obtained from Eq. (5.25).

It is desired to compare the values of C_{W_a} resulting from the conventional and conformal flap configurations defined in Figures 6.1 and 6.2. The first case to be considered, shown in Figure 5.13, compares the C_{W_a} required for a given ΔC_L , x_b , and τ^* while varying k . It is seen that the

C_{wa} required by the conformal flap is less than that required by the conventional flap for any k when $\eta = 0$. For the $\eta = 1$ case, there is a small range of k values where C_{wa} is slightly less for the conventional flap. Overall though, the conformal flap requires less C_{wa} than the conventional flap.

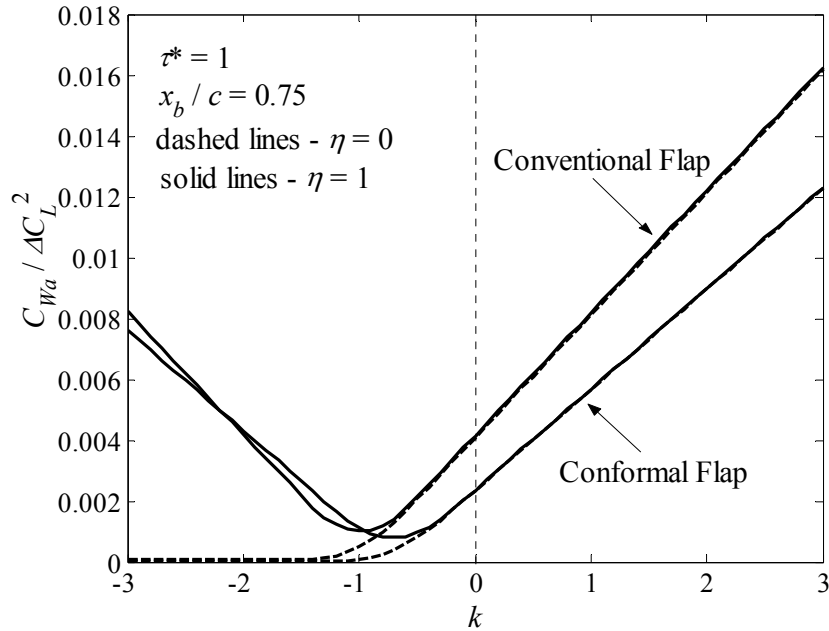


Figure 5.13: A comparison of the C_{wa} required for a conformal or conventional flap

The reason for the smaller C_{wa} for the conformal flap is that it requires less overall camberline deformation for a given change in lift than does the conventional flap. Figure 5.14 illustrates this result along with the corresponding load distribution at $\tau = 1/2$. It is seen that the angle of deflection at the trailing edge of the conformal flap is larger than that for the conventional flap for a given change in lift, but the overall Δz of the camberline is less for the conformal flap. The load distribution for the conventional flap is centered more towards the hinge-line than for the conformal flap, which is favorable for the conventional flap. Nevertheless, the larger Δz overshadows the favorable load distribution for the conventional flap. It should be mentioned that the shape of the load distributions shown in Figure 5.14 apply only at $\tau = 1/2$. As shown in Eq. (5.36), the load distribution does not simply scale linearly with the ramp input of β .

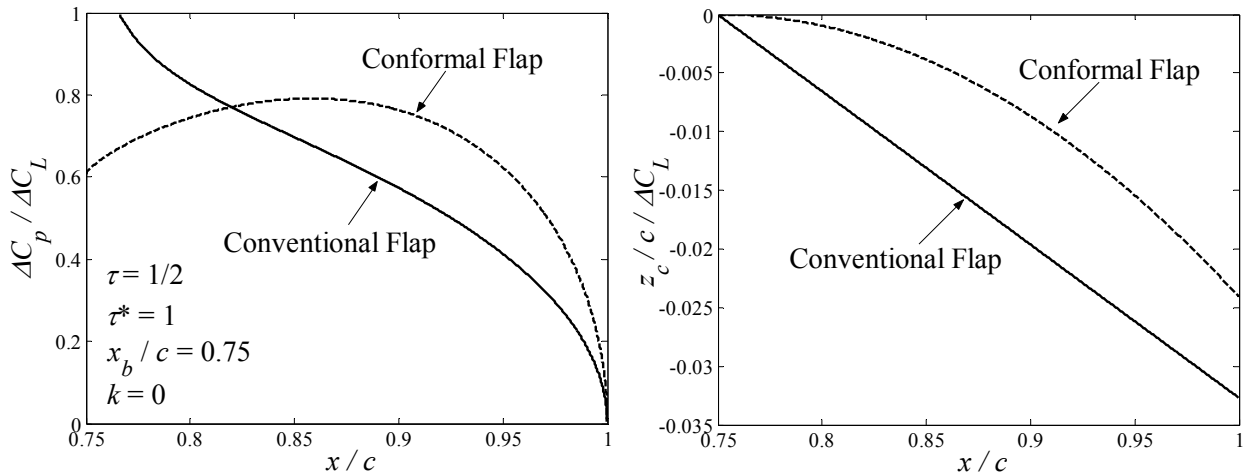


Figure 5.14: The load distribution over the flap and the corresponding shape of the flap deflections

Figure 5.15 shows how C_{wa} varies with τ^* and x_b for the conformal and conventional flap. It is seen that the conformal flap requires less C_{wa} for every case. It is also apparent that the benefit of the conformal flap becomes larger as τ^* decreases. Hence, the conformal flap is ideal in situations where rapid changes in lift are required. The values of C_{wa} in the limit as τ^* goes to infinity are shown in Figure 5.15. These values, which can be obtained from steady thin airfoil theory, show that C_{wa} is 18% less for the conformal flap in the steady limit. The considerable difference between the steady and unsteady values in Figure 5.15 indicates the importance of including the unsteady aerodynamic terms in this analysis. It should be mentioned that the values of C_{wa} for a given change in quarter chord pitching moment (C_M), produce results similar to those in Figure 5.15. In particular, the value of C_{wa}/C_M^2 decreases continuously as x_b varies from midchord to the trailing edge. This is true even though the flap deflection required to produce a pitching moment has a minimum at $x_b/c = 0.75$ for the conventional case.

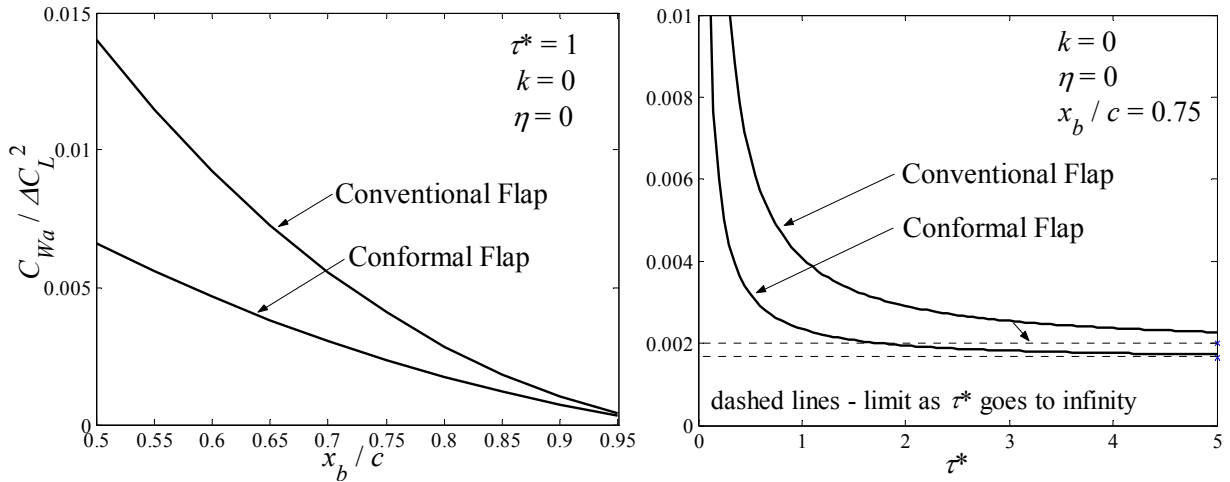
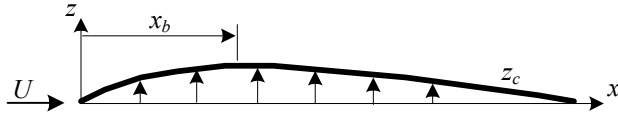


Figure 5.15: The effect of flap size and τ^* on the C_{W_a} required for the conformal or conventional flap

The next cases to be considered are the variable camber configurations shown in Figures 6.6 and 6.7, which are defined as NACA 4-digit camberlines with time-dependent magnitudes of maximum camber. These cases were discussed in Section 3.5. Configuration A, shown in Figure 5.16, is defined so that the *leading and trailing edges* remain on the x -axis as the camber changes. Configuration B, shown in Figure 5.17, is defined so that the *location of maximum camber* (x_b) remains on the x -axis as the camber changes. Figure 3.1 shows that in steady thin airfoil theory, these two configurations produce the same aerodynamic forces. But, the addition of the aerodynamic damping component, shown in Figure 3.2, makes the unsteady thin airfoil results different between the two cases. In considering the actuator energy for each case, it is assumed that each configuration is actuated with a single actuator. This implies that some type of linkage system is used to produce the desired camberline shape. Also, as has been done throughout this paper, only the aerodynamic forces are considered for the actuator energy. It is recognized that this is a big assumption for these variable camber configurations, but nonetheless, we feel that the present analysis provides significant insight into the actuation properties of a variable camber airfoil.



$$\begin{aligned}
 &0 \leq x < x_b, \\
 &\psi(x) = -\frac{1}{x_b^2}x^2 + \frac{2}{x_b}x \\
 &x_b \leq x \leq c, \\
 &\psi(x) = -\frac{1}{(1-x_b)^2}x^2 + \frac{2x_b}{(1-x_b)^2}x + \frac{1-2x_b}{(1-x_b)^2}
 \end{aligned}$$

Figure 5.16: The camberline geometry for a variable camber airfoil with the leading and trailing edges fixed to the x-axis (Configuration A)



$$\begin{aligned}
 &0 \leq x < x_b, \\
 &\psi(x) = -\frac{1}{x_b^2}x^2 + \frac{2}{x_b}x - 1 \\
 &x_b \leq x \leq c, \\
 &\psi(x) = -\frac{1}{(1-x_b)^2}x^2 + \frac{2x_b}{(1-x_b)^2}x - \frac{x_b^2}{(1-x_b)^2}
 \end{aligned}$$

Figure 5.17: The camberline geometry for a variable camber airfoil with x_b fixed to the x-axis (Configuration B)

The dependence of C_{wa} on k and x_b/c is shown in Figure 5.18 for both configurations and $\eta = 0$. It is seen that configuration B requires significant C_{wa} for positive k cases while configuration A requires very little for these cases. This result is explained by recognizing that the camberline motion for configuration B is downwards for a positive change in lift, which must therefore move against the upward acting lift forces. On the other hand, the camberline motion for configuration A is upwards and is therefore not resisted by the aerodynamic forces. For negative k values, the situation reverses and this configuration requires significant C_{wa} . Figure 5.18 shows that configuration B requires less C_{wa} for a given positive k than configuration A requires for a negative k of the same magnitude. This means that if the airfoil is intended to produce an equal number of positive changes in lift as negative changes in lift, then configuration B is favorable from an energy standpoint. The second plot in Figure 5.18 shows that this conclusion is true for any location of maximum camber (x_b). It is also seen that as x_b moves closer to the leading edge, configuration B becomes even more favorable.

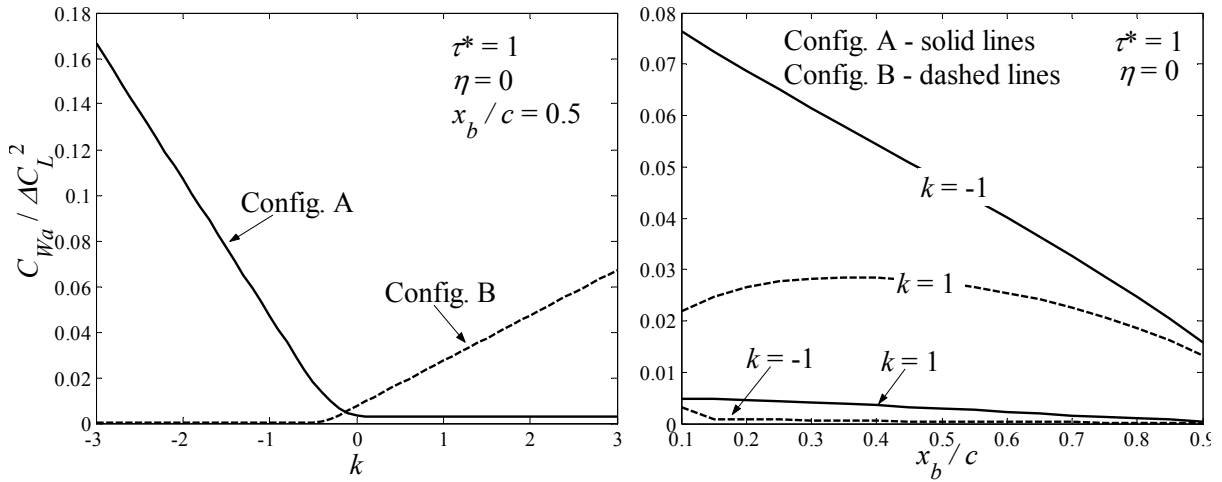


Figure 5.18: The effect of k and x_b/c on the C_{wa} required for configuration A and B

The load distribution and corresponding camberline shape at $\tau = 1/2$ are shown in Figure 5.19. This figure illustrates the point made previously that the camberline motion for configuration B is resisted by the aerodynamic forces for k greater than or equal to zero. Note that the difference between the load distributions shown in this figure comes from the $K_{0,d}$ and $\bar{A}_{0,d}$ terms in Eq. (5.36). This figure makes clear the reasons why configuration B requires less C_{wa} (when considering the entire range of k values) than configuration A. The first reason is that configuration B simply requires less overall camberline deflection than configuration A. The second reason is that for configuration A, the largest camberline deflections are towards the center of the camberline while for configuration B they are at the leading and trailing edges. Combining this fact with the shape of the load distribution makes clear the advantage of configuration B.

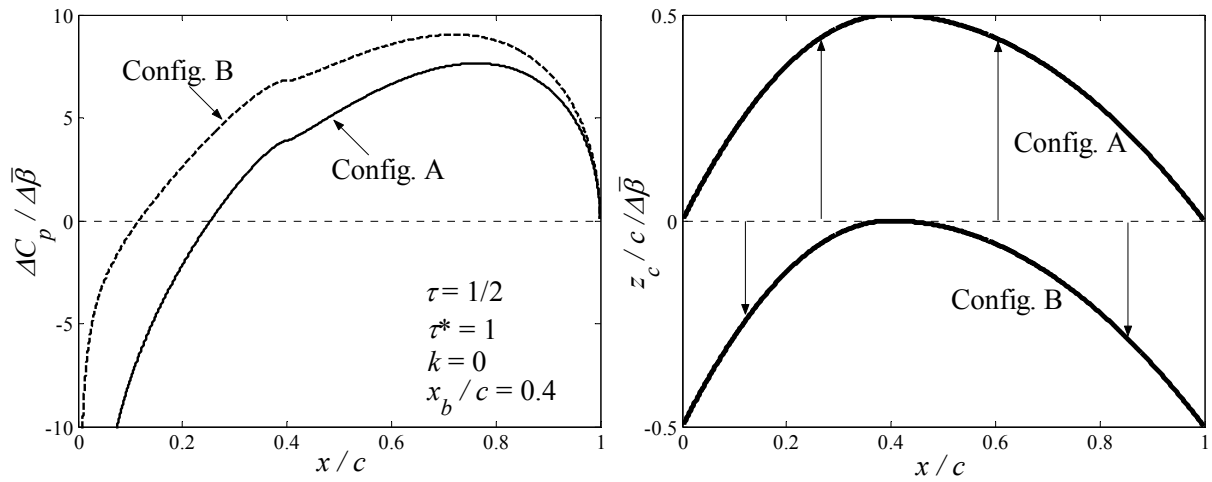


Figure 5.19: Example of the unsteady load distribution and corresponding camberline shape for configuration A and B

Chapter 6

Flapping Wing Propulsion

6.1 Introduction

The discussion in the previous chapters on the aerodynamic characteristics of oscillating camberlines provides the foundation for studying flapping wing propulsion. This section will develop a flapping wing analysis based on the unsteady thin airfoil theory method presented in this report. Using the actuator model presented in Chapter 5, the influence of negative power on the efficiency of flapping wing propulsion will be discussed. The influence of springs and elastic mechanism will be shown to be important in order to maintain high actuator efficiency. The application of this method to a three-dimensional wing will be discussed. An example for two birds will be presented and shown to agree with previous studies. Negative power is found to be present in these examples, which when considered in the efficiency, leads to a change in the optimal flight speed.

6.2 The Energy Required for Flapping

For an oscillating airfoil with a steady-state component, the parameter β from Eq. (2.55) can be written as

$$\beta = \bar{\beta}_0 + \bar{\beta} \cos(\bar{k}\tau) \quad (6.1)$$

where $\bar{\beta}_0$ is the steady component and $\bar{\beta}$ is the amplitude of the oscillating component. Although $\bar{\beta}_0$ does not affect the time-averaged values of C_P and C_d , it does change their instantaneous values. For C_d , we are not interested in the time-history, but for C_P we are

interested to allow for the calculation of the actuator energy discussed in Chapter 5. From Eqs. (5.10), (2.89), (2.55), and (6.1), C_P is written as follows

$$C_P(\tau) = \frac{\bar{\beta}^2 \bar{k}}{c^2} \int_0^c [\Pi_1(\bar{k}, \theta) \cos(\bar{k}\tau) + \Pi_2(\bar{k}, \theta) \sin(\bar{k}\tau)] \psi \sin(\bar{k}\tau) dx + \frac{\bar{\beta}_0 \bar{\beta} \bar{k}}{c^2} \int_0^c \Pi_3(\theta) \psi \sin(\bar{k}\tau) dx \quad (6.2)$$

where the Π_1 and Π_2 terms are rewritten from Eq. (2.89) and Π_3 is defined here as simply the steady load distribution

$$\begin{aligned} \Pi_1(\bar{k}, \theta) &= \left[\bar{A}_{0,s} \chi(\theta) + T_{0,s}(\theta) - T_{1,d}(\theta) \bar{k}^2 + \frac{\chi(\theta)}{2\pi} (K_{0,s} F - K_{0,s} - \bar{k} K_{0,d} G) \right] \\ \Pi_2(\bar{k}, \theta) &= - \left[(\bar{A}_{0,d} \chi(\theta) + T_{0,d}(\theta) + T_{1,s}(\theta)) \bar{k} + \frac{\chi(\theta)}{2\pi} (K_{0,s} G + \bar{k} K_{0,d} F - \bar{k} K_{0,d}) \right] \\ \Pi_3(\theta) &= \chi(\theta) \bar{A}_{0,s} + T_{0,s}(\theta) \end{aligned} \quad (6.3)$$

It will be convenient to write Eq. (6.2) as follows

$$C_P(\tau) = \bar{\beta}^2 [\Phi_1(\bar{k}) \cos(\bar{k}\tau) + \Phi_2(\bar{k}) \sin(\bar{k}\tau)] \sin(\bar{k}\tau) + \bar{\beta}_0 \bar{\beta} \Phi_3(\bar{k}) \sin(\bar{k}\tau) \quad (6.4)$$

where the Φ terms are defined as

$$\begin{aligned} \Phi_1(\bar{k}, \theta) &= \int_0^c (T_{0,s}(\theta) - T_{1,d}(\theta) \bar{k}^2) \bar{k} \psi(\theta) dx + \bar{k} \left(\frac{1}{2} \bar{A}_{1,d} - \bar{A}_{0,d} \right) (2\pi \bar{A}_{0,s} + K_{0,s} F - K_{0,s} - \bar{k} K_{0,d} G) \\ \Phi_2(\bar{k}, \theta) &= -2\bar{k}^2 \int_0^c T_{0,d}(\theta) \psi(\theta) dx - \bar{k} \left(\frac{1}{2} \bar{A}_{1,d} - \bar{A}_{0,d} \right) (2\pi \bar{A}_{0,d} \bar{k} + K_{0,s} G + \bar{k} K_{0,d} F - \bar{k} K_{0,d}) \\ \Phi_3(\theta) &= 2\pi \bar{k} \left(\frac{1}{2} \bar{A}_{1,d} - \bar{A}_{0,d} \right) \bar{A}_{0,s} + \bar{k} \int_0^c T_{0,s}(\theta) \psi(\theta) dx \end{aligned} \quad (6.5)$$

Recall that, as illustrated in Figure 5.1, C_P represents the power required to overcome only the aerodynamic forces. The average value of C_P over one cycle can be written as

$$\bar{C}_P = \frac{\bar{\beta}^2}{2} \Phi_2(\bar{k}) \quad (6.6)$$

Combining the average drag defined in Eq. (4.32) and the above equation for the average power, the aerodynamic efficiency is written as

$$\eta_{aero} = -\frac{\bar{C}_d}{\bar{C}_P} \quad (6.7)$$

Note that this efficiency is only an aerodynamic efficiency; if it was total efficiency for the flapping mechanism, the denominator would be the average total actuator energy. This will be defined later.

To determine the energy required by the flapping actuators, the structural and inertial power components shown in Figure 5.1 must also be known. Although in Chapter 5 these components were neglected for fixed-wing control surface motions, for flapping wings, these components may be significant. The power to overcome the inertial forces will be written as

$$C_{P,inertia}(\tau) = \bar{\beta}^2 K_I \bar{k}^3 \cos(\bar{k}\tau) \sin(\bar{k}\tau) \quad (6.8)$$

where K_I is defined as

$$K_I = \frac{m_a}{\rho c^2} \quad (6.9)$$

where m_a is the mass per-unit-length of the airfoil in the spanwise direction. The power required to overcome the structural forces will be simplified as the power required to overcome a spring connected to the flapping device. There are two different arrangements possible for a single actuator and spring: parallel and series. These are shown in Figure 6.1, where $\beta_{actuator}$ is the actuator output displacement and β is the prescribed camberline displacement. For the parallel arrangement, $\beta_{actuator}$ and β are the same while for the series arrangement they are added together. Conversely, for the series arrangement, the force acting at $\beta_{actuator}$ and β is the same while for the parallel arrangement they are added together.

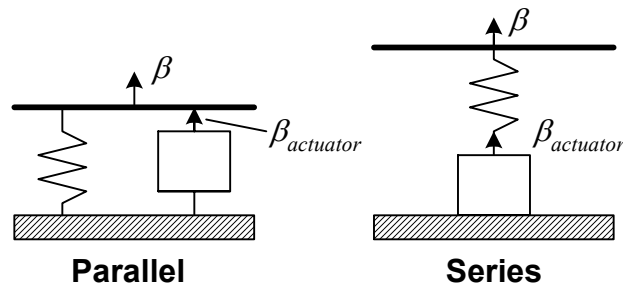


Figure 6.1: Illustration of a spring and actuator in parallel and in series

Brooks *et al.* [1985] used a series arrangement for a flapping pterosaur model and showed that this resulted in a large reduction in the required actuator current. Bennett *et al.* [1985] studied the muscles in the tails of whales and found that the muscles were in series with elastic tissue. They attempted to show that this configuration minimized the negative work required by the muscles, but found the opposite. Blickhan and Cheng [1994] revisited this study and found that the elastic tissues did in fact reduce the amount of negative work required by the muscles. They used an unsteady vortex lattice method to model the aerodynamics and showed that Bennett's simplified quasi-steady aerodynamic model was insufficient. Pennycuik [1976] studied the elastic

properties of feather shafts in birds and showed that they were capable of acting as an efficient spring. It is not clear whether this would be a parallel or series arrangement because it depends on how the muscles are attached and what part of the wing is deforming. Weis-Fogh [1960] studied the elastic properties of insect cuticles, which acted as springs in the hinges of insect wings. Because the spring was at the hinge, it was a parallel configuration. Weis-Fogh [1973] later concluded from an energy analysis, which considered only the positive work ($\eta = 0$), that these elastic mechanisms *must* be present for insect flight to be possible. In another similar study, Weis-Fogh [1972] discussed the possible benefits of elastic elements in hummingbirds, but mentioned that he was unable to find any such system upon dissecting a hummingbird. More importantly, he also mentioned that he was unaware of anybody describing an elastic system in any bird. Of course, as was mentioned previously, Pennycuick later found a type of elastic mechanism, but it is not clear whether this mechanism is effective.

For the present analysis a parallel spring arrangement will be considered. A similar discussion for the series arrangement is presented by Blickhan and Cheng [1994]. For a given reduced frequency, the parallel and series arrangements may be designed to give the same optimal performance. The difference between the two comes in their off-design operation. Generally, the series arrangement is significantly better in off-design conditions. For the parallel arrangement, the required power can be written as

$$C_{P,spring}(\tau) = -K_S [\bar{\beta} \cos(\bar{k}\tau) - \bar{\beta}_s] \bar{\beta} \bar{k} \sin(\bar{k}\tau) \quad (6.10)$$

where $\bar{\beta}_s$ is the value of β at which the spring produces no force and K_S is nondimensional spring stiffness per-unit length, which is defined as $K_S = G/q$, where G is the dimensional spring stiffness per-unit length (N/m²) and q is the dynamic pressure.

Combining Eqs. (6.4), (6.8), and (6.10), the total output power required by the actuator to maintain the prescribed flapping motion can be written as

$$\begin{aligned} C_{P,out}(\tau) &= C_P + C_{P,inertial} + C_{P,spring} \\ &= A \sin^2(\bar{k}\tau) + B \sin(\bar{k}\tau) \cos(\bar{k}\tau) + C \sin(\bar{k}\tau) \\ &= \frac{A}{2} - \frac{A}{2} \cos(2\bar{k}\tau) + \frac{B}{2} \sin(2\bar{k}\tau) + C \sin(\bar{k}\tau) \end{aligned} \quad (6.11)$$

where

$$\begin{aligned}
A &= \bar{\beta}^2 \Phi_2 \\
B &= \bar{\beta}^2 (\Phi_1 + K_I \bar{k}^3 - K_S \bar{k}) \\
C &= (\bar{\beta}_0 \Phi_3 + K_S \bar{\beta}_s \bar{k}) \bar{\beta}
\end{aligned} \tag{6.12}$$

The average value of $C_{P,out}$ is equal to $A/2$, which is the same as \bar{C}_p in Eq. (6.6), meaning the spring and inertia do not contribute. The last line in Eq. (6.11) shows that $C_{P,out}$ will be positive for every value of τ if B and C are zero and Φ_2 is positive. The likelihood of Φ_2 being positive will be discussed later, but let us assume that it is true for the current discussion. If K_S and $\bar{\beta}_s$ are free design variables, then from Eq. (6.12) they can be chosen to make B and C equal to zero. This leads to the following

$$\begin{aligned}
K_{S,opt} &= \Phi_1 / \bar{k} + K_I \bar{k}^2 \\
\bar{\beta}_{S,opt} &= -\frac{\bar{\beta}_0 \Phi_3}{\Phi_1 + K_I \bar{k}^3}
\end{aligned} \tag{6.13}$$

Because $K_{S,opt}$ is a nondimensional coefficient, it makes things more clear if G_{opt} is written instead, which results in

$$\begin{aligned}
G_{opt} &= \frac{1}{2} \rho U^2 (\Phi_1 / \bar{k} + K_I \bar{k}^2) \\
&= \frac{1}{2} \rho (\Phi_1 U^3 / (\omega c) + K_I (\omega c)^2)
\end{aligned} \tag{6.14}$$

For a given design condition, which is defined by ω and U separately (i.e. not just \bar{k}), G_{opt} and $\bar{\beta}_{S,opt}$ may be chosen from Eqs. (6.13) and (6.14) therefore resulting in Eq. (6.11) reducing to the following for $C_{P,out}$

$$C_{P,out}(\tau) = \frac{A}{2} - \frac{A}{2} \cos(2\bar{k}\tau) \tag{6.15}$$

Assuming G_{opt} and $\bar{\beta}_{S,opt}$ cannot be varied during flight, it is important to know what range of ω and U values that the spring system remains beneficial compared to having no spring. A simplified case of practical significance considers the range of U values for a fixed ω and a $\bar{\beta}_s$ that is always optimal, or $\bar{\beta}_0$ and $\bar{\beta}_s$ may be considered zero (meaning C is always zero). From Eq. (6.12), if there is no spring the value of B in Eq. (6.11) is

$$B_0 = \bar{\beta}^2 \left(\Phi_1(\omega, U) + K_I \left(\frac{\omega c}{U} \right)^3 \right) \tag{6.16}$$

At the design value of U (U_{des}), the design value of G is obtained from Eq. (6.14) and the corresponding B is equal to zero. At an off-design value of U defined as

$$U_{off} = U_{des} + \Delta U \quad (6.17)$$

which corresponds to the following value of B

$$B_{off} = \bar{\beta}^2 \left(\Phi_1(\omega, U_{des} + \Delta U) + K_I \left(\frac{\omega c}{U_{des} + \Delta U} \right)^3 - \frac{2G_{des}\omega}{\rho(U_{des} + \Delta U)^2} \right) \quad (6.18)$$

For the spring to be beneficial, the following equation must be true

$$B_0(U_{des} + \Delta U) > B_{off}(U_{des} + \Delta U) \quad (6.19)$$

which leads to the following equation

$$0 < \frac{2G_{des}\omega}{\rho(U_{des} + \Delta U)^2} < \Phi_1(\omega, U_{des} + \Delta U) + K_I \left(\frac{\omega c}{U_{des} + \Delta U} \right)^3 \quad (6.20)$$

The lower limit indicates that ΔU may become as large (positive) as desired and the spring will remain beneficial. The upper limit requires knowledge of Φ_1 , but once this is known Eq. (6.20) allows for the largest negative value of ΔU to be determined. This will be discussed later.

Returning to Eq. (6.11), the values of τ at which $C_{P,out}$ is zero (τ_0) must be known to determine the required actuator energy (C_{Wa}) as discussed in Chapter 5. For our purposes, the first five roots of Eq. (6.11) are required, which are equal to the following

$$\begin{aligned} \tau_{0,1} &= 0 \\ \tau_{0,2} &= \frac{1}{\bar{k}} \left[\cos^{-1} \left(-\frac{C}{\sqrt{A^2 + B^2}} \right) - \tan^{-1} \frac{-A}{B} \right] \\ \tau_{0,3} &= \pi / \bar{k} \\ \tau_{0,4} &= \frac{1}{\bar{k}} \left[2\pi - \cos^{-1} \left(-\frac{C}{\sqrt{A^2 + B^2}} \right) - \tan^{-1} \frac{-A}{B} \right] \\ \tau_{0,5} &= 2\pi / \bar{k} \end{aligned} \quad (6.21)$$

where in some cases $\tau_{0,2}$ may be larger than $\tau_{0,3}$. The inverse cosine term in these equations indicate that if $C > \sqrt{A^2 + B^2}$, then $\tau_{0,2}$ and $\tau_{0,4}$ are imaginary and therefore only $\tau_{0,1}$, $\tau_{0,3}$, and $\tau_{0,5}$ are physically realized. Figure 6.2 shows an example of $C_{P,out}$ and the corresponding τ_0 values.

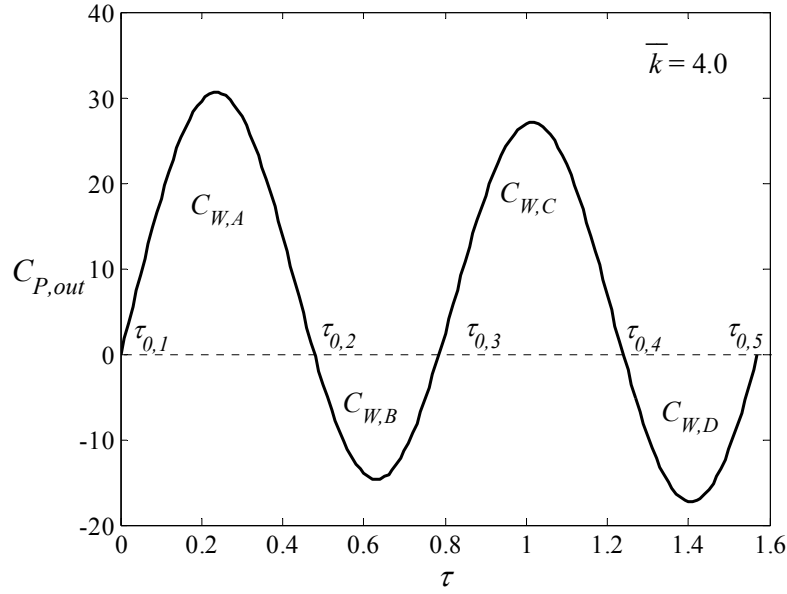


Figure 6.2: Example of the variation of $C_{P,out}$ with τ and an illustration of the C_W and τ_0 terms

Also shown in Figure 6.2 are the four distinct components of C_W obtained by integrating $C_{P,out}$ over the appropriate regions of τ . From Eq. (6.11), these components evaluate to the following

$$\begin{aligned}
 C_{W,A}(\tau) &= \frac{1}{4\bar{k}} \left(B + 4C + 2\bar{k}A\tau_{0,2} - A \sin(2\bar{k}\tau_{0,2}) - B \cos(2\bar{k}\tau_{0,2}) - 4C \cos(\bar{k}\tau_{0,2}) \right) \\
 C_{W,B}(\tau) &= \frac{1}{4\bar{k}} \left(-B + 4C + 2A\pi - 2\bar{k}A\tau_{0,2} + A \sin(2\bar{k}\tau_{0,2}) + B \cos(2\bar{k}\tau_{0,2}) + 4C \cos(\bar{k}\tau_{0,2}) \right) \\
 C_{W,C}(\tau) &= -\frac{1}{4\bar{k}} \left(-B + 4C + 2A\pi - 2\bar{k}A\tau_{0,4} + A \sin(2\bar{k}\tau_{0,4}) + B \cos(2\bar{k}\tau_{0,4}) + 4C \cos(\bar{k}\tau_{0,4}) \right) \\
 C_{W,D}(\tau) &= \frac{1}{4\bar{k}} \left(-B - 4C + 2A\pi - 2\bar{k}A\tau_{0,4} + A \sin(2\bar{k}\tau_{0,4}) + B \cos(2\bar{k}\tau_{0,4}) + 4C \cos(\bar{k}\tau_{0,4}) \right)
 \end{aligned} \tag{6.22}$$

These equations must be changed accordingly if $\tau_{0,2}$ is larger than $\tau_{0,3}$. To apply Eq. (5.24) for the input energy to the actuator (C_{W_a}), C_{W+} and C_{W-} are defined from Figure 6.2 as

$$\begin{aligned}
 C_{W+} &= C_{W,A} + C_{W,C} \\
 C_{W-} &= -(C_{W,B} + C_{W,D})
 \end{aligned} \tag{6.23}$$

which is true for most practical configurations. Note the negative sign is present in the C_{W-} equation because, as defined in Chapter 5, C_{W-} is the absolute value of the negative work. From Eq. (5.24), C_{W_a} is written as

$$C_{W_a} = C_{W+} + \eta C_{W-} \tag{6.24}$$

which depends on the actuator parameter η . Note that an actuator is not 100% efficient at producing positive work as indicated by Eq. (6.24). Another efficiency to account for this could

be introduced and multiply the right-hand side of Eq. (6.24). This is not done here because we are interested in observing the relative effect of the required negative work on the input energy to the actuator, which requires only the relative efficiency represented by η .

From C_{W_a} in Eq. (6.24), the average value of C_{P_a} can be written as

$$\bar{C}_{P_a} = \frac{\bar{k}}{2\pi} C_{W_a} \quad (6.25)$$

Similarly to Eq. (6.7), the efficiency of the system is defined as

$$\eta_{act} = -\frac{\bar{C}_d}{\bar{C}_{P_a}} \quad (6.26)$$

which is equal to η_{aero} when $\eta = -1$ or when C_{W_a} is zero.

6.3 Flapping by Heave Motions

The fundamental motion for flapping propulsion is the heave motion with ψ defined in Eq. (2.75) and $\bar{\beta}$ representing the maximum value of z_c/c . To allow a steady-state lift to be present throughout the motion, a constant value of angle of attack is superimposed on the heave motion ($\bar{\beta}_0 = \alpha_0$), which defines Φ_3 . From Tables 2.1 and 2.2 and Eq. (6.5), the Φ terms are found to equal the following

$$\begin{aligned} \Phi_1(\bar{k}, \theta) &= 2\pi\bar{k}^2 \left(\frac{\bar{k}}{4} + G \right) \\ \Phi_2(\bar{k}, \theta) &= 2\pi\bar{k}^2 F \\ \Phi_3(\theta) &= 2\pi\bar{k} \end{aligned} \quad (6.27)$$

From this equation and Eq. (6.6), the average power coefficient is simply

$$\bar{C}_p = \bar{\beta}^2 \pi\bar{k}^2 F \quad (6.28)$$

Also, from Eq. (4.32) the average drag coefficient is found to equal

$$\bar{C}_d = -\pi\bar{k}^2 \bar{\beta}^2 (F^2 + G^2) \quad (6.29)$$

which allows the aerodynamic efficiency in Eq. (6.7) to be written as

$$\eta_{aero} = -\frac{F^2 + G^2}{F} \quad (6.30)$$

This equation was first presented in the English-speaking literature by Garrick [1936]. Experimental validation of this theory has been provided by, for example, Anderson *et al.* [1998] and Delaurier and Harris [1982].

Results for the total efficiency (η_{act}) of a heaving airfoil with no spring or inertia forces are shown in Figures 6.3 and 6.4. In Figure 6.3 the effect of negative work is seen to greatly reduce the efficiency for large values of reduced frequency. Recall that the $\eta = -1$ case corresponds to η_{aero} , given by Eq. (6.30). The cases shown in this figure have no constant lift component ($\bar{\beta}_0 = 0$). Figure 6.4 shows the effect of $\bar{\beta}_0$ being nonzero, where in these cases $\bar{\beta}_0$ represents a constant angle of attack (α_0). For small values of reduced frequency, the difference in the efficiency with $\eta = 1$ is seen to be large. For large values of reduced frequency, the different values of α_0 converge to the zero lift case shown in Figure 6.3.

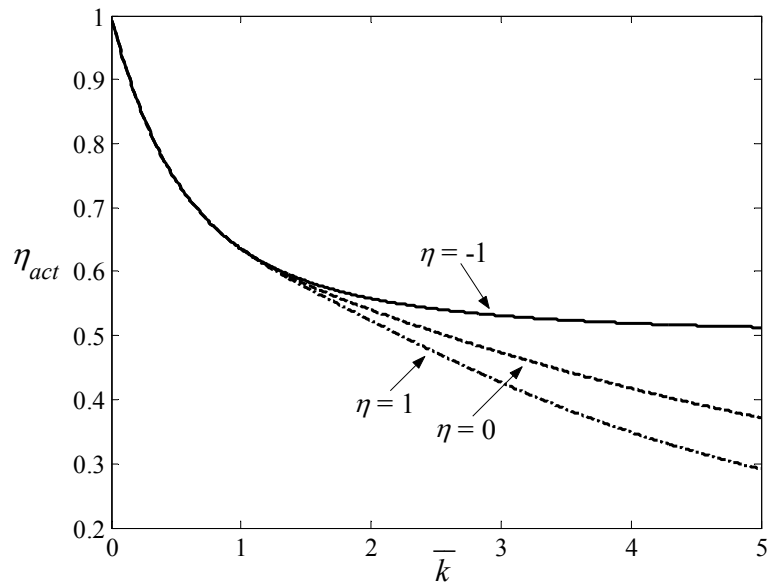


Figure 6.3: The efficiency of propulsion for a heaving airfoil (no inertia or spring components)

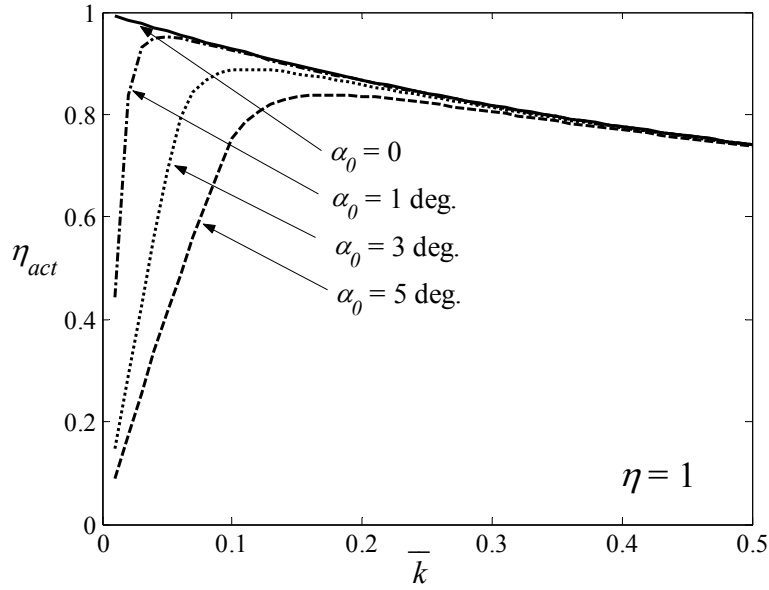


Figure 6.4: The efficiency (no inertia or spring components) for different α_0 values

The discussion of the range of U values for which a spring of fixed stiffness was beneficial ended at Eq. (6.20), which required Φ_2 to be specified. Substituting Φ_2 in Eq. (6.25) into Eq. (6.20) results in the following

$$0 < \frac{2G_{des}\omega}{\rho(U_{des} + \Delta U)^2} < 2\pi \left(\frac{\omega c}{U_{des} + \Delta U} \right)^2 F + K_I \left(\frac{\omega c}{U_{des} + \Delta U} \right)^3 \quad (6.31)$$

where F is a function of ω and U . Because we already found that the spring remains beneficial as ΔU becomes large, meaning \bar{k} becomes small, we are not concerned with the small \bar{k} case. Considering the large \bar{k} case, F may be approximated by Eq. (2.46), rewritten as follows in terms of \bar{k}

$$F = \frac{1}{2} \left(1 + \frac{1}{2\bar{k}^2} + O(k^{-4}) \right) \quad (6.32)$$

Substituting this into Eq. (6.31) and considering the right inequality, the following equation is obtained after some algebra which may be solved for the lower (negative) limit of ΔU .

$$\frac{\pi}{2} (U_{des} + \Delta U)^3 + \left(\pi(\omega c)^2 - \frac{2G_{des}\omega}{\rho} \right) (U_{des} + \Delta U) + (\omega c)^3 K_I = 0 \quad (6.33)$$

In summary, ΔU may be as large and positive as desired for the spring designed for U_{des} to be beneficial over the no spring case, but beyond the negative ΔU found from Eq. (6.33), the system requires more energy than if there was no spring.

6.4 Flapping Wing Performance Analysis

This section will investigate the actuator input energy required by a full flapping wing vehicle using the theoretical developments of the previous sections. There has been a significant amount of past research to determine the energy required for flapping flight (a review is presented by Shyy *et al.*), although nearly all of it has been concerned with determining the output energy required by actuators or muscles instead of the input energy required. Because the role of negative work could be large, the required output energy required by actuators does not provide sufficient guidance towards an energy efficient flapping device.

To apply the two-dimensional theory that has been used throughout this report to a three-dimensional wing, some approximations suggested by DeLaurier [1993] are made. But first, the wing geometry and motion must be defined. Figure 6.5 shows the front view of a half-span, where the dark line is the wing surface and s is the wing half-span. The amplitude of the total flapping motion is defined by $\bar{\sigma}$ and the instantaneous flap angle measured from the y -axis is defined as

$$\sigma(\tau) = \frac{\bar{\sigma}}{2} \cos(\bar{k}\tau) \quad (6.34)$$

We will treat the airfoil section at the span location $s/2$ as the representative section for the half span. To applying the heaving airfoil equations to this section, the maximum arc-length measured from the y -axis is β , which is written as

$$\begin{aligned} \beta(\tau) &= \frac{s\bar{\sigma}}{4c} \cos(\bar{k}\tau) \\ \bar{\beta} &= \frac{s\bar{\sigma}}{4c} \end{aligned} \quad (6.35)$$

Figure 6.6 shows the side view of a half-span, which shows that the flapping axis is assumed to remain parallel to the free-stream velocity. The steady-state lift is assumed to be produced by the angle of attack of the wings relative to the flapping axis. The difference between the flapping axis being at an angle of attack and the wings relative to the flapping axis being at an angle of attack is not large if $\bar{\sigma}$ is less than 45 degrees. The normal force coefficient of the entire wing can be written as

$$C_N = 2\pi(\theta - w_0) + \text{unsteady terms} \quad (6.36)$$

where the three-dimensional downwash correction used by DeLaurier is defined as

$$w_0 = \frac{2\theta}{2 + AR} \quad (6.37)$$

where AR is the wing aspect ratio. To obtain the average lift coefficient for one cycle of oscillation, the following equation is used

$$\bar{C}_L = \frac{\bar{k}}{2\pi} \int_0^{2\pi/\bar{k}} C_N \cos(\sigma) d\tau \quad (6.38)$$

which from Eq. (6.34) and (6.36) results in

$$\bar{C}_L = 2\pi\theta J_0(\bar{\sigma}/2) \left(1 - \frac{2}{2 + AR}\right) \quad (6.39)$$

where J_0 is a zeroth order Bessel function of the first kind. Note that the unsteady terms in Eq. (4.34) do not contribute to the average lift coefficient.

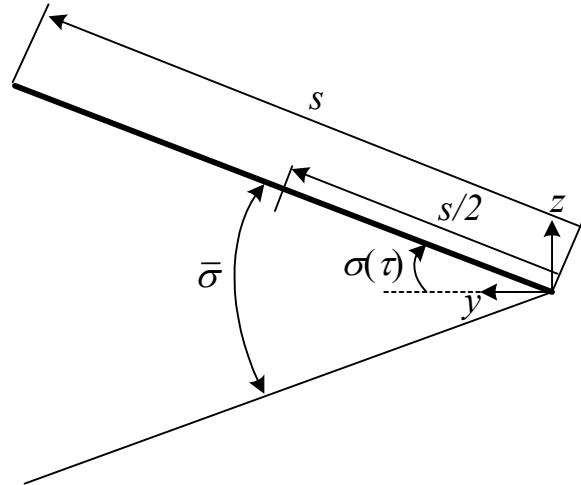


Figure 6.5: Front view of a half-span of the flapping wing

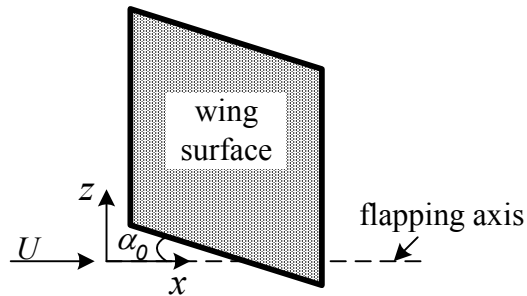


Figure 6.6: Side view of a half-span of the flapping wing

For steady level flight, the average lift must balance the weight of the aircraft, which is expressed in the following equation

$$qS\bar{C}_L - mg = 0 \quad (6.40)$$

where S is the wing area, m is the aircraft mass, and g is gravity. Also, for steady flight the thrust must equal the drag, which is expressed as

$$\frac{(qS\bar{C}_L)^2}{4e\pi q s^2} + qS(C_{d,pro} + C_{d,par}) + qS\bar{C}_d = 0 \quad (6.41)$$

where the first term is the induced drag, the second term is the profile drag, the third term is the parasite drag, and the fourth term is the unsteady component determined in Section 4.6 (which is actually the thrust). The profile and parasite drag terms are discussed by Pennycuick [1968], Tucker [1973] and Rayner [1979a and 1979b] in the context of bird flight. Although the present analysis is not specific to bird flight, the value for $C_{d,pro}$ given by Rayner and the expression for $C_{d,par}$ given by Tucker will be used:

$$\begin{aligned} C_{d,pro} &= 0.02 \\ C_{d,par} &= 3.34 \times 10^{-3} m^{2/3} / S \end{aligned} \quad (6.42)$$

where m is in kg and S is in m^2 . For a given aircraft mass (m), wing area (S), half-span (s), and dynamic pressure (q), the thrust due to flapping ($-\bar{C}_d$) must equal the combination of induced, parasite, and profile drag. From Eq. (6.41), this results in the following required value of \bar{C}_d

$$\bar{C}_{d,req} = -\frac{(mg)^2}{4Se\pi q^2 s^2} - (C_{d,pro} + C_{d,par}) \quad (6.43)$$

From Eqs. (6.29 and 6.35) the average drag due to flapping produced by a given $\bar{\sigma}$ and \bar{k} is written as

$$\bar{C}_d = -\pi\bar{k}^2 \left(\frac{s\bar{\sigma}}{4c} \right)^2 [F^2 + G^2] \quad (6.44)$$

which must be negative to indicate thrust. The components of the Theodorsen function, F and G , in Eq. (6.44) are incorrect for finite aspect ratio wings. Jones [1940] presented aspect ratio corrections and DeLaurier [1993] presented a simplified form of Jones's equations, which are written as follows

$$\begin{aligned} F(\bar{k}) &= \frac{AR}{(2+AR)} \left(1 - \frac{C_1\bar{k}^2}{4(\bar{k}^2/4 + C_2^2)} \right) \\ G(\bar{k}) &= -\frac{AR}{(2+AR)} \left(\frac{C_1C_2\bar{k}}{2(\bar{k}^2/4 + C_2^2)} \right) \end{aligned} \quad (6.45)$$

where

$$\begin{aligned} C_1 &= \frac{0.5AR}{2.32 + AR} \\ C_2 &= 0.181 + \frac{0.772}{AR} \end{aligned} \quad (6.46)$$

Equating Eq. (6.44) with Eq. (6.43) and assuming U and ω are given, the required flapping amplitude is found to equal

$$\bar{\sigma} = \frac{4c}{s} \sqrt{\frac{\frac{(mg)^2}{e\pi q^2 S b^2} + 0.02 + 3.34 \times 10^{-3} m^{2/3} / S}{\pi \bar{k}^2 (F^2 + G^2)}} \quad (6.47)$$

Substituting this into Eqs. (6.6) and (6.35), the average aerodynamic power for one cycle is written as

$$\bar{C}_P = \left(\frac{(mg)^2}{4Se\pi q^2 s^2} + 0.02 + 3.34 \times 10^{-3} m^{2/3} / S \right) \frac{F}{F^2 + G^2} \quad (6.48)$$

which, as mentioned while discussing Eq. (6.11), is the same as the average output power required by the actuators ($\bar{C}_{P,out}$). Note that this equation is just the average required thrust divided by the aerodynamic efficiency: $-\bar{C}_{d,req} / \eta_{aero}$. Also, this equation is independent of the spanwise location of the chosen representative airfoil section.

With $\bar{\sigma}$ known from Eq. (6.47), the required angle of attack (θ) is determined by combining Eqs. (6.39) and (6.40), which results in

$$\theta = \frac{mg}{2\pi q S J_0(\bar{\sigma}/2) \left(1 - \frac{2}{2 + AR} \right)} \quad (6.49)$$

This is the last term required to calculate $C_{P,out}$ from Eqs. (6.11) and (6.12) for a given aircraft configuration (AR, S, s, m, m_a), flight speed (U), and flapping frequency (ω); where $\bar{\beta}_0 = \theta$ and $\bar{\beta}$ is defined in Eq. (6.35). From the procedure discussed with Eqs. (6.21-6.25), the average actuator input power (\bar{C}_{Pa}) may be determined. Note that \bar{C}_{Pa} is dependent upon θ , which represents the steady lift component, whereas $\bar{C}_{P,out}$ is not. In the case of swimming flapping wing propulsion, the value for m in the above analysis is set to zero. Also, the parasite and profile drag coefficients in Eq. (6.42) must be changed to account for the fluid being water instead of air.

The above procedure was applied to two flapping wing cases: a Pigeon and a Pied Flycatcher, which have been studied previously by Pennycuick [1968], Rayner [1979b], and Phlips *et al.* [1981]. Phlips *et al.* presents a comparison of the three studies. These past studies only calculated the average aerodynamic power (\bar{C}_p), therefore ignoring the difference in the energy cost of positive and negative muscular work. The present analysis will calculate the average input power (\bar{C}_{pa}) to the flapping actuators, or in this case the flapping muscles. The relative energy cost of positive and negative work, represented by η in Eq. (5.7), is just as applicable to muscles as to actuators (Margarita [1976]). From Weis-Fogh's [1972] statement that there are no elastic mechanisms in the wing of a bird, no spring will be present in our analysis. The inertia will also be ignored, which has been assumed negligible in past studies. To be consistent with the comparison presented by Phlips *et al.*, the results are presented in terms of the dimensional average power, which for the three-dimensional wing is defined as

$$\bar{P}_a = qUS\bar{C}_{pa} \quad (6.50)$$

Figures 6.7 and 6.8 present the defining parameters for each bird as well as the power curves resulting from the present method. Recall that for the $\eta = -1$ case, $\bar{C}_{pa} = \bar{C}_p$, which should therefore be in closest agreement with the curves presented by Phlips *et al.*. This is the case, and the present method with $\eta = -1$ predicts a minimum power of nearly equal magnitude at about the same flight speed as the past studies. For the η equal to zero and one cases, the required power is noticeably increased at low flight speeds. This means that there is a significant amount of negative power required during the flapping cycle. An important consequence of this is seen to be the change in the minimum power flight speed, which is marked by an X in both figures. For both birds, the minimum power flight speed increases as η increases. The reason for the large amount of negative power at low flight speeds, which correspond to large values $\theta (= \alpha_0)$, is apparent from Figure 6.4. If a spring was added to this system with a K_s and $\bar{\beta}_s$ determined from Eq. (6.13), the η equal to zero and one curves would reduce to the $\eta = -1$ curve. Thus, a significant reduction in the required power would be obtained. Note that adding an inertia term to this case would increase the amount of negative power; meaning a spring would be even more beneficial. The importance of springs in flapping wing flight does not seem to be emphasized enough in the literature. The only mention of this significance in a non-Biological study seems to be that of Brooks *et al.* [1985]. They show experimentally a reduction in the required current for a flapping motor with a spring system. They also mention that this is an issue that has not been

“adequately addressed” by past research and many past ornithopter designs operate inefficiently as a result.

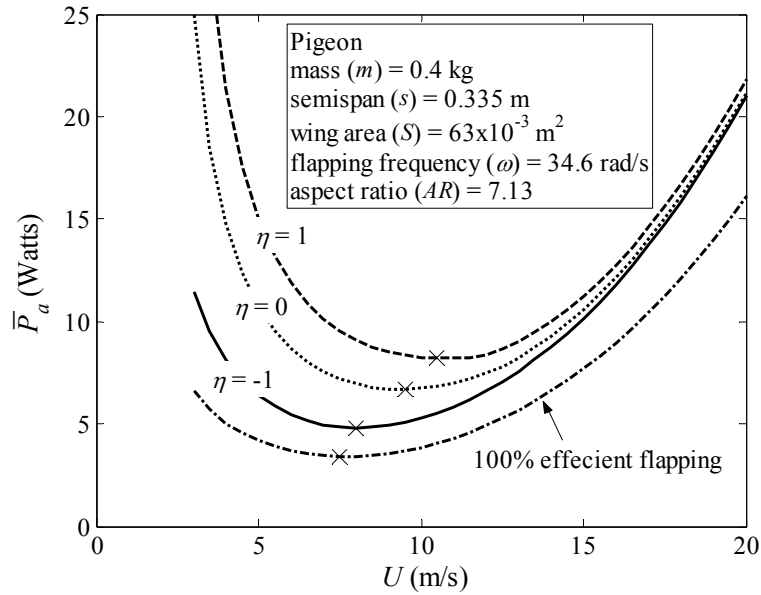


Figure 6.7: Average actuator input power versus flight speed for a Pigeon

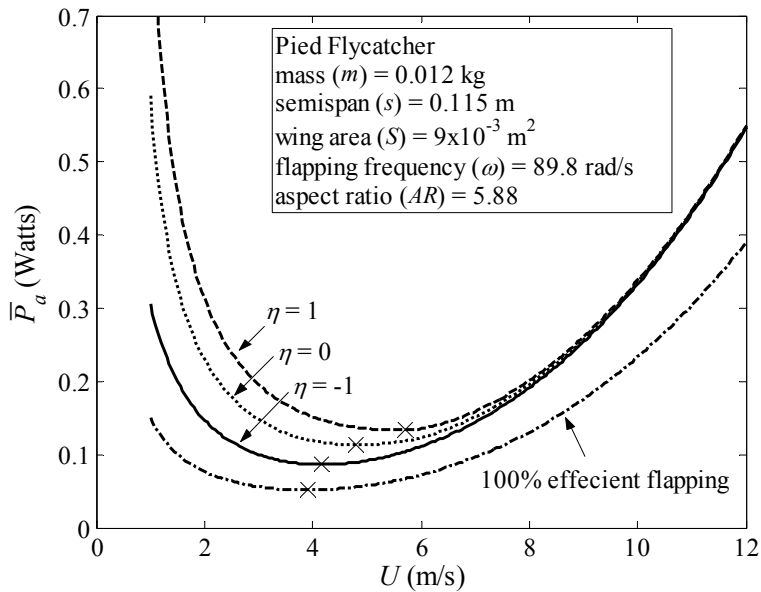


Figure 6.8: Average actuator input power versus flight speed for a Pied Flycatcher

The curve labeled “100% flapping efficiency” in Figures 6.7 and 6.8 represents the required thrust from Eq. (6.43) multiplied by the velocity. This is the power that would be required from

the engine of a fixed wing aircraft of the same size and mass. Thus, there is an apparent penalty for flapping wing propulsion. It could be argued that a fixed wing aircraft would require a larger mass to account for an engine, and therefore this penalty would not be present. Woods *et al.* [2001] compared the power requirements of flapping wings, rotary wings, and fixed wings for micro air vehicles. For a 50 g vehicle, flapping wings were shown to require less power in a range of flight velocities between 3 and 10 m/s. Spedding and Lissaman [1998] also discussed the power requirements for small flapping or fixed wing vehicles. They found that flapping and rotary wings have similar power requirements.

6.5 Multi-Degree-of-Freedom Flapping

This chapter has been limited so far to single-degree-of-freedom flapping propulsion using heave motions. In general, flapping propulsion may use multiple-degrees-of-freedom, and it is not required that any of these degrees-of-freedom be heaving. For example, Wu [1961] and Daniel [1987] studied the propulsion characteristics of progressive chordwise waves on a thin airfoil and Nakashima and Ono [1996 and 200] studied the propulsion of an airfoil modeled as a three-joint bending mechanism. The most common mode of flapping wing propulsion, though, uses a combination of pitch and heave. This has been studied extensively by, for example, Lighthill [1970], Wu, [1971], Jones *et al.* [2001], and Neef and Hummel [2001]. Lighthill and Wu both studied the problem using thin airfoil theory and determined the ratio of pitch and heave amplitudes and the phase angle that resulted in the maximum propulsive efficiency. Jones *et al.* and Neef and Hummel studied the problem numerically and showed agreement with the thin airfoil theory results. From Appendix B of this report, the thrust for a general multi-degree-of-freedom system may be determined analytically. The required power can be derived similarly to Section 6.2, although this is not presented. To determine the actuator input energy, the actuator layout must be specified. For example, are the degrees of freedom actuated independently with different actuators or are they linked? We will assume that one actuator is used for the entire system. The separation of $C_{P,out}$ into negative and positive work can be done similarly to Section 6.2 although a numerical approach to determining the τ_θ values simplifies the problem. This section will show how negative work influences the optimal pitching axis determined by Lighthill.

In his study of flapping, Lighthill defined a “feathering parameter” as

$$\theta = \frac{U\alpha}{\omega h} \quad (6.49)$$

where α and h are the pitch and heave amplitudes, respectively. He also made the assumption that the pitch and heave motions were 90 degrees out-of-phase. This allowed the pitching axis to be a free parameter. On the other hand, Wu fixed the pitching axis and allowed the phase angle to be the free parameter. Lighthill also defined a thrust coefficient as follows

$$C_T = -\frac{\overline{D}c}{\omega^2 h^2 x_a} \quad (6.50)$$

where x_a is the pitching axis. In Figure 4 of Lighthill [1970], the aerodynamic efficiency (η_{aero}) and C_T are plotted as a function of reduced frequency. The conclusion is made that for highest efficiency with large thrust, the pitching axis should be towards the trailing edge. Figures 6.9 and 6.10 present a similar analysis, except in this case, η_{act} is presented instead of η_{aero} . The thick lines in Figure 6.9 represent the $\eta = -1$ case, which as mentioned before, means that $\eta_{aero} = \eta_{act}$. In other words, the thick lines reproduce Lighthill's results. Examining both figures for this case, it can be concluded that for high reduced frequency, the $x_a/c = 1.0$ and $\theta = 0.8$ case is the best for maintaining both high thrust and high efficiency (which is Lighthill's conclusion). The thin line present the $\eta = 0$ case, which means the influence of negative power is accounted for. It turns out, that for the $x_a/c = 0.5$ and $\theta = 0.6$ case, the $\eta = 0$ and -1 lines lie on top of each other, meaning that there is a very small amount of negative power. But more importantly, for large values of reduced frequency η_{act} is largest for this case. In Figure 6.10 it is seen that this case also produces nearly the same amount of thrust as does the $x_a/c = 1.0$ and $\theta = 0.8$ case. Also, the component of the thrust due to leading edge suction is smallest for the $x_a/c = 0.5$ and $\theta = 0.6$ case. This means that, as pointed out by Lighthill, the actual flow is less likely to have leading edge separation and thrust is less sensitive to viscous effects. We can conclude from this discussion that the $x_a/c = 0.5$ and $\theta = 0.6$ case is more effecient than the $x_a/c = 1.0$ and $\theta = 0.8$ case suggested by Lighthill. If there is an optimal elastic mechanism, though, as shown before the results for the $\eta = -1$ case are true, and therefore Lighthill's result is applicable. Note also that this analysis assumed there was a single actuator operating both the heaving and pitching motions. If this was not assumed, the phase angle between the pitch and plunge would become a free parameter and could not be assumed to be 90 degrees.

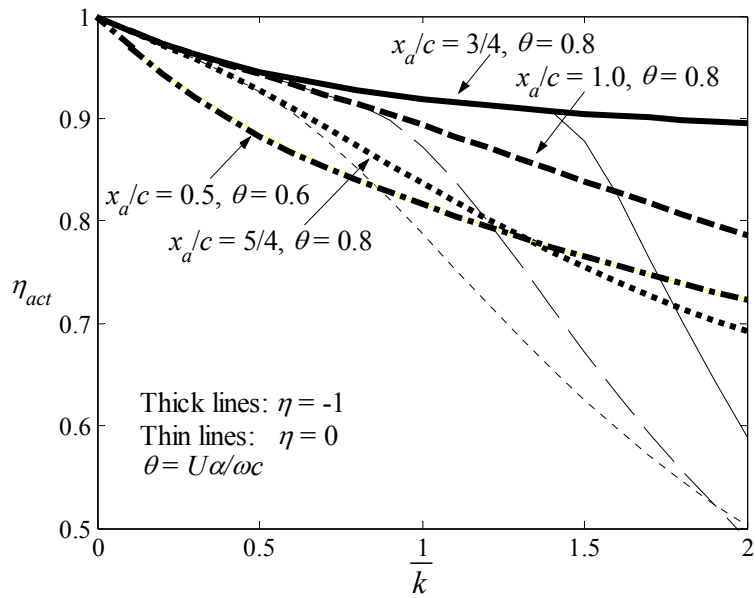


Figure 6.9: The influence of negative work on Lighthill's conclusion regarding the pitching axis and feathering parameter for highest efficiency

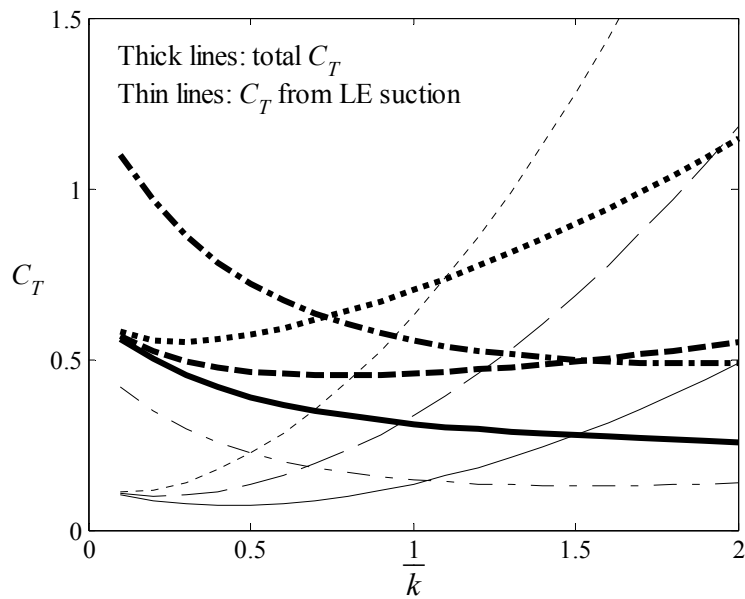


Figure 6.10: The influence thrust coefficient, as defined by Lighthill, for the cases shown in the previous figure

References

Abbot, B. C., Bigland, B., and Ritchie, J. M., "The Physiological Cost of Negative Work," *Journal of Physiology*, Vol. 117, 1952, pp. 380-390.

Abzug, M. J., "Estimation of the Lift and Moment Parameters of Leading-Edge Flaps," *Journal of the Aeronautical Sciences*, Vol. 22, No. 9, September 1955, pp. 655-656.

Albano, E., and Rodden, W. P., "A Doublet Lattice Method for Calculating Lift Distributions on Oscillating Surfaces in Subsonic Flows," *AIAA Journal*, Feb. 1969, pp. 279-285.

Alexander, R., McN., "Springs for Wings," *Science*, Vol. 268, April 1995, pp. 50-51.

Alexander, R., McN., "Storage of Elastic Strain Energy in Muscle and Other Tissues," *Nature*, Vol. 265, April 1977, pp. 114-117.

Allen, H. J., "Calculation of the Chordwise Load Distribution over Airfoil Sections with Plain, Split, or Serially Hinged Trailing-Edge Flaps," NACA Report No. 634, 1938.

Allen, H. J., "General Theory of Airfoil Sections Having Arbitrary Shape or Pressure Distribution," NACA Report No. 833, 1943.

Amiet, R. K., "Gust Response for Flat-Plate Airfoils and the Kutta Condition," *AIAA Journal*, Vol. 28, Oct. 1990, pp. 1718-1727.

Amiet, R. K., "Compressibility Effects in Unsteady Thin-Airfoil Theory," *AIAA Journal*, Vol. 12, Nov. 1974, pp. 252-255.

Anderson, G., Forster, E., Kolonay, R., and Eastep, F., "Multiple Control Surface Utilization in Active Aeroelastic Wing Technology," *Journal of Aircraft*, Vol. 34, July-August 1997, pp. 552-557.

Anderson, J. M., Streitlien, K., Barrett, D. S., Triantafyllou, M. S., "Oscillating Foils of High Propulsive Efficiency," *Journal of Fluid Mechanics*, Vol. 360, 1998, pp. 41-72.

Ardonceanu, P. L., "Unsteady Pressure Distribution over a Pitching Airfoil," *AIAA Journal*, Vol. 27, No. 5, May 1989, pp. 660-662.

Ashley, H., Dugundji, J., Neilson, D. O., "Two Methods for Predicting Air Loads on a Wing in Accelerated Motion," *Journal of the Aeronautical Sciences*, Vol. 19, No. 8, August 1952, pp. 543-552.

Bennett, M. B., Ker, R. F., Alexander, R. McN., "Elastic Properties in the Tails of Cetaceans (*Phocaena* and *Lagenorhynchus*) and their Effect on the Energy Cost of Swimming," *Journal of the Zoological Society of London*, Vol. 211, 1987, pp. 177-192.

Betz, A., *Tragflugeltheorie* (Dissertation), *Berichte u. Abhandlungen der WGL*, 1 Jahrgang, Heft 2, 1920.

Bisplinghoff, R. L., Ashley, H., and Halfman, R. L., *Aeroelasticity*, Addison-Wesley, 1955.

Blickhan, R., Cheng, J., "Energy Storage by Elastic Mechanisms in the Tail of Large Swimmers – a Re-evaluation," *Journal of Theoretical Biology*, Vol. 168, 1994, pp. 315-321.

Boyd, E. A., "Comment on a Conjecture of Tanner," *Journal of the Royal Aeronautical Society*, Vol. 67, 1963, pp. 127-129.

Boyd, E. A., "Generalisation of the Condition for Waviness in the Pressure Distribution on a Cambered Plate," *Journal of the Royal Aeronautical Society*, Vol. 67, 1963, pp. 529-530.

Boyd, E. A., "Comment on the "The Load Distribution on a Polynomial Mean Line and the Converse,"" *Journal of the Royal Aeronautical Society*, Vol. 68, 1964, pp. 59.

Brooks, A. N., MacCready, P. B., Lissaman, P. B. S., and Morgan, W. R., "Development of a Wing-Flapping Flying Replica of the Largest Pterosaur," AIAA paper 85-1446, 1985.

Chopra, M. G., "Wake Effects in Finite Amplitude Nonsteady Motion of Slender Profiles," *AIAA Journal*, Vol. 14, No. 8, August 1976, pp. 1145-1148.

Chuen, C., Huang M., "The Initial Lift and Drag on an Impulsively Started Airfoil of Finite Thickness," *Journal of Fluid Mechanics*, Vol. 118, 1982, pp. 393-409.

Daniel, T. L., "Forward Flapping Flight from Flexible Fins," *Canadian Journal of Zoology*, Vol. 66, 1988, pp. 630-638.

DeLaurier, J. D. and Harris, J. M., "Experimental Study of Oscillating Wing Propulsion," *Journal of Aircraft*, Vol. 19, No. 5, 1982, pp. 368-373.

DeLaurier, J. D., "An Aerodynamic Model for Flapping-Wing Flight," *Aeronautical Journal*, Vol. 97, April 1993, pp. 125-130.

Dengler, M. A., Goland, M., Luke, Y. L., "Notes on the Calculation of the Response of Stable Aerodynamic Systems," *Journal of the Aeronautical Sciences*, Vol. 19, No. 3, March 1952, pp. 213.

Dietze, F., "The Air Forces on a Harmonically Oscillating Self-Deforming Plate," *Luftfahrtforschung*, Vol. 16, No. 2, 1939, pp. 84.

Dietze, F., "Law of Aerodynamic Force of a Jointed Plate in Harmonic Motion," *Luftfahrtforschung*, Vol. 18, No. 4, 1941, pp. 135.

Dietze, F., "Comparative Calculations Concerning Aerodynamic Balance of Control Surfaces," in *Three Papers from Conference on Wing and Tail Surface Interactions*, (Translated from Lilienthal-Gesellschaft fur Luftfahrtforschung, March 1941, pp. 61-74), NACA TM 1306, 1951.

Dowell, E. H., *Modern Course in Aeroelasticity*, Kluwer Academic Publishers, 3rd Ed., 1995.

Ericsson, L. E., Reding, J. P., “Unsteady Airfoil Stall, Review and Extension,” *Journal of Aircraft*, Vol. 8, August 1971, pp. 609-616.

Fleischer, H., *Manual of Pneumatic Systems Optimization*, McGraw Hill, Inc., 1995.

Forster, E., Sanders, B., and Eastep, F., “Synthesis of a Variable Geometry Trailing Edge Control Surface,” AIAA paper 2003-1717, April 2003.

Forster, E., Sanders, B., and Eastep, F., “Modeling and Sensitivity Analysis of a Variable Geometry Trailing Edge Control Surface,” AIAA paper 2003-1807, April 2003.

Fung, Y. M., *An Introduction to the Theory of Aeroelasticity*, Dover, New York, 1969.

Garrick, I. E., “Propulsion of a Flapping and Oscillating Airfoil,” NACA Report No. 567, 1936.

Garrick, I. E., “On Some Reciprocal Relations in the Theory of Nonstationary Flows,” NACA Report No. 629, 1938.

Garrick, I. E., “A Review of Unsteady Aerodynamics of Potential Flows,” *Applied Mechanics Review*, Vol. 5, No. 3, March 1952, pp. 89-91.

Garrick, I. E., “Nonsteady Wing Characteristics,” in *Aerodynamic Components of Aircraft at High Speeds*, Vol. VII of *High Speed Aerodynamics and Jet Propulsion*, edited by Donovan, A. F., and Lawrence, H. R., 1957.

Gern, F. H., Inman, D. J., and Kapania, R. K., “Computation of Actuation Power Requirements for Smart Wings with Morphing Airfoils,” AIAA Paper 2002-1629, April 2002.

Giesing, J. P., “Vorticity and Kutta Condition for Multienergy Flows,” *ASME Journal of Applied Mechanics*, Sept. 1969, pp. 608-613.

Giurgiutiu, V., Rogers C. A., Ruscovici, R., “Power and Energy Issues in the Induced-Strain Actuation for Aerospace Adaptive Control,” AIAA paper 96-1300, 1996.

Glauert, H., *The Elements of Aerofoil and Airscrew Theory*, 2nd Edition, Cambridge University Press, 1947.

Goland, M., “The Quasi-Steady Air Forces for Use in Low-Frequency Stability Calculations,” *Journal of the Aeronautical Sciences*, Vol. 17, No. 10, October 1952, pp. 601-672.

Gradshteyn, I. S., and Ryzhik, I. M., *Tables of Integrals Series and Products*, Academic Press, New York and London, 1965, pp. 148.

Graham, J.M.R., “Similarity Rules for Thin Airfoils in Non-Stationary Flows,” *Journal of Fluid Mechanics*, Vol. 43, 1970, pp. 753-766.

Green, W. L., *Aircraft Hydraulic Systems*, John Wiley and Sons, 1985.

Halfman, R. L. “Experimental Aerodynamic Derivatives of a Sinusoidally Oscillating Airfoil in Two-Dimensional Flow,” NACA Report No. 1108, 1952.

Hancock, G. J., and Mabey, D. G., “Unsteady Aerodynamics of Controls,” AGARD CP-465, Aerodynamics of Combat Aircraft Controls and of the Ground, Oct. 1989.

Hariharan, N., and Leishman, J. G., “Unsteady Aerodynamics of a Flapped Airfoil in Subsonic Flow by Indicial Concepts,” *Journal of Aircraft*, Vol. 33, No. 5, March-April 1996, pp. 855-868.

Henderson, J. A., Weisshaar, T. A., and Sanders, B. “Integrated Wing Design with Adaptive Control Surfaces,” AIAA Paper 2001-1428, 2001.

Homentcovschi, D., “The Theory of the General Motion of a Thin Profile at a Small Incidence in an Inviscid Incompressible Fluid,” *ZAMM*, Vol. 65, No. 11, November 1985, pp. 537-544.

Jaekel, K., “On the Calculation of the Circulation Distribution for a Two-Dimensional Wing Having Periodic Motion,” *Luftfahrtforschung*, Vol. 16, No. 3, 1939, pp. 135.

Johnson, W., *Helicopter Theory*, Princeton University Press, 1980.

Johnston, C. O., *et al.* “A Model to Compare the Flight Control Energy Requirements of Morphing and Conventionally Actuated Wings,” AIAA paper 2003-1716, 2003.

Johnston, C. O., *Actuator-Work Concepts Applied to Morphing and Conventional Aerodynamic Control Devices*, M.S. Thesis, Virginia Tech, 2003.

Jones, K. D., and Platzer, M. F., “Numerical Computation of Flapping-Wing Propulsion and Power Extraction,” AIAA paper 97-0826, Jan. 1997.

Jones, K. D., Lund, T.C., and Platzer, M. F., “Experimental and Computational Investigation of Flapping Wing Propulsion for Micro Air Vehicles,” in *Fixed and Flapping Wing Aerodynamics for Micro Air Vehicles*, Chapter 16, 2001, pp. 307-339.

Jones, R. T., “The Unsteady Lift of a Wing of Finite Aspect Ratio,” NACA Report No. 681, 1940.

Jones, R. T., Cohen, D., “An Analysis of the Stability of an Airplane with Free Controls,” NACA Report No. 709, 1941.

Jones, R. T., *Wing Theory*, Princeton University Press, 1990, pp. 59-65.

Jones, W. P., “The Generalized Theodorsen Function,” *Journal of the Aeronautical Sciences*, Vol. 19, No. 3, March 1952, pp. 213.

Silverstein, A., Joyner, U. T., “Experimental Verification of the Theory of Oscillating Thin Airfoils,” NACA Report No. 673, 1939.

Katz, J., and Weihs, D., “The Effect of Chordwise Flexibility on the Lift of a Rapidly Accelerated Airfoil,” *Aeronautical Quarterly*, Vol. 30, 1979, pp. 360-370.

Katz, J., and Weihs, D., "Wake Rollup and the Kutta Condition for Airfoils Oscillating at High Frequency," *AIAA Journal*, Vol. 19, Dec. 1981, pp. 1604-1606.

Katz, J., and Plotkin, A., *Low-Speed Aerodynamics*, 2nd Edition, Cambridge University Press, 2001.

Kemp, N. H., "On the Lift and Circulation in Some Unsteady Flow Problems," *Journal of the Aeronautical Sciences*, Vol. 19, No. 10, October 1952, pp. 713-714.

Kemp, N. H., "Closed-Form Lift and Moment for Osborne's Unsteady Thin-Airfoil Theory," *AIAA Journal*, Vol. 11, Sept. 1973, pp. 1358-1360.

Kemp, N. H. and Homicz, G., "Closed-Approximate Unsteady Thin-Airfoil Theory for Subsonic Flow," *AIAA Journal*, Vol. 14, August 1976, pp. 1083-1089.

Kemp, N. H., "Simplified Formulas for Lift and Moment in Unsteady Thin Airfoil Theory," *AIAA Journal*, Vol. 16, August 1978, pp. 851-852.

Kussner, H. G., Schwarz, L., "The Oscillating Wing with Aerodynamically Balanced Elevator," NACA TM 991, 1941 (Translation).

Laitone, E. V., Walters, E. R., "The Application of Nonstationary Airfoil Theory to Dynamic Stability Calculations," *Journal of the Aeronautical Sciences*, Vol. 18, No. 3, March 1951, pp. 214-216.

Laitone, E. V., "Theodorsen's Circulation Function for Generalized Motion," *Journal of the Aeronautical Sciences*, Vol. 19, No. 3, March 1952, pp. 211-213.

Leishman, J. G., "Unsteady Lift of a Flapped Airfoil by Indicial Concepts," *Journal of Aircraft*, Vol. 31, No. 2, March-April 1994, pp. 288-297.

Leishman, J. G., "Two-Dimensional Model for Airfoil Unsteady Drag Below Stall," *Journal of Aircraft*, Vol. 25, No. 7, July 1988, pp. 665, 666.

Leishman, J. G., "A Semi-Empirical Model for Dynamic Stall," *Journal of the American Helicopter Society*, Vol. 34, July 1989, pp. 3-17.

Leishman, J. G., Comment on "Induced Drag Based on Leading-Edge Suction for a Helicopter in Forward Flight," *AIAA Journal*, Vol. 29, No. 9, September 1991, pp. 1532-1533.

Leishman, J. G., "Unsteady Aerodynamics of Airfoils Encountering Traveling Gusts and Vortices," *Journal of Aircraft*, Vol. 34, Nov.-Dec. 1997, pp. 719-729.

Leishman, J. G., *Principles of Helicopter Aerodynamics*, Cambridge University Press, 2000.

Li, C., Poling, D., and Wu, D., "Induced Drag Based on Leading Edge Suction for a Helicopter in Forward Flight," *AIAA Journal*, Vol. 28, No. 2, July 1990, pp. 201-204.

Li, C., Poling, D., and Wu, D., "Reply by the Authors to J. G. Leishman," *AIAA Journal*, Vol. 29, No. 9, July 1991, pp. 1534-1535.

Lighthill, M. J., "Aquatic Animal Propulsion of High Hydromechanical Efficiency," *Journal of Fluid Mechanics*, Vol. 44, part 2, 1970, pp. 265-301.

Llewelyn, R. P., "The Velocity Distribution on a Polynomial Mean Line and the Converse," *Journal of the Royal Aeronautical Society*, Vol. 68, 1964, pp. 57-58.

Lomax, H., "Indicial Aerodynamics," in *AGARD Manual on Aeroelasticity*, Part II, Chapter 7, June, 1960.

Luke, Y. L., and Dengler, M. A., "Tables of the Theodorsen Circulation Function for Generalized Motion," *Journal of the Aeronautical Sciences*, Vol. 18, No. 7, July 1951, pp. 478.

Margarita, R., *Biomechanics and Energetics of Muscular Exercise*, Clarendon Press, Oxford, 1976.

Mateescu, D., and Abdo, M., "Unsteady Aerodynamic Solutions for Oscillating Airfoils," AIAA paper 2003-227, 2003.

Maclean, B. J., and Decker, R. A., "Lift Analysis of a Variable Camber Foil Using the Discrete Vortex Blob Method," *AIAA Journal*, Vol. 32, No. 7, July 1994, pp. 1525-1527.

McCroskey, W. J., "Inviscid Flowfield of an Unsteady Airfoil," *AIAA Journal*, Vol. 11, August 1973, pp. 1130-1137.

McCroskey, W. J., "Unsteady Airfoils," *Annual Review of Fluid Mechanics*, Vol. 14, 1982, pp. 285-311.

McCune, J. E., "Unsteady Wing Theory – The Karman/Sears Legacy," AIAA paper No. 88-3539, 1988.

McCune, J. E., "Nonlinear Aerodynamics of Two-Dimensional Airfoils in Severe Maneuver," *AIAA Journal*, Vol. 28, No. 3, March 1990, pp. 385-393.

McCune, J. E., and Tavares, T. S., "Perspective: Unsteady Wing Theory - The Karman/Sears Legacy," Vol. 115, No. 12, December 1993, pp. 548 – 560.

McKinney, W., DeLaurier, J., "The Wingmill: An Oscillating-Wing Windmill," *Journal of Energy*, Vol. 5, No. 2, March-April, 1981, pp. 109-115.

Mesaric, M., and Kosel, F., "Unsteady Airload of an Airfoil with Variable Camber," *Aerospace Science and Technology*, Vol. 8, 2004, pp. 167-174.

Miles, J. W., "Quasi-Stationary Thin Airfoil Theory," *Journal of the Aeronautical Sciences*, Vol. 16, No. 7, July 1949, pp. 440.

Miles, J. W., "Quasi-Stationary Airfoil Theory in Compressible Flow," *Journal of the Aeronautical Sciences*, Vol. 16, No. 8, August 1949, pp. 509.

Miles, J. W., "Unsteady Flow Theory in Dynamic Stability," *Journal of the Aeronautical Sciences*, Vol. 17, No. 1, Jan. 1950, pp. 62-63.

Miles, J. W., "On the Compressibility Correction for Subsonic Unsteady Flow," *Journal of the Aeronautical Sciences*, Vol. 17, No. 3, Jan. 1950, pp. 181-182.

Munk, M., "The Minimum Induced Drag of Aerofoils," NACA Report No. 121, 1923.

Munk, M., "General Theory of Thin Wing Sections," NACA Report No. 142, 1923.

Nakashima, M., and Ono, K., "Numerical and Experimental Study of the Propulsive Speed of the Three Joint Bending Propulsion Mechanism," *Journal of Fluids Engineering*, Vol. 118, March 1996, pp. 134-141.

Nakashima, M., and Ono, K., "Numerical Study of the Thrust, Energy Consumption, and Propulsive Efficiency of a Three Joint Bending Propulsion Mechanism," *Journal of Fluids Engineering*, Vol. 122, Sept. 2000, pp. 614-618.

Narkiewicz, J. P., Ling, A., Done, G. T. S., "Unsteady Aerodynamic Loads on an Aerofoil with a Deflecting Tab," *Aeronautical Journal*, August/ September 1995, pp. 282-292.

Neef, M. F., Hummel, D., "Euler Solutions for a Finite-Span Flapping Wing," in *Fixed and Flapping Wing Aerodynamics for Micro Air Vehicles*, Chapter 19, 2001, pp. 429-451.

Nekrasov, A. I., "Theory of Wings in Nonstationary Flow," NACA TM 1154, 1947.

Neumark, S., "Pressure Distribution on an Airfoil in Nonuniform Motion," *Journal of the Aeronautical Sciences*, Vol. 19, No. 3, March 1952, pp. 214-215.

Osborne, C., "Unsteady Thin-Airfoil Theory for Subsonic Flow," *AIAA Journal*, Vol. 11, Feb. 1973, pp. 205-209.

Patil, M. J., "From Fluttering Wings to Flapping Flight: The Energy Connection," *Journal of Aircraft*, Vol. 40, No. 2, March-April, 2003.

Pennycuik, C. J., "Elastic Energy Storage in the Primary Feather Shafts," *Journal of Experimental Biology*, Vol. 64, 1976, pp. 677-689.

Pennycuik, C. J., "Power Requirements for Horizontal Flight in the Pigeon *Columba Livia*," *Journal of Experimental Biology*, Vol. 49, 1968, pp. 527-555.

Pettit, G. W., Robertshaw, H. H., Gern, F. H., and Inman, D. J., "A Model to Evaluate the Aerodynamic Energy Requirements of Active Materials in Morphing Wings," 2001 ASME Design Engineering Technical Conference, September 2001.

Phlips, P. J., East, R. A., Pratt, N. H., "An Unsteady Lifting Line Theory of Flapping Wings with Application to the Forward Flight of Birds," *Journal of Fluid Mechanics*, Vol. 112, 1981, pp. 97-125.

Pinkerton, R. M., "Calculated and Measured Pressure Distributions over the Midspan Section of the NACA 4412 Airfoil," NACA Report No. 563, 1936.

Poling, D. R., Telionis, D. P., "The Response of Airfoils to Periodic Disturbances – The Unsteady Kutta Condition," *AIAA Journal*, Vol. 24, No. 2, 1986, pp. 193-199.

Postel, E. E., and Leppert, E. L., "Theoretical Pressure Distribution for a Thin Airfoil Oscillating in Incompressible Flow," *Journal of the Aeronautical Sciences*, Vol. 15, No. 8, August 1948, pp.486-492.

Prock, B. C., Weisshaar, T. A., and Crossley, W. A., "Morphing Airfoil Shape Change Optimization with Minimum Actuator Energy as an Objective," AIAA Paper 2002-5401, September 2002.

Rayner, J. M. V., "A Vortex Theory of Animal Flight: Part 2. The Forward Flight of Birds," *Journal of Fluid Mechanics*, Vol. 91, 1979, pp. 731-763.

Rayner, J. M. V., "A New Approach to Animal Flight Mechanics," *Journal of Experimental Biology*, Vol. 80, 1979, pp. 17-54.

Rainey, A. G., "Measurement of Aerodynamic Forces for Various Mean Angles of Attack of an Airfoil Oscillating in Pitch and on Two Finite-Span Wings Oscillating in Bending with Emphasis on Damping in Stall," NACA Report No. 1305, 1957.

Reid, E. G., Vincenti, W., "An Experimental Determination of the Lift of an Oscillating Airfoil," *Journal of the Aeronautical Science*, Vol. 8, No. 1, 1940, pp. 1-6.

Rennie, R. M., and Jumper, E. J., "Experimental Measurements of Dynamic Control Surface Effectiveness," *Journal of Aircraft*, Vol. 33, No. 5, September-October 1996, pp. 880-887.

Rennie, R. M., and Jumper, E. J., "Dynamic Leading-Edge Flap Scheduling," *Journal of Aircraft*, Vol. 34, No. 5, September-October 1997, pp. 606-611.

Rennie, R. M., and Jumper, E. J., "A Case for Pseudo-Steady Aerodynamic Behavior at High Motion Rates," AIAA paper 97-0617, 1997.

Sanders B., Eastep, F. E., and Forster, E., "Aerodynamic and Aeroelastic Characteristics of Wings with Conformal Control Surfaces for Morphing Aircraft," *Journal of Aircraft*, Vol. 40, Jan.-Feb. 2003, pp. 94-99.

Satyanarayana, B., Davis, S., "Experimental Studies of Unsteady Trailing Edge Conditions," *AIAA Journal*, Vol. 16, No. 2, Feb. 1978, pp. 125-129.

Scanlan, R. H., "Pressure Distribution on an Airfoil in Nonuniform Motion," *Journal of the Aeronautical Sciences*, Vol. 19, No. 7, July 1952, pp. 502.

Schwarz, L., "Calculation of the Pressure Distribution of a Wing Harmonically Oscillating in Two-Dimensional Flow," *Luftfahrtforschung*, Vol. 17, No. 11, 1940, pp. 379.

Schwarz, L., "Aerodynamically Equivalent Systems for Various Forms of Control Surfaces within the Scope of the Two-Dimensional Wing Theory," in *Three Papers from Conference on Wing and Tail Surface Interactions*, (Translated from Lilienthal-Gesellschaft für Luftfahrtforschung, March 1941, pp. 61-74), NACA TM 1306, 1951.

Sears, W. R., *A Systematic Presentation of the Theory of Thin Airfoils in Non-Uniform Motion*, PhD. Thesis, California Institute of Technology, 1938.

Sears, W. R., Kuethe, A. M., "The Growth of the Circulation of an Airfoil Flying Through a Gust," *Journal of the Aeronautical Sciences*, Vol. 6, No. 7, July 1939, pp. 376-378.

Sears, W. R., "Operational methods in the Theory of Airfoils in Non-Uniform Motion," *Journal of the Franklin Institute*, Vol. 130, July 1940, pp. 95-111.

Sears, W. R., "Some Aspects of Non-Stationary Airfoil Theory and Its Practical Applications," *Journal of the Aeronautical Sciences*, Vol. 8, 1941, pp. 104-108.

Sears, W. R., "Some Aspects Recent Developments in Airfoil Theory," *Journal of the Aeronautical Sciences*, Vol. 23, No. 5, May 1956, pp. 490-499.

Sears, W. R., and Telionis, D. P., "Boundary Layer Separation in Unsteady Flow," *SIAM Journal on Applied Mathematics*, Vol. 28, No. 1, 1975, pp. 215-235.

Sears, W. R., "Unsteady Motion of Airfoils with Boundary Layer Separation," *AIAA Journal*, Vol. 14, No. 2, Feb. 1976, pp. 216-219.

Sedov, L. I., *Two Dimensional Problems in Hydrodynamics and Aerodynamics*, John Wiley & Sons, 1965.

Send, W., "The Mean Power of Forces and Moments in Unsteady Aerodynamics," *ZAMM*, Vol. 72, 1992, pp. 113-132.

Shyy, W., Berg, M., and Ljungqvist, D., "Flapping and Flexible Wings for Biological and Micro Air Vehicles," *Progress in Aerospace Sciences*, Vol. 35, 1999, pp. 455-505.

Singh, J., "Unsteady Aerodynamics of Deforming Airfoils – A Theoretical and Numerical Study," AIAA paper 96-2162, 1996.

Sohngen, H., "Remarks Concerning Aerodynamically Balanced Control Surfaces," in *Three Papers from Conference on Wing and Tail Surface Interactions*, (Translated from Lilienthal-Gesellschaft fur Luftfahrtforschung, March 1941, pp. 61-74), NACA TM 1306, 1951.

Sohngen, H., "Determination of the Lift Distribution for Optionally Non-Uniform Movement," *Luftfahrtforschung*, Vol. 17, No. 11, 1940, pp. 401.

Spedding, G. R., Lissaman, P. B. S., "Technical Aspects of Microscale Flight Systems," *Journal of Avian Biology*, Vol. 29, 1998, pp. 458-468.

Spence, D. A., "The Lift on a Thin Airfoil with a Jet-Augmented Flap," *Aeronautical Quarterly*, Vol. 9, Aug. 1958, pp. 287-299.

Spielburg, I. N., "The Two-Dimensional Incompressible Aerodynamic Coefficients for Oscillatory Changes in Airfoil Camber," *Journal of the Aeronautical Sciences*, Vol. 20, No. 6, June 1953, pp.432-433.

Stanewsky, E., "Aerodynamic Benefits of Adaptive Wing Technology," *Aerospace Sciences and Technology*, Vol. 4, 2000, pp. 439-452.

Stanewsky, E., "Adaptive Wing and Flow Control Technology," *Progress in Aerospace Sciences*, Vol. 37, 2001, pp. 583-667.

Tavares, T. S., and McCune, J. E., "Aerodynamics of Maneuvering Slender Wings with Leading-Edge Separation," *AIAA Journal*, Vol. 31, No. 6, June 1993, pp. 977-986.

Theodorsen, T., "On the Theory of Wing Sections with Particular Reference to the Lift Distribution," NACA Report No. 383, 1931.

Theodorsen T., "General Theory of Aerodynamic Instability and the Mechanism of Flutter," NACA Report No. 496, 1935.

Tucker, V. A., "Bird Metabolism During Flight, Evolution of a Theory," *Journal of Experimental Biology*, Vol. 58, 1973, pp. 689-709.

Van de Vooren, A. I., "Generalization of the Theodorsen Function to Stable Oscillations," *Journal of the Aeronautical Sciences*, Vol. 19, No. 3, March 1952, pp. 209-211.

von Karman, T., and Sears, W. R., "Airfoil Theory for Non-Uniform Motion," *Journal of the Aeronautical Sciences*, Vol. 5, No. 10, August, 1938, pp. 378-390.

von Karman, T., and Burgers, J. M., "General Aerodynamic Theory – Perfect Fluids," *Aerodynamic Theory*, W. F. Durand, ed., Vol. II, Julius Springer, 1935.

Wagner, H., "Über die Entstehung des dynamischen Auftriebes von Tragflugeln," *ZAMM*, Vol. 5, 1925, pp. 17-35.

Weih, D., and Katz, J., "Transient Induced Drag," *AIAA Journal*, Vol. 24, No. 7, July 1986, pp. 1203-1205.

Weis-Fogh, T., "A Rubber-Like Protein in Insect Cuticle," *Journal of Experimental Biology*, Vol. 37, 1960, pp. 889-907.

Weis-Fogh, T., "Energetics of Hovering Flight in Hummingbirds and in *Drosophila*," *Journal of Experimental Biology*, Vol. 56, 1972, pp. 79-104.

Weis-Fogh, T., "Quick Estimates of Flight Fitness in Hovering Animals, Including Novel Mechanisms for Lift Production," *Journal of Experimental Biology*, Vol. 59, 1973, pp. 169-230.

White, R. J., Klampe, G. "Force and Moment Coefficients for a Thin Airfoil with Flap and Tab in a Form Useful for Stability and Control Calculations," NACA TN 960, 1945.

Williams, M. H., "Exact Solutions in Oscillating Airfoil Theory," *AIAA Journal*, Vol. 15, June 1977, pp. 875-877.

Williams, M. H., "Aerodynamic Coefficients in Generalized Unsteady Thin Airfoil Theory," *AIAA Journal*, Vol. 18, July 1980, pp. 850-852.

Woods, M. I., Henderson, J. F., Lock, G. D., "Energy Requirements for the Flight of Micro Air Vehicles," Vol. 105, 2001, pp. 135-147.

Wu, T. Y., "Swimming of a Waving Plate," *Journal of Fluid Mechanics*, Vol. 10, 1961, pp. 321-344.

Wu, T. Y., "Hydromechanics of Swimming Propulsion, Part 1. Swimming of a Two-Dimensional Flexible Plate at Variable Forward Speeds in an Inviscid Fluid," *Journal of Fluid Mechanics*, Vol. 46, part 2, 1971, pp. 337-355.

Wu, T. Y., "Hydromechanics of Swimming Propulsion, Part 2. Some Optimum Shape Problems," *Journal of Fluid Mechanics*, Vol. 46, part 3, 1971, pp. 521-544.

Wu, T. Y., "Hydromechanics of Swimming Propulsion, Part 3. Swimming and Optimum Movements of Slender Fish with Side Fins," *Journal of Fluid Mechanics*, Vol. 46, part 3, 1971, pp. 545-568.

Wu, T. Y., "Extraction of Flow Energy by a Wing Oscillating in Waves," *Journal of Ship Research*, March 1972, pp. 66-78.

Yates, G. T., "Optimum Pitching Axes in Flapping Wing Propulsion," *Journal of Theoretical Biology*, Vol. 120, 1986, pp. 255-276.

Yates, J. E., "Viscous Thin Airfoil Theory and the Kutta Condition," AIAA paper 78-152, 1978.

Yates, J. E., "Unsteady Viscous Thin Airfoil Theory," AGARD Report No. 671, 1978.

Yurkovitch, R. "Status of Unsteady Aerodynamic Prediction for Flutter of High-Performance Aircraft," *Journal of Aircraft*, Vol. 40, Sept.-Oct. 2003, pp. 832-841.

Zbeikowski, R., "On Aerodynamic Modeling of an Insect-like Flapping Wing in Hover for Micro Air Vehicles," *Phil. Trans. R. Soc. Lond. A*, Vol. 360, Jan. 2003, pp.273-290.

Appendix A

Useful Integral Formulas for Determining the Unsteady Load Distribution

The following integrals are used in determining the apparent mass pressure distribution for the general camberline:

$$\int_0^{\theta} \ln \left(\frac{\sin \theta \tan(\theta_B / 2) - \cos \theta + 1}{\sin \theta \tan(\theta_B / 2) + \cos \theta - 1} \right) \sin \theta d\theta$$

$$= \left\{ \cos \theta_B \ln \left[-\frac{\sin \left(\frac{\theta_B + \theta}{2} \right)}{\sin \left(\frac{\theta_B - \theta}{2} \right)} \right] - \cos \theta \ln \left[\frac{\sin \left(\frac{\theta_B + \theta}{2} \right)}{\sin \left(\frac{\theta_B - \theta}{2} \right)} \right] + \theta \sin \theta_B \right\} \quad (\text{A.1})$$

$$\int_0^{\theta} \ln \left(\frac{\sin \theta \tan(\theta_B / 2) - \cos \theta + 1}{\sin \theta \tan(\theta_B / 2) + \cos \theta - 1} \right) \cos \theta \sin \theta d\theta$$

$$= \frac{1}{4} \left\{ 2 \sin \theta_B \sin \theta + \cos 2\theta_B \ln \left[-\frac{\sin \left(\frac{\theta_B + \theta}{2} \right)}{\sin \left(\frac{\theta_B - \theta}{2} \right)} \right] - \cos 2\theta \ln \left[\frac{\sin \left(\frac{\theta_B + \theta}{2} \right)}{\sin \left(\frac{\theta_B - \theta}{2} \right)} \right] + \theta \sin 2\theta_B \right\} \quad (\text{A.2})$$

$$\int_0^{\theta} \ln \left(\frac{\sin \theta \tan(\theta_B / 2) - \cos \theta + 1}{\sin \theta \tan(\theta_B / 2) + \cos \theta - 1} \right) \cos 2\theta \sin \theta d\theta$$

$$= \frac{1}{12} \left\{ \begin{aligned} & 2 \sin \theta_B \sin 2\theta + 4 \sin \theta_B \sin 2\theta + (2 \cos 3\theta_B + 6 \cos \theta_B) \ln \left[-\frac{\sin \left(\frac{\theta_B + \theta}{2} \right)}{\sin \left(\frac{\theta_B - \theta}{2} \right)} \right] \\ & + (6 \cos \theta - 2 \cos 3\theta) \ln \left[\frac{\sin \left(\frac{\theta_B + \theta}{2} \right)}{\sin \left(\frac{\theta_B - \theta}{2} \right)} \right] - 6\theta \sin \theta_B + 2\theta \sin 3\theta_B \end{aligned} \right\} \quad (\text{A.3})$$

Appendix B

The Drag for a Three-Degree-of-Freedom Oscillating Airfoil

Many practical oscillating airfoil applications deal with multi-degree-of-freedom airfoil motions, such as the combination of pitch and plunge oscillations. For the lift, pitching moment, and load distribution, each degree of freedom is treated separately and then linearly combined. As discussed in Chapter 4, the drag (and in Chapter 5, the work) is not linear with respect to the camberline deformation or airfoil motion. Thus, to accommodate multi-degree-of-freedom situations, the drag must be derived specifically for the combination of various camberline deformations or airfoil motions. This appendix will derive the drag for a three degree-of-freedom configuration, where each degree of freedom is defined by a magnitude and phase angle. This derivation is similar to Garrick's [1936] derivation for pitch, plunge, and flap motions, although the present case treats three general degrees-of-freedom.

From Eq. (2.76), the n^{th} degree-of-freedom of the airfoil motion will be defined as follows

$$\begin{aligned}\beta_n &= \bar{\beta}_n e^{i(\bar{k}\tau + \phi_n)} \\ &= \bar{\beta}_n [\cos(\bar{k}\tau + \phi_n) + i \sin(\bar{k}\tau + \phi_n)] \quad n=1,2,3\end{aligned}\tag{B.1}$$

which allows the corresponding camberline for each degree-of-freedom to be defined similarly to Eq. (2.55) as

$$z_n(x, \tau) = \psi_n(x) \beta_n(\tau), \quad n=1,2,3\tag{B.2}$$

To calculate the drag from Eq. (4.7), the load distribution and leading edge suction must be known. From Eqs. (2.73) and (2.74), the load distribution for each n can be written as

$$\Delta C_{p,n} = \Pi_{1,n} \bar{\beta}_n \cos(\bar{k}\tau + \phi_n) + \Pi_{2,n} \bar{\beta}_n \sin(\bar{k}\tau + \phi_n)\tag{B.3}$$

where the Π terms are defined in Eq. (2.89). From Eq. (4.16), the leading edge suction is extended to the three degree-of-freedom oscillating case as follows

$$C_a(\tau) = 2\pi \left[\sum_{n=1}^{n=3} \bar{A}_{0,s,n} \beta_n(\tau) + \bar{A}_{0,d,n} \beta_n'(\tau) + \alpha_{un,n}(\tau) \right]^2\tag{B.4}$$

From Eqs. (4.15) and (2.72), $\alpha_{un,n}$ is defined as

$$\alpha_{un,n}(\tau) = \frac{\bar{\beta}_n}{2\pi} [K_{0,s,n}(F-1) - K_{0,d,n}\bar{k}G] \cos(\bar{k}\tau + \phi_n) + \frac{\bar{\beta}_n}{2\pi} [-K_{0,s,n}G - K_{0,d,n}\bar{k}(F-1)] \sin(\bar{k}\tau + \phi_n) \quad (\text{B.5})$$

which will be written as

$$\alpha_{un,n}(\tau) = \alpha_{A,n}\bar{\beta}_n \cos(\bar{k}\tau + \phi_n) + \alpha_{B,n}\bar{\beta}_n \sin(\bar{k}\tau + \phi_n) \quad (\text{B.6})$$

where

$$\begin{aligned} \alpha_{A,n}(\tau) &= \frac{1}{2\pi} [K_{0,s,n}(F-1) - K_{0,d,n}\bar{k}G] \\ \alpha_{B,n}(\tau) &= \frac{1}{2\pi} [-K_{0,s,n}G - K_{0,d,n}\bar{k}(F-1)] \end{aligned} \quad (\text{B.7})$$

From Eq. (B.1) and (B.6), the terms within the summation in Eq. (B.4) will be written as

$$C_a(\tau) = 2\pi \left[\sum_{n=1}^{n=3} \bar{\beta}_n B_{A,n} \cos(\bar{k}\tau + \phi_n) + \bar{\beta}_n B_{B,n} \sin(\bar{k}\tau + \phi_n) \right]^2 \quad (\text{B.8})$$

where

$$\begin{aligned} B_{A,n} &= (\bar{A}_{0,s,n} + \alpha_{A,n}) \\ B_{B,n} &= (-\bar{A}_{0,d,n}\bar{k} + \alpha_{B,n}) \end{aligned} \quad (\text{B.9})$$

Substituting Eqs. (B.2), (B.3), and (B.8) into Eq. (4.7) allows the drag to be written as

$$\begin{aligned} C_d(\tau) &= -\int_0^c \left[\sum_{n=1}^{n=3} \Pi_{1,n}(x) \bar{\beta}_n \cos(\bar{k}\tau + \phi_n) + \Pi_{2,n}(x) \bar{\beta}_n \sin(\bar{k}\tau + \phi_n) \right] \left[\sum_{n=1}^{n=3} \frac{d\psi_n}{dx}(x) \bar{\beta}_n \cos(\bar{k}\tau + \phi_n) \right] dx \\ &\quad - 2\pi \left[\sum_{n=1}^{n=3} \bar{\beta}_n B_{A,n} \cos(\bar{k}\tau + \phi_n) + \bar{\beta}_n B_{B,n} \sin(\bar{k}\tau + \phi_n) \right]^2 \end{aligned} \quad (\text{B.10})$$

The complexity of the drag for a multi degree-of-freedom system is apparent from Eq. (B.10). It is common practice to define the average drag over one period of oscillation (\bar{C}_d) as

$$\bar{C}_d = \frac{\bar{k}}{2\pi} \int_0^{2\pi/\bar{k}} C_d(\tau) d\tau \quad (\text{B.11})$$

Substituting Eq. (B.10) into Eq. (B.11) and performing the integration over τ results in a very long expression, which is not presented here. The integration over x in Eq. (B.10) is performed numerically to obtain \bar{C}_d . The value of the formulation presented here lies in the fact that it applies to the general deforming camberline presented in Chapter 3.